SEISMIC VULNERABILITY OF FLAT-SLAB STRUCTURES

TECHNICAL REPORT
MID-AMERICA EARTHQUAKE CENTER
DS-9 PROJECT (RISK ASSESSMENT MODELING)

M. Altug ERBERIK and Amr S. ELNASHAI

Civil and Environmental Engineering Department
University of Illinois at Urbana-Champaign

December 2003

TABLE OF CONTENTS

1. INTRODUCTION

The devastating social and economic impacts of recent earthquakes in urban areas have resulted in an increased awareness of the potential seismic hazard and the corresponding vulnerability of the built environment. Greater effort has been given to reasonably estimates, predictions and mitigation of the risks associated with these potential losses.

In order to be successful in mitigation efforts and post-disaster decision-making processes, the expected damage and the associated loss in urban areas caused by severe earthquakes should be properly estimated. It is appropriate to consider the expected damage as a measure of seismic vulnerability. The determination of such a vulnerability measure requires the assessment of the seismic performances of all types of building structures typically constructed in an urban region when subjected to a variety of potential earthquakes. The vulnerability study generally focuses on the generic types of construction due to the enormous size of the problem. Hence simplified structural models with random properties to account for the uncertainties in the structural parameters are employed for all representative building types.

As being one of the special reinforced concrete structural forms, flat-slab systems need further attention. They possess many advantages in terms of architectural flexibility, use of space, easier formwork and shorter construction time. However the structural efficiency of the flat-slab construction is hindered by its poor performance under earthquake loading. This undesirable behavior has originated from the insufficient lateral resistance due to the absence of deep beams or shear walls in the flat-slab system. This gives rise to excessive deformations that cause damage in non-structural members even when subjected to earthquakes of moderate intensity. Flat-slab type of construction is in widespread use in Mediterranean and Middle Eastern countries, which are known as earthquake vulnerable regions of the world. Hence it becomes even more important to investigate the vulnerability of this special structural form.

Risk assessment is a process or application of a methodology for evaluating risk as defined by the probability and frequency of occurrence of a seismic hazard, exposure of people and infrastructure to the hazard and the consequences of that exposure. Different methodologies exist

for assessing the risk of natural hazard events. FEMA's HAZUS (National Institute of Building Sciences, 1999a) is an earthquake loss estimation methodology that can be applied throughout the nation by local, State and regional officials. The methodology provides a detailed method for the prediction of the effects of a potential seismic hazard within urban areas or across large regions and leads to a greater understanding of the problem, highlighting the most efficient ways in which the associated risk can be mitigated. HAZUS is an evolving methodology that has several drawbacks. However greater efforts are being given to enhance the framework of the methodology in order to obtain more plausible loss estimates.

1.1 Research Objectives

The study has three main objectives. The first objective is to investigate the fragility of flat-slab reinforced concrete systems. Developing the fragility information of flat-slab construction will be a novel achievement since the issue has not been the concern of any research in the literature.

The second objective is to assess HAZUS as an open-source, nationally accepted earthquake loss estimation software environment. It is important to understand the potentials and the limitations of the methodology, the relationship between the hazard, damage and the loss modules, and the plausibility of the results before using it for the purposes of hazard mitigation, preparedness or recovery.

The last objective is to implement the fragility information obtained for the flat-slab structural system into HAZUS. The methodology involves many built-in specific building types, but does not include flat-slab structures. Hence it will be extra achievement to develop HAZUS-compatible fragility curves to be used within the methodology.

1.2 Report Organization

The report is composed of two parts. The first part (Chapters 2 and 3) deals with the development of the fragility information of flat-slab systems. Chapter 2 gives information about fragility studies in general. The advantages and disadvantages of different methodologies employed in developing fragility curves are explained. Example fragility studies from the literature are reviewed. Chapter 3 focuses on the fragility curve development for the flat-slab system. The chapter begins with preliminary information about the significance of flat-slab construction. Then the methodology used in this study to develop the fragility curves is explained. The methodology includes the design and construction of the analytical model, selection of ground motions, evaluation of the seismic response through the analytical model, attainment of the limit states, treatment of material variability and the development of the structural simulations in order to construct the curves. At the end of the chapter, the obtained fragility curves are compared with the similar fragility information in the literature for the sake of verification.

The second part of the report is devoted to the loss estimation analysis of flat-slab structures (Chapters 4 and 5). Chapter 4 gives detailed information about HAZUS, FEMA's Earthquake Loss Estimation Methodology. It begins by listing the features and limitations of HAZUS for a better understanding of the methodology. The uncertainty in the methodology is investigated in detail, focusing on the treatment of this uncertainty. Next, the building related damage and loss modules of HAZUS are explained in detail. Chapter 5 is devoted to the implementation of the fragility curves developed for the flat-slab system into HAZUS. First a procedure to modify the fragility information to fit into HAZUS format is proposed. Next the employment of HAZUS modules in the implementation process is discussed. Two study regions are employed and the results of the loss estimation analysis are evaluated, focusing on the comparison of the flat-slab system with other structural forms embedded into HAZUS.

Chapter 6 includes a brief summary of the report and the conclusions drawn during different phases of the study.

PART I

RISK ASSESSMENT OF FLAT-SLAB STRUCTURES

2. SEISMIC FRAGILITY

Definition of seismic risk involves three different components: the earthquake hazard; the structural inventory; and the fragility of the inventory with respect to seismic hazard. While developing the fragility information, the inherent uncertainties in hazard and inventory should be taken into account and should be combined with the uncertainties arising from the employed methodologies.

Fragility curves provide estimates for the probabilities of a population of structures reaching or exceeding various limit states at given levels of ground shaking intensity. A limit state usually represents a damage condition, or a limitation of usage, in the same terms as the response. In recent studies, limit states have been defined in terms of deformation rather than load and multiple limit state satisfaction has been widely accepted.

Fragility information can be used by design engineers, researchers, reliability experts, insurance experts and administrators of critical systems such as hospitals and highway networks. The information can be used to analyze, evaluate and improve the seismic performance of both structural and non-structural systems. Fragility curves can be developed either for a specific system or component for a class of systems and components.

Different sources of information can be utilized in the derivation of fragility curves. These approaches are summarized briefly in the next section. Then the analytical-based fragility curves existing in the literature are examined in more detail.

2.1 Different Methodologies for Fragility Curve Derivation

There are several approaches to construct seismic fragility curves. The first approach to construct seismic fragility curves is empirically based using the available damage data from previous earthquakes. The second approach is by using expert opinion or by using experimental-based

damage information. The third approach to construct seismic fragility curves is to use engineering analysis.

The first approach using historical damage data in the construction of the empirical fragility curves and contains information about the degree of damage, the intensity of ground motion and the construction category of the building. This approach is the most realistic one because it is based on actual damage data. However, there are shortcomings using this approach. It is very difficult to find a suitable observational-based set of fragility functions for a particular region with site specific seismo-tectonic, geotechnical and building stock characteristics. Furthermore, this approach is inherently category-based, or in other words, it cannot reflect any details of a particular building in the category. Information on the vulnerability of buildings with new configurations or materials that are not represented in the available earthquake damage database can not be provided using this approach. Consequently this becomes an issue when assessing the future benefits of proposed code changes or seismic retrofits.

The second approach, using expert opinion for the derivation of fragility functions, is used generally in the case where there is inadequate existing data. In this approach, the opinions of multiple experts can be used as data to create a probability distribution on response, conditioned on hazard intensity. The varying degrees of knowledge of the experts are obtained by having each one self-rate his or her expertise. The advantage of this approach is that it is versatile and does not require costly or unavailable damage data. The drawback to this approach is that expert opinion lacks a scientific basis which makes the data arguable (or biased). One area that may be problematic in obtaining reliable data is in the case of new conditions in which the experts have no experience.

Experimental-based fragility studies are becoming popular by enhancements in the structural testing facilities to test large, realistic structures and full-scale structures. Since large-scale testing is an expensive and time-consuming process, it is not possible to test many structures to obtain the necessary response statistics for fragility studies.

The third approach is to use analytical methods for the derivation of the fragility curves. The most significant advantage of using this approach is the ease and efficiency by which the response statistics can be obtained. Advances in computational structural engineering make it possible to simulate more realistic structures with many characteristic features. Additionally, new analysis techniques speed up the process and enable the formation of a huge analytical database.

However just like all the other approaches, computational-based fragility functions have limitations. One limitation is that it is difficult to use this method for macroscopic loss estimation. This approach can only be used for a specific type of building or a building category. Also, detailed modeling of many structural assemblages is still questionable and should be verified through experimental investigation. As of the computational procedures used, convergence issues may arise when structures are subjected to very large demands, hence obtaining realistic response output near collapse may not be numerically possible.

Each approach has both pros and cons. In fact, there is no universally applicable best method for calculating fragility functions. Depending on the circumstances, one method to construct fragility curves may be preferred over another.

2.2 Review of Analytical Fragility Studies

Analytical methods can be employed for the derivation of the fragility curves for which there is no existing damage database, or for which experimentation would be prohibitively expensive.

For creating seismic fragility curves, structural analysis can be employed with different levels of sophistication: linear or nonlinear, pseudo-static or dynamic. Obviously, the level of effort and computational time increases along with the accuracy of the results. The most commonly used analytical approaches in fragility studies are the nonlinear time-history analyses and the nonlinear static procedures (e.g. capacity spectrum method). These methods have been used to assess the vulnerability of different engineering structures and subassemblages such as buildings,

bridges, structural components. The following paragraphs focus on some of the recent studies related with the vulnerability of the building structures only.

A recent study being conducted by Wen et al. (2003) is in the area of Vulnerability Function Framework for Consequence Based Engineering. Different methods are proposed to evaluate the vulnerability of a system depending on the problem and the information available. The proposed methods include probabilistic displacement demand analysis, limit state probability analysis and fragility curve analysis.

In the fragility analysis, if the system stays within the linear range, the relationship between the system response and the intensity measure can be constructed via a linear structural dynamic analysis using the method of modal superposition. Since there exists an analytical relationship, only the structural modeling and the response analysis methods are the additional sources of uncertainty. On the other hand, the system can behave in the inelastic range when subjected to a severe excitation. Obviously, it is not possible to use simple modal analysis in this case. Time history analyses are required with ground motions ranging from low to high intensities and reflecting the seismicity of the region. Then, a regression analysis of the responses related to the limit state of interest as a function of the excitation intensity measure is performed. At this stage, the nonlinear regression analysis of the power-law form is recommended due to the general nonlinearity of the problem and the large scatter in response caused by the ground motion variation. It should be noted that the power-law form allows linear regression analysis by a simple logarithmic transformation. The regression constants obtained through the analysis determine the conditional expectation and coefficient of variation of the structural response given the hazard intensity. Finally, a proper distribution function, preferably lognormal, can be selected to construct the fragility curve.

Wen et al. have also conducted research on alternative intensity measures. The ones used in the literature are generally scalar parameters derived either from ground motion or from response characteristics. However, they cannot predict all structural response characteristics, particularly higher mode contribution and very complex behavior of some building types (e.g. various failure modes of masonry structures). Hence the authors have worked on an alternative approach called

Uniform Hazard Ground Motions (UHGM) Method in order to predict the complex structural response by employing the entire time-history of ground motions. By definition, UHGM represents events of various magnitudes, distance and attenuation having frequency and intensity such that the median response of the structures gives an accurate estimate of the demand on the structure for a given probability of exceedence.

The proposed vulnerability analysis framework is demonstrated by a masonry building located in Memphis. The performance of the building is measured by the wall-drift ratio. Spectral acceleration is used as the hazard parameter for fragility analysis. The ground motions are generated according to the regional seismicity and uniform hazard response spectra. Four different limit states are used: Immediate Occupancy, Life Safety, Collapse Prevention and Incipient Collapse. The first three limit states are defined according to FEMA 273 (1997). The definition of the fourth limit state, Incipient Collapse, was obtained from the Incremental Dynamic Analysis. Studies on the vulnerability evaluation of reinforced concrete buildings and steel frame buildings have been in progress at the completion time of this report.

Another group of researchers, Hwang and Huo (1997), studied the development of fragility curves on concrete frame and shear wall buildings for the Loss Assessment of Memphis Buildings (LAMB) project. The buildings were classified in three different categories: 1-3 story frame buildings, 4-6 story shear wall buildings and 7-9 story shear-wall buildings. These categories represent low, mid and high-rise construction, respectively. The researchers employed two different sets of synthetic ground motions generated for a site close to the University of Memphis, in the central part of the Mississippi embayment and located close to the New Madrid Seismic Zone.

Two different modeling approaches were employed to obtain the dynamic response: multi degree of freedom (MDOF) structural models and a simplified single degree of freedom (SDOF) stick model by which the inelastic behavior of the buildings is simulated using the modified Takeda model with a bilinear skeleton curve. The results obtained by the simplified method were promising when compared with the ones obtained by conventional analysis.

Four damage states were considered in terms of maximum story drift ratio, δ_{max}: (1) no damage, when $\delta_{max} < 0.2\%$, (2) insignificant damage, when $0.2\% < \delta_{max} < 0.5\%$, (3) moderate damage, when $0.5\% < \delta_{max} < 1.0\%$ and (4) heavy damage, when $\delta_{max} < 1.0\%$. The damage criteria were assumed to be the same for both frame and shear-wall buildings.

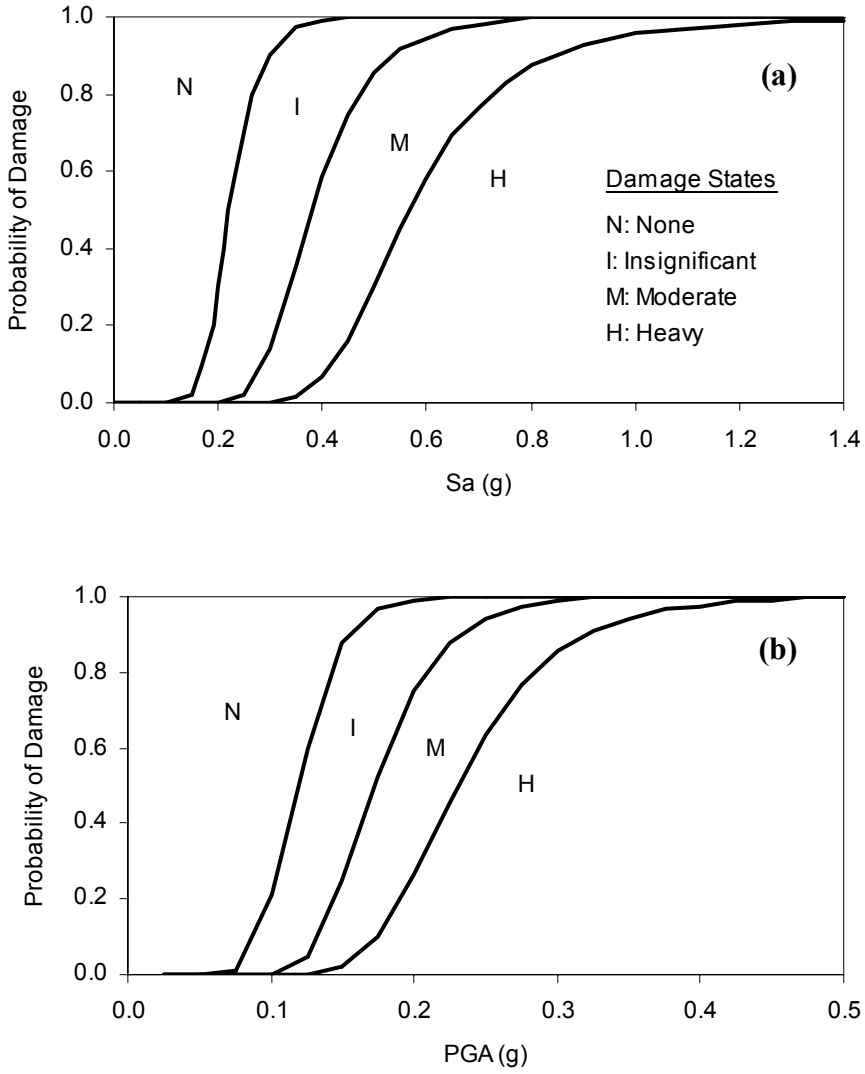

Figure 2.1 Fragility Curves of Generic 1-3 Story RC Frame Building (Hwang & Huo) **a)** Ground Motion Parameter: S_a, **b)** Ground Motion Parameter: PGA

Hwang and Huo employed peak ground acceleration (PGA) and spectral acceleration (S_a) at the fundamental period of the generic buildings to represent the intensity of ground shaking whereas δ_{max} is used to quantify the structural response. Typical fragility curves obtained for low-rise frame buildings and for the two different types of ground motion intensity parameters are illustrated in Figure 2.1.

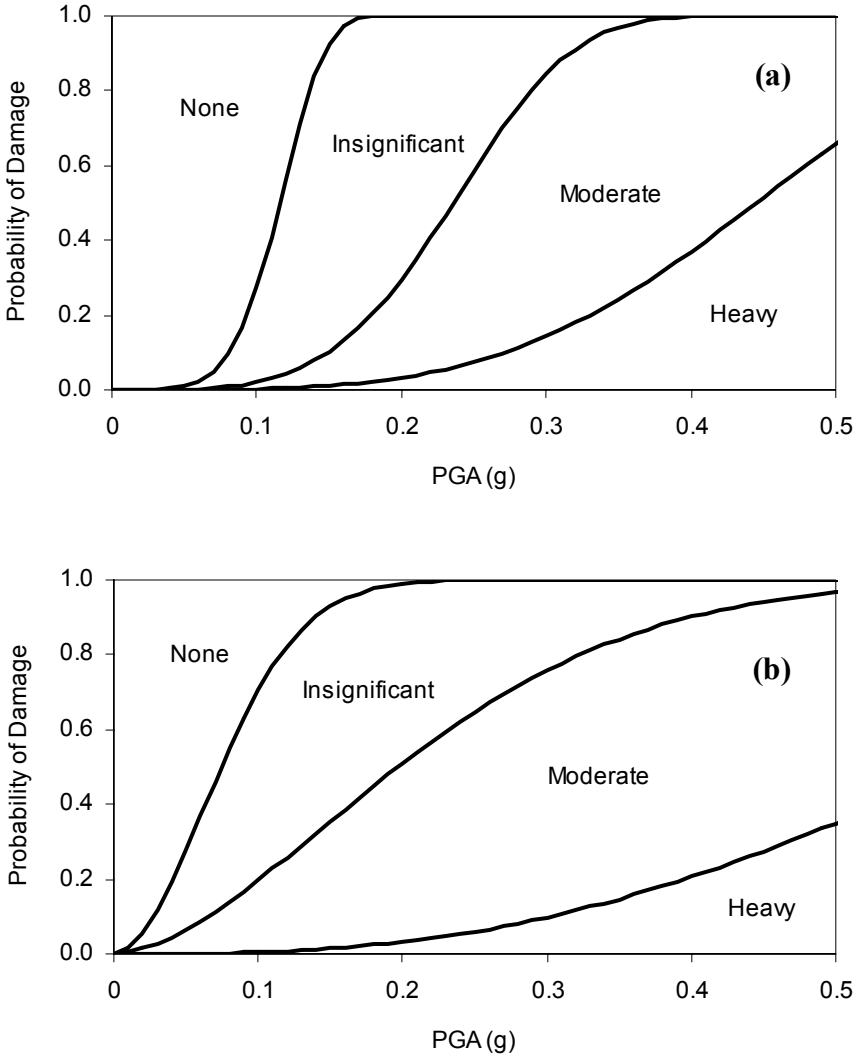

Figure 2.2 Fragility Curves of LRC Frames (Mosalam et al.) **a)** Bare Frame, **b)** Infilled Frame

In the context of the same (LAMB) project, Mosalam et al. (1997) developed fragility curves for low-rise and mid-rise Lightly Reinforced Concrete (LRC) frames with masonry infill walls. The same ground motion sets of the previously mentioned study were employed in the analysis. The researchers employed a different computation method, the Dynamic Plastic Hinge Method (DPHM), which is a simplified method to minimize the effort and the expense involved in determination of the structural response. DPHM reduces MDOF structure to an equivalent SDOF oscillator with equivalent nonlinear properties. In the implementation of DPHM, properties of equivalent SDOF are obtained by using the Adaptive Pushover Analysis.

In the generation of the curves for LRC frames with and without infill walls, PGA was used as the hazard parameter whereas maximum interstory drift ratio was employed as the response parameter. The limit states established in the previous study was considered to be valid for bare LRC frames. For infilled frames, an arbitrary criterion of 1/10 of the limits specified for bare frames were established. Figure 2.2 represents the fragility curves for bare and infilled LRC frames.

Singhal and Kiremidjian (1997) used three different classes (low, mid and high-rise) of reinforced concrete frames as the test-bed in their fragility study. The ARMA model is employed to generate artificial time histories. Spectral acceleration at the fundamental period of the structure is used for the hazard parameter. The Park and Ang damage index is used as the response parameter. Damage states are also identified based on this damage index after calibration with observed damage to several buildings caused by different earthquakes. According to the damage scale, minor damage occurs when the index uses values between 0.1 and 0.2. For index values between 0.2 and 0.5 the damage state is moderate whereas for values between 0.5 and 1.0 it is severe. Exceedence of unity for the index value corresponds to the collapse limit state. Fragility curves for low and mid-rise frames are illustrated in Figure 2.3.

It is also worth mentioning two other recent fragility studies in which nonlinear dynamic structural analysis is employed. One study conducted by Porter (2000) proposed a rigorous methodology called “Assembly-based Vulnerability” for developing building specific seismic fragility functions. The methodology utilizes the damage to individual building components and

accounts for the building seismic location, structural and non-structural design and use. A simulation approach to implementing assembly-based vulnerability applies a ground motion time history to a structural model to determine structural response. The response is applied to assembly fragility functions to simulate damage to each structural and non-structural element in the building and to its contents. Because the methodology produces detailed damage simulations at the assembly level, the analyst can calculate the probability that a particular building will meet detailed performance–based design objectives. The assembly level resolution also means that a designer or analyst can examine the benefits of alternative designs, rehabilitation, or retrofit details to which a category-based approach is not sensitive.

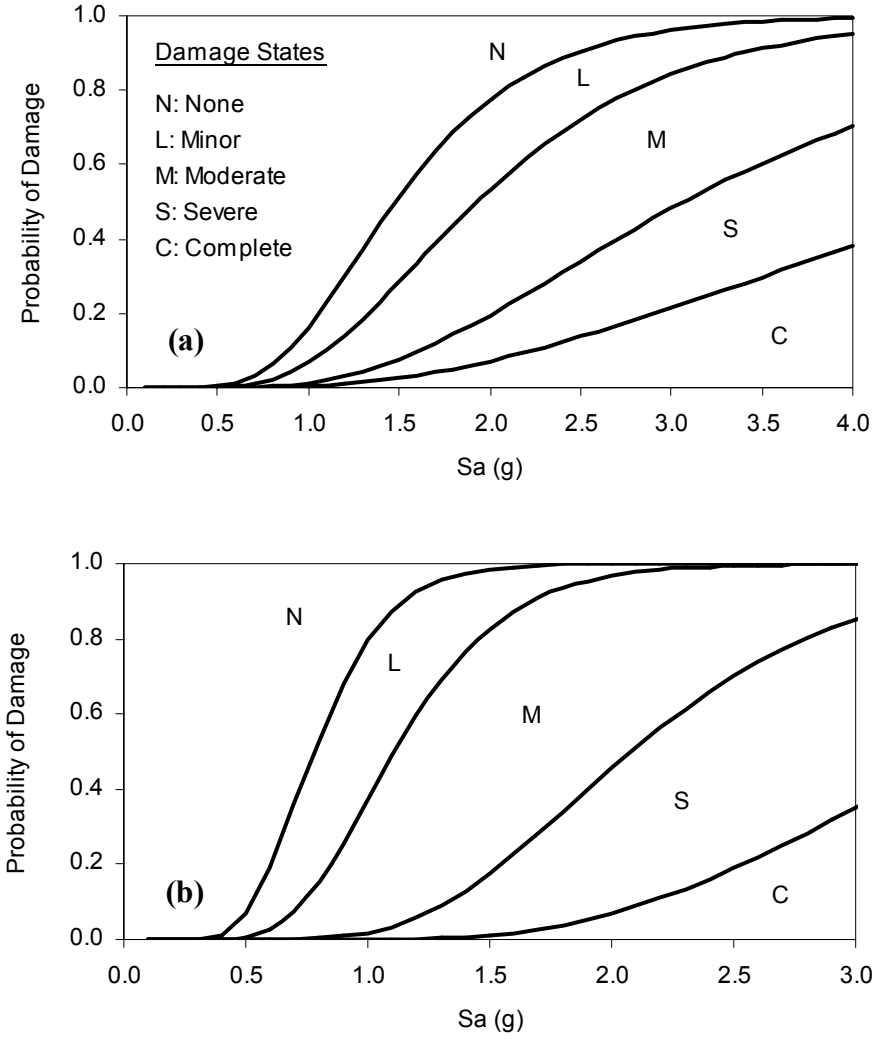

Figure 2.3 Fragility Curves of RC Frames (Singhal & Kremidjian); **a)** Low-rise, **b)** Mid-rise

Tantala and Deodatis (2002) studied the reliability assessment of tall buildings subjected to earthquake loadings. Their study is one of the first to relate the vulnerability of tall buildings to different earthquake intensity measures. The methodology to develop the fragility curves follows a Monte-Carlo simulation approach incorporating uncertainties in the ground motion and in the structural characteristics. They also evaluated the effect of the assumption of Gaussianity and the role of duration of strong ground motion.

Recently, there has also been an increasing interest in the simplified nonlinear analysis methods. The Capacity Spectrum Method (CSM) is widely used by researchers to assess the seismic vulnerability functions of civil engineering structures.

The best example of the implementation of simplified methods is the HAZUS Earthquake Loss Estimation Methodology (National Institute of Building Sciences, 1999a). The HAZUS building fragility curves are lognormal functions which take into account the uncertainty associated with capacity curve properties, damage states and ground shaking. Databases from previous earthquakes and expert opinions were also considered in developing the curves. Figure 2.4 provides two examples of HAZUS fragility curves. These curves belong to model building types of unreinforced masonry with low-code seismic design level (URM-L) and reinforced concrete moment frames with moderate-code seismic design level (C1M-M), respectively. There are 36 different model building types in HAZUS. Each fragility curve is defined by a median value and the variability associated with the damage state. Structural fragility is expressed in terms of spectral displacement. Median values of fragility are based on inter-story drift ratios that describe the threshold of damage states. HAZUS defines damage by one of four discrete damage states: Slight, Moderate, Extensive or Complete. Detailed information about the HAZUS Loss Estimation Methodology and the building classifications is provided in Chapter 4.

A similar procedure is proposed by Barron-Corvera (2000). The basic idea of their method is the assumption that the expected median response is determined by the intersection of the spectral capacity and spectrum demand curves. This intersection is called the expected response point. If either or both of the curves are random, the response is random. This method was applied to a four story structure with RC frames and shear walls. In addition, the influence of various

structural parameters such as yield strength level, initial period and post yield stiffness ratio was considered in evaluating the probabilistic response of nonlinear systems.

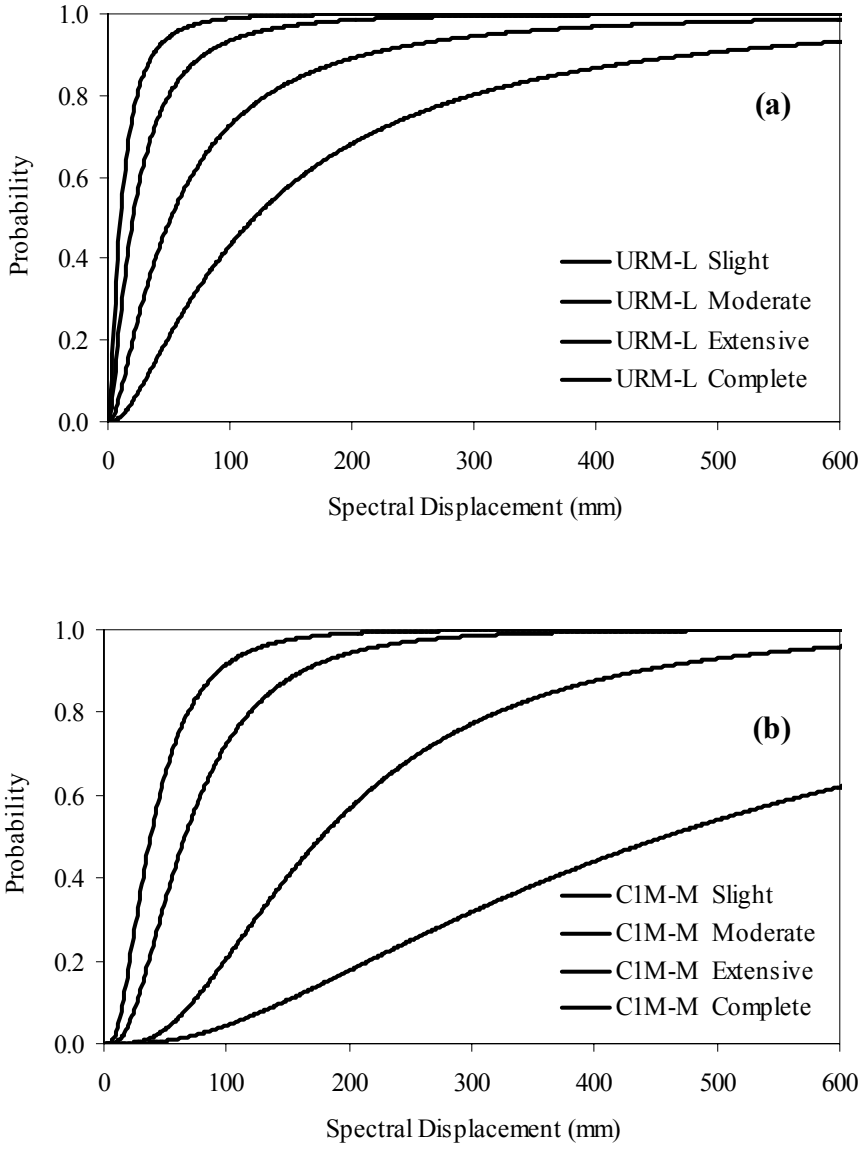

Figure 2.4 HAZUS Fragility Curves; **a)** Low-rise Unreinforced Masonry Buildings (URM-L), **b)** Mid-rise Concrete Moment Frame (C1M-M)

3. FRAGILITY ANALYSIS OF FLAT-SLAB STRUCTURES

Flat-slab construction possesses major advantages over conventional slab-beam-column construction and are in wide spread use in most Middle East and Mediterranean countries. Their structural efficiency, however, is often hindered by poor performance under earthquake loading. The absence of deep beams or shear walls in the flat-plate system gives rise to excessive lateral deformations; hence drift limits associated with non-structural damage can be prematurely attained. This study is an attempt to perform risk assessment of flat-slab construction. The goal of this novel work is to derive the vulnerability curves for flat-slab construction and then compare it with the built-in vulnerability functions of reinforced concrete buildings in HAZUS.

The first section will introduce flat-slab structures, their features and the advantages and disadvantages of this type of construction. It will also cover other studies on flat-slab structures. The next section will discuss the methodology for the derivation of the fragility parameters of a generic flat-slab structure.

3.1 Overview of Design and Analysis Considerations in Flat-Slab Construction

One of the most common floor systems for the construction practice in many earthquake vulnerable parts of the world (Mediterranean, Middle East) is the flat-slab (Figure 3.1). This practice is generally used for relatively light loads and for spans from 4.5m to 6m. For heavy industrial loads and for larger spans, flat-slabs are used with drop panels or column capitals. In such structural systems, the load is transferred to the column by thickening the slab near the column, using drop panels and/or by flaring the top of the column to form a column capital. The drop panel commonly extends about one sixth of the span each way from each column, giving extra strength in the column region while minimizing the amount of concrete at midspan (MacGregor, 1997). The flat-slab type of construction provides architectural flexibility, more clear space, less building height, easier formwork, and, consequently, shorter construction time. Furthermore, the absence of sharp corners improves fire resistance, so there is less danger of the concrete spalling and exposing the reinforcement. However, a serious problem that can arise in

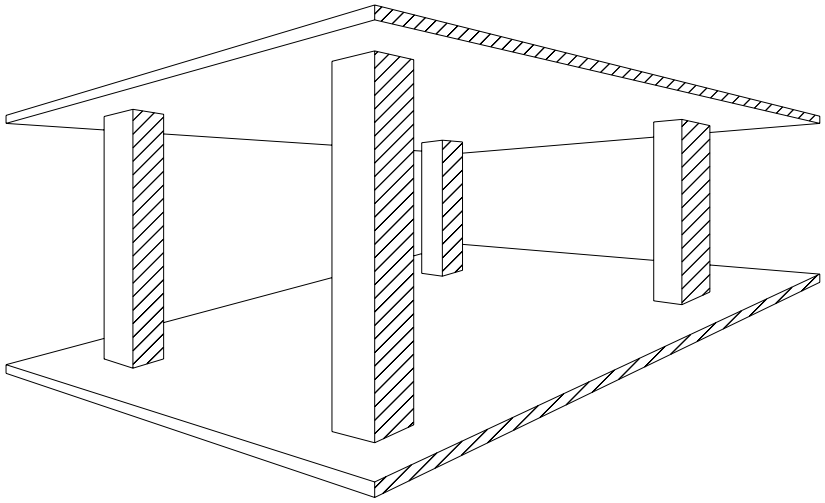

Figure 3.1 Illustration of a typical flat-slab structural form

flat plates is brittle punching failure due to the transfer of shearing forces and unbalanced moments between slabs and columns (Hueste and Wight, 1997; Megally and Ghali, 2000). Under earthquake actions, the unbalanced moments can produce high shear stresses in the slab. In addition to this, flat-slabs are susceptible to significant reductions in stiffness as a consequence of slab cracking that can arise from construction loads, service gravity loads, temperature and shrinkage effects and lateral loads (Moehle, 1986; Pan and Moehle, 1989). Hence in regions of high seismic risk, flat-slab construction should only be used as the vertical load carrying system in structures braced by frames or shear walls, which are responsible for the lateral capacity of the structure (ACI-ASCE Committee, 1988). In such cases, slab-column connections must undergo the lateral deformations of the primary lateral load-resisting structural elements without punching failure in order to sustain the gravity loads acting at the instance of earthquake occurrence in addition to unbalanced moments resulting from earthquake lateral forces. Megally and Ghali (1994) suggested that the primary lateral load resisting structural elements, such as shear walls, should be combined with flat plates in seismic zones to keep the lateral drift ratio lower than 1.5%. Therefore the slab-column connections must be capable of withstanding 1.5 %

drift ratio without punching failure. They also stated that for ductility and drift capacity, slab-column connections without shear reinforcement must satisfy

$$V_u \leq 0.4\, V_o \qquad \textbf{(3.1)}$$

where V_u is the factored axial force and V_o is the nominal capacity in the absence of unbalanced moment. In the presence of shear reinforcement, the above criterion is no longer required. Thus, slab-column connections in seismic zones must possess (a) adequate strength against punching shear failure during and after earthquake occurrence and (b) adequate ductility to undergo inelastic deformations without failure, that is, the ability to undergo a specified minimum lateral inter-story drift ratio.

In spite of the above recommendations, flat-slabs are often adopted as the primary lateral load resisting system and their use proves popular in seismically active regions, such as most of the Mediterranean basin. In these cases, the design of flat-slab buildings is typically carried out in a similar manner to ordinary frames. Where this practice is followed, the response under moderate earthquakes indicates extensive damage to non-structural elements even when code provisions for drift limitation are satisfied (Chow and Selna, 1995). Prevention of such damage is important, as it accounts for the greatest portion of total repair costs (Penelis and Kappos, 1997).

According to ACI-318 (1999), flat-slabs can be designed by any procedure that satisfies equilibrium and geometric compatibility provided that every section has strength at least equal to the required strength, and that the serviceability conditions are satisfied. Two methods employed for the design of flat-slabs are the Direct Design Method and Equivalent Frame Method.

These two methods differ primarily in the way in which the slab moments are calculated. The Equivalent Frame Method uses an elastic frame analysis to compute the positive and negative moments in the various panels in the slab while the Direct Design Method uses coefficients to compute the moments. In Equivalent Frame Method, a flat-slab building is modeled as a set of parallel plane frames in which the columns are modeled as equivalent columns whose flexibility is taken as the sum of the flexibility of the columns above and below the slab and the flexibility

of the torsional members, and the slabs are modeled as equivalent beams. The equivalent beam has a depth equal to that of the original slab and an effective width that targets both the strength and the stiffness of the slab (Luo and Durrani, 1995a and b; Luo et al., 1995; ACI-318, 1999). Direct Design Method is easier to use than the Equivalent Frame Method, but it has limitations. One limitation is that it is only applicable to fairly regular multi-panel slabs. A multi-panel is a panel with a minimum of three continuous spans in each direction. In addition to this, rectangular panels must have a long span / short span ratio not greater that two. Another serious limitation is that the direct design method cannot be used for unbraced laterally loaded frames; all loads must be due to gravity only.

The main issues in lateral load design of flat-slab frames can be listed as lateral load stiffness, lateral load strength and ductility and resistance to progressive collapse (Moehle, 1986). These issues are discussed briefly in the following paragraphs.

Lateral Load Stiffness

Lateral drift is likely to be a significant design issue for flat-slab frames. In many cases, lateral drift considerations rather than strength considerations will control the frame proportions. Large flexibility of flat-slab frames causes concern in seismic design for several reasons including possible damage to structural and non-structural components and overall stability of the frame under excessive drifts. For example, the five story three bay flat plate building analyzed by Chow and Selna (1995) has the fundamental calculated period of 1.66 seconds and the seismic coefficient, which is defined as the base story yield shear divided by the weight of the structure of 15.8%. The value of the predominant period is pretty much higher than the corresponding reinforced concrete moment resisting frames with conventional beams and columns. In addition, the calculated story drift values of the model building when subjected to the 1940 El Centro earthquake are higher than the levels specified by Uniform Building Code (UBC) limits. Even if the building survives such a moderate earthquake, the non-structural systems will be heavily damaged and the safety of the occupants will be jeopardized by the failure of these systems. Using conservative procedures, if not accurate procedures, for estimating stiffness are desirable in flat-slab structures.

Lateral load strength and ductility

Both shear and unbalanced moment result in slab shear stresses in the vicinity of the column and shear stresses due to the combination of both may control strength. Under combined shear and moment transfer, a linear variation of shear stresses is presumed to develop according to the ACI Building Code (ACI, 1999). The model predicts a linear interaction between shear and unbalanced moment transfer strengths. Shear and unbalanced moment strength of edge and corner slab-column connections are generally affected by the same parameters that influence the behavior of interior connections, when design and analysis procedures are similar. However, for frames located in regions of high seismic risk, most building codes require the use of perimeter frames to comprise conventional beam-column framing.

Resistance to progressive collapse

Slab-column connections are susceptible to punching shear failures when subjected to inelastic load reversals. The methods for strengthening the slab-column connections against punch-shear failures include the use of drop panels or slab shear reinforcement or the use of high strength concrete in the slab at the vicinity of the columns. Among these, drop panels (or shear capitals) tend to increase the length of the perimeter of the punching shear critical section. Drop panels with small plan dimensions are not effective in an earthquake when lateral forces can produce reversals of relatively high unbalanced moments in slab in column vicinity. In such cases, an inverted punching failure can occur for which the additional slab depth provided by the shear capital is not effective in increasing punching shear capacity. An alternative to preventing the punching shear failure is the use of slab shear reinforcement generally in the form of vertical legs of stirrups. Anchorage is provided by means of hooks, bends and the longitudinal slab flexural reinforcing bars lodged at the corners of the stirrup. With stud shear reinforcement, anchorage is provided mechanically by means of a forged head at one end and a steel strip at the other end. Megally and Ghali (2000) stated that providing stud shear reinforcement increases the punching resistance and prevents brittle failure even in a severe earthquake. Finally, the use of high strength concrete instead of normal strength concrete delays the punching failure until the yield strength of more flexural reinforcing bars is developed. Punching strength is directly proportional to the tensile strength of concrete different than other types of failures in ordinary

structures that are dominated by steel; therefore in flat-slab structures, concrete quality is extremely important (Ersoy, 1994).

Although all the methods discussed above were successful in increasing the punching strength, the effects of the three different strengthening methods on ductility are substantially different. In addition, when a single connection fails, loads originally supported at the connection will be transferred to surrounding connections if no provisions were made to suspend the slab at the punched connection. These may, in turn, fail under increased loads, possibly resulting in a progressive collapse. To avoid a progressive collapse, either original punching failure must be prevented or progressive collapse must be arrested by suspending the slab from the columns after punching of the individual connections. The first method of avoiding the original punching shear failure can be achieved either by ensuring very low shear stresses under gravity loads or by providing slab stirrup reinforcement. Both of these methods are often considered unsatisfactory because of apparent economic reasons. An alternative method of preventing progressive collapse by suspending the slab from the columns is, in many cases, the more acceptable solution. To achieve this goal, the bottom longitudinal reinforcement (minimum amount of which is specified by the ACI-ASCE Committee 352) should be continuous over the columns at slab-column connections since it is capable of significant post-punching resistance.

3.2 Derivation of Fragility Functions for Flat-Slab Structures

The seismic fragility of a building structure is the probability that a given intensity of earthquake input will cause a limit state criterion to be achieved or exceeded. Fragility studies are in general undertaken employing relationships that express the probability of damage as a function of a ground motion parameter, since neither the input motion nor the structural behavior can be described deterministically. The two widely used forms of motion-versus-damage relationships are fragility curves and damage probability matrices (DPM). A plot of the computed conditional probability versus the ground motion parameter is defined as the fragility curve for that damage state, whilst the discrete probability of reaching or exceeding a damage state for a certain input motion severity represents an element of the DPM. The damage level is randomly described

corresponding to random input variables. Out of the large number of parameters that affect the behavior of structures under seismic action, only those considered to influence significantly the response are assumed as random variable.

The principal considerations in the evaluation of fragility curves are:

i. identification of random input variables and hence likely scenarios of systems based on a prototype structure;
ii. quantification of potential ground motion;
iii. determination of the limit states of the considered structural system
iv. evaluation of structural response;
v. construction of the curves by comparing the demand, corresponding to the hazard, and the limit states.

The general methodology will be introduced in the next section and each of the above steps will be explained in detail in the proceeding sections.

3.2.1 Methodology

The methodology used in the derivation of fragility curves for flat-slab construction is presented as a flowchart in Figure 3.2.

For the construction of the fragility functions, there is not a definite method or strategy. A great degree of uncertainty is involved in each step of the procedure originated from the ground motion characteristics, analytical models, materials used, selection of the limit states etc. Hence, this study aims at developing a consistent approach for the derivation of the fragility curves. The process begins with the selection of the building configuration and the material properties. Then the building is designed according to some predefined objectives and the detailing of the structural members is performed. The next step is to prepare a realistic analytical model of the building structure under concern. There should be a compromise between the simplicity of the model and the ability to capture the required response characteristics (like local damage). After this step, there are three different tasks to be fulfilled. The first task is the selection of the ground

motions to be used in the analysis. The number and the characteristics of the records depend on the objectives of the analysis. The second task is to conduct the nonlinear static analysis and determine the limit states of the structure. And the final task is the modeling of the material variability. There may be a large number of variables, but the issue is to select the ones which significantly affect the response. Then the dynamic analyses are conducted with varying structural characteristics, for different ground motions, each scaled to different levels of seismic intensity. This is the most elaborate step of the analysis, since thousands of runs are required even for a small number of random variables and grounds motion records. In the final step, the analysis results are processed by considering the previously defined limit states and the statistical distribution of data for each damage state is established. Each of these steps will be explained in detail for the flat-slab building selected for this study.

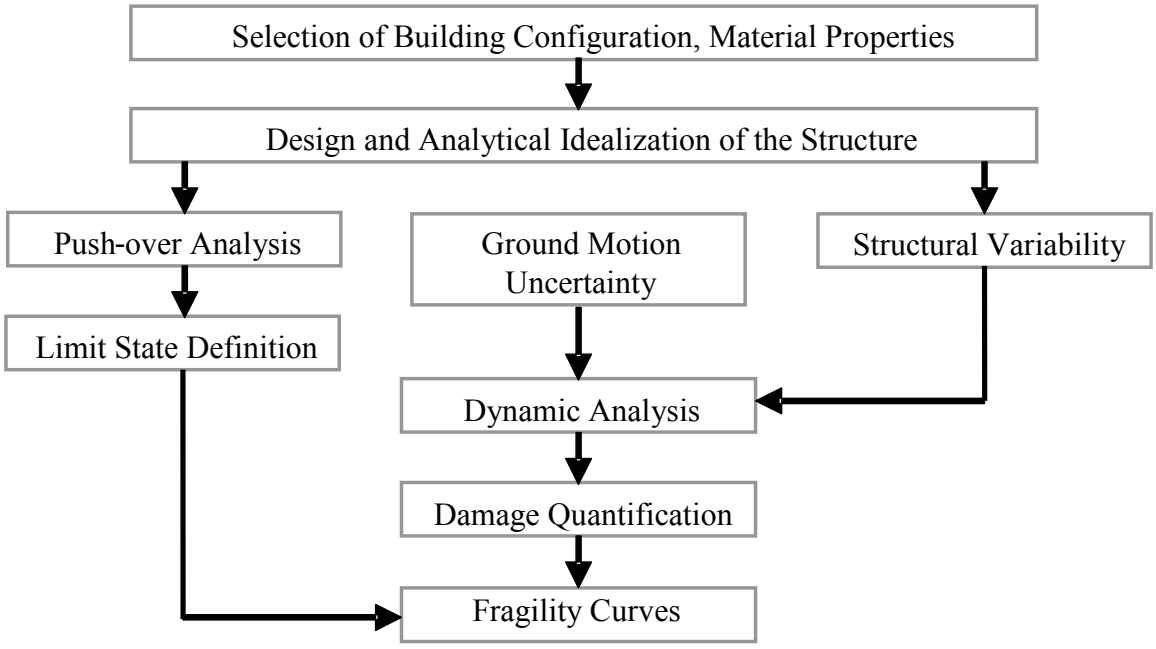

Figure 3.2 The Methodology Used in the Derivation of Vulnerability Curves.

3.2.2 Structural Configuration and Design

Since probabilistic nonlinear analysis of reinforced concrete buildings is computationally intensive, the analysis will be conducted only for a typical five-story flat-slab building. Such a building may be treated as a mid-rise construction. The reason of choosing a mid-rise building is two-fold on the basis of applicability of flat-slab construction: Because of the inherent flexibility of the flat-slab buildings, it may not be possible to satisfy the drift demands of high-rise construction. On the other hand, low-rise buildings may be regarded sufficiently stiff to warrant particular consideration. The selected dimensions of the building in preliminary design are shown in Figure 3.3. For simplicity, the building is symmetric in plan with three bays in both horizontal directions. This symmetry enables the use of 2-D models in both design and analysis. Each story contains nine square slab panels with dimensions 6 m x 6 m. This span length is considered to represent typical values for this type of construction in earthquake-vulnerable regions, especially in Mediterranean countries (Limniatis, 2001). Furthermore, equal span lengths in both directions are frequently preferred in flat and ribbed/waffle slabs, thus maximizing the efficiency of two-way slab reinforcement. The story height is selected as 2.8 m. It should be noted that the story height parameter has a significant effect on the flexibility of structures, thus it is beneficial in design to retain it as short as practically possible.

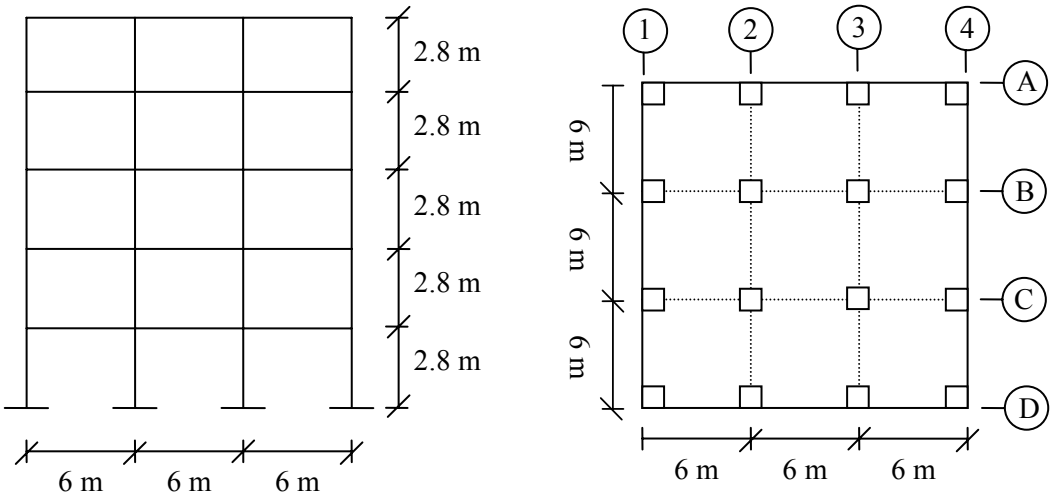

Figure 3.3 Five-Story Flat-Slab Building, **a)** Elevation, **b)** Plan

The building was designed according to the ACI 318-99 (ACI, 1999) for both gravity and seismic loads. The materials used are 4000 psi (28 MPa) concrete and Grade 60 (414 MPa) reinforcing bars which represent the common practice. The gravity load consists of dead load and live load. In the calculation of dead load, the weight of the structural members and masonry infill walls are included. The live load is taken as 2.5 kN/m^2, which is typical for an office building. Other types of loading, such as wind and snow, are not accounted for.

The seismic design is carried out according to FEMA 368, NEHRP Recommended Provisions for Seismic Regulations for New Buildings and Other Structures (Building Seismic Safety Council, 2001). Design spectra can be constructed from the maps of spectral response accelerations at short period S_S (defined as 0.2 sec) and at 1.0 sec period S_1 corresponding to the maximum considered earthquake. An alternative way to obtain S_S and S_1 is to enter the USGS Web Site* with the ZIP Code of the building site. The flat-slab building is assumed to be located in Urbana, IL. Hence the corresponding values of S_S and S_1 are determined from the web site using the ZIP code 61801. Then the spectral acceleration values are multiplied by the site

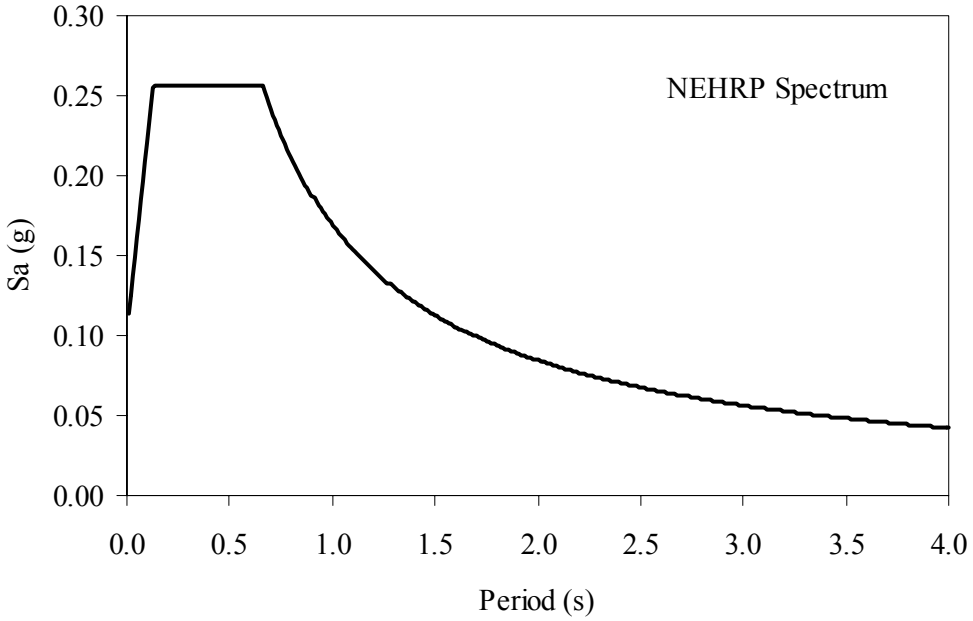

Figure 3.4 NEHRP Design Spectrum

* http://eqint.cr.usgs.gov/eq/html/zipcode.shtml

coefficients F_a and F_v in the short and mid to long period ranges, respectively. These coefficients depend on the soil category and the shaking intensity. Finally the adjusted spectral ordinates at the maximum considered earthquake are multiplied by 2/3 to construct the spectra for the design earthquake. The 5% damped design spectra constructed according to 2000 NEHRP Guidelines, FEMA-368 is shown in Figure 3.4.

The design base shear for the building is calculated as 420 kN and then used in the equivalent lateral force procedure to obtain the vertical distribution of seismic forces. Since the building is symmetric in plan, design forces are calculated based on one of the planar interior frames. Design axial forces, shears and moments are obtained by subjecting the selected frame to the factored design dead, live and seismic (lateral) loads. The detailing of the structural members is carried out according to ACI 318-99.

Design of Structural Members

In this study, the flat-slabs are designed as frames, in which the beams are concealed within the slab. The flexural design of the slabs is carried out according to ACI provisions whereas the design for shear and ductility of the support strips called as the slab-beams follows the conventional ACI regulations for beams.

Slab reinforcement was designed by employing direct design method. The first step in this method is the determination of the total static design moment, M_o.

$$M_o = \frac{wl_2 l_n^2}{8} \qquad \textbf{(3.2)}$$

In this equation, wl_2 is the load per unit length and l_n is the clear length of the span. Next, M_o is distributed to negative and positive moment sections (i.e. at supports and mid-spans). The final step is to redistribute the negative and positive moments to column and middle strips. These strips are defined as shown in Figure 3.5 for a single frame of the flat-slab building.

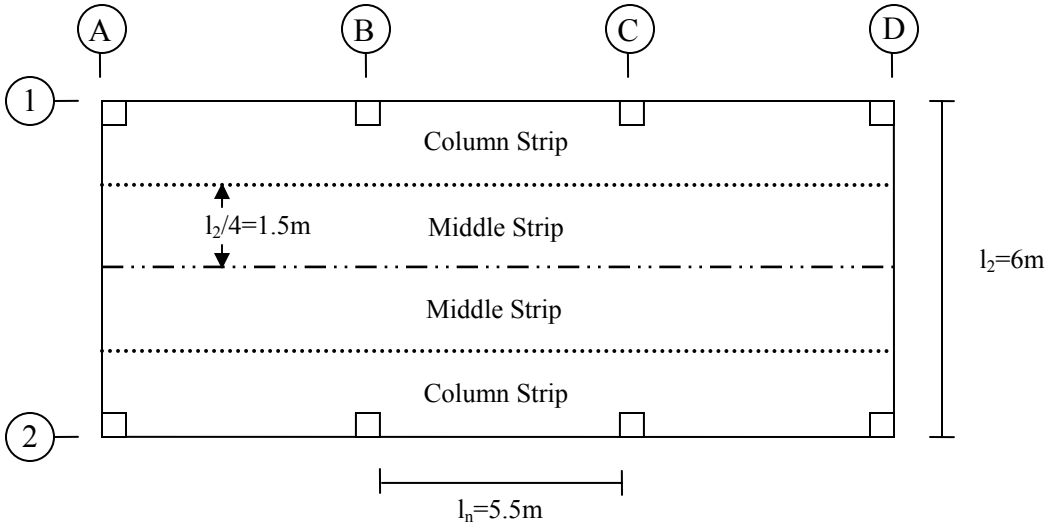

Figure 3.5 Column and Middle Strips Used in Slab Reinforcement Calculations

The required amount of reinforcement in both directions is obtained after distributing the moments to the strips and by using the conventional beam design formulation given by

$$A_s = \frac{M}{\phi f_y jd} \qquad \textbf{(3.3)}$$

where ϕ is taken as 0.90 and j as 0.925 for slabs. Typical reinforcement diagrams for a selected column and middle strip in each direction, respectively, are illustrated in Figure 3.6.

Since the most significant problem of the flat-slab systems is the punching shear failure, precautions should be taken in the design stage to prevent this undesired behavior. First, the depth of the slab should be selected according to the requirements in the code in order to prevent this type of failure. For the flat-slab building under consideration, the slab depth is taken as 22 cm, satisfying the punching shear check of ACI 318-99.

$$\phi V_c > V_u \qquad \textbf{(3.4)}$$

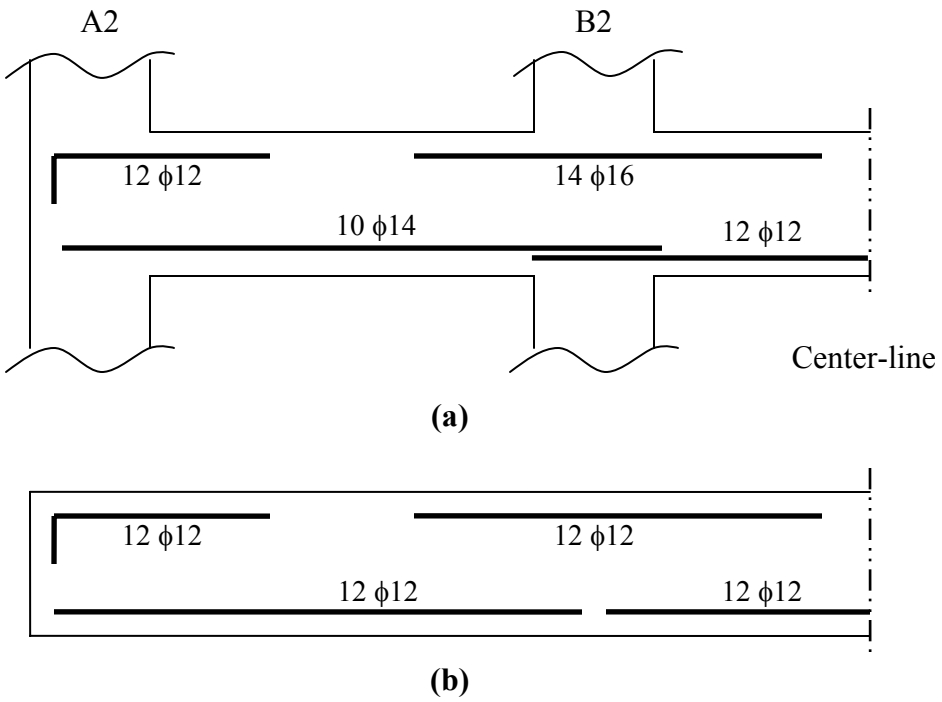

Figure 3.6 Schematic Diagram of Reinforcement for **a)** Column Strip along Line 2, **b)** Middle Strip between Lines A & B.

In Equation 3.4, V_u is the factored shear force, V_c is the allowable nominal shear strength and ϕ is the strength reduction factor. V_c is taken as the smallest of

$$V_c = \left(2 + \frac{4}{\beta_c}\right)\sqrt{f_c'}\, b_o d \qquad \textbf{(3.5)}$$

$$V_c = \left(\frac{\alpha_s\, d}{b_o} + 2\right)\sqrt{f_c'}\, b_o d \qquad \textbf{(3.6)}$$

$$V_c = 4\sqrt{f_c'}\, b_o d \qquad \textbf{(3.7)}$$

In the above equations, d is the depth of the slab, β_c is the ratio of the long side to the short side of the column, concentrated load or reaction areas, b_o is the perimeter of the critical section, f_c' is

the specified compressive strength of concrete and α_s is a constant with a value of 40 for interior columns, 30 for edge columns and 20 for corner columns. Some of the parameters given in Equations 3.5-3.7 are illustrated in Figure 3.7.

The reinforcement of the slab-beams is properly detailed to prevent failure induced by the combination of forces in the slab including shear, torsion and moment transferred from the column. In other words, the slab-column connections are designed and detailed to withstand moment reversals.

Moreover, the bottom reinforcement of the slab system in the case study building is continuous with a reasonable amount passing through the columns. This prevents progressive vertical collapse of slabs in the event of a local punching failure.

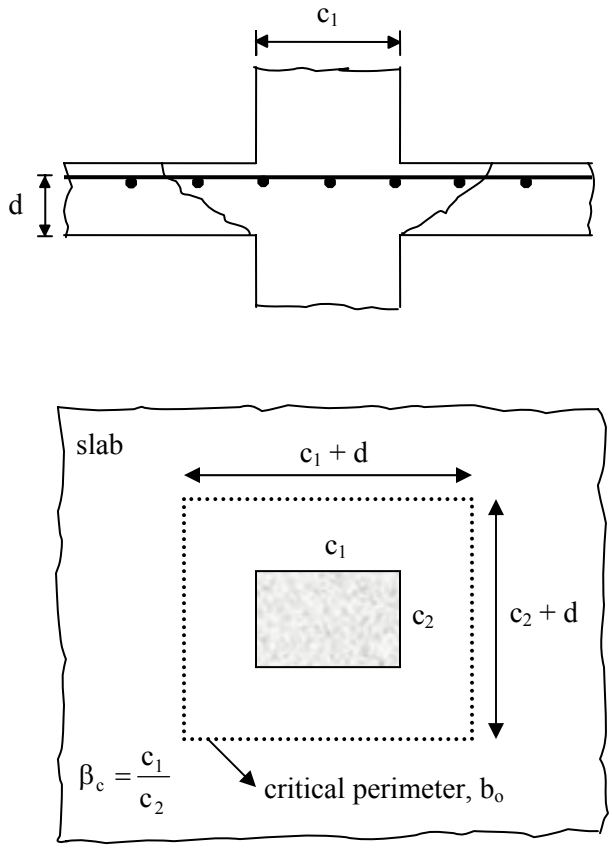

Figure 3.7 Illustration of Punching Failure Phenomenon at a Slab-column Connection

The column dimensions are taken as 40 cm x 40 cm throughout the height of the building. Longitudinal and lateral reinforcement are determined according to ACI provisions. These provisions state that the column should have adequate capacity to withstand the excessive drift demand that the building is imposed under seismic action. Design calculations endorse the use of 8 ϕ24 bars as the longitudinal reinforcement which yields a reinforcement ratio, ρ_t=0.022. The lateral reinforcement is selected as ϕ14 bars with a spacing of 10 cm. Although the column dimensions are kept constant throughout the structure, 8ϕ20 bars are employed as the longitudinal reinforcement for the top three floors, yielding a reinforcement ratio of ρ_t=0.016. As lateral reinforcement, ϕ12 bars are used with a spacing of 10 cm. It should be kept in mind that column confinement is extremely important with regard to the flexible response of the flat plate system, since the ductility capacity of the column should cope with the high drift demands. Moreover, the strength of concrete increases with increasing confinement.

Capacity design principles are also valid for the structure under concern, ensuring a beam hinging collapse mechanism by the employment of "weak beam-strong column" concept. Hence it becomes possible to obtain the plastic hinging at the slab-beams, which has more flexure dominant behavior, rather than columns, which are relatively non-ductile compression members.

3.2.3 Modeling of the Flat-Slab Structure

The regularity of the buildings in terms of mass and stiffness in both plan and elevation enables the utilization of two-dimensional analysis in the assessment of seismic response. In this study, the three dimensional flat-slab building is modeled as 2-D planar frame with lumped masses. The program utilized for the inelastic analysis of the flat-slab structure is ZeusNL (Elnashai et al., 2002). The program is employed herein to perform static non-linear (pushover) and dynamic time history analysis. In addition to the inelastic analysis, eigenvalue analysis is performed with the program, to obtain modal characteristics.

Slab-beams

For the modeling of the slabs, the portion of the slab that will contribute to the frame analysis should be determined as well as the width of the concealed beam within this slab portion. Two simplified methods exist for the former, namely the Effective Beam Width and the Equivalent Frame Method, in which the effect of the slab is accommodated by appropriate modification of the beam width or the column stiffness, respectively. In this study, the Effective Beam Width Method is employed.

The effective beam width is defined as the slab width for which uniform rotation across its width gives the same column displacement as the original slab. In this method, the columns of the model structure remain the same, but floor slabs are replaced with equivalent slab-beams. Determination of an accurate effective width is an issue of paramount importance with respect to modeling of the structures. Overestimation of the beam width will result in a stronger and stiffer beam than appropriate, possibly leading to premature column failure; hence the capacity design concept envisaged in design may not be identifiable in the assessment. Furthermore, the increase inertia of the shallow beam, although related linearly with width, may lead to an underestimation of lateral drifts. On the other hand, underestimation of the effective width can trigger premature beam failure if the predicted capacity is exceeded by the imposed demand.

The use of effective beam width concept for the analysis of flat plate systems subjected to earthquake loading has been recommended by Luo and Durrani (1995a and 1995b), amongst others. For the purpose of developing a rational method for the selection of the effective width, the authors conducted extensive analytical research based on the results of numerous tests on slab-column connections reported in the literature. Their study considered as variables the column and slab aspect ratios, the magnitude of the gravity loads, the location of the connection (interior or exterior) and the presence of the stirrups and spandrel beams as part of the slab. The suggested expressions of the effective width coefficient for interior and exterior connections, α_i and α_e respectively, take the form:

$$\alpha_i = \chi \frac{R_{12}\left(\frac{c_1}{l_2}\right)}{0.05 + 0.002\left(\frac{l_1}{l_2}\right)^4 - 2\left(\frac{c_1}{l_1}\right)^3 - 2.8\left(\frac{c_1}{l_1}\right)^2 + 1.1\left(\frac{c_1}{l_1}\right)} \quad \textbf{(3.8)}$$

where

$$R_{12} = -0.0221\left(\frac{c_1}{c_2}\right)^4 + 0.0281\left(\frac{c_1}{c_2}\right)^3 + 0.1535\left(\frac{c_1}{c_2}\right)^2 + 0.773\left(\frac{c_1}{c_2}\right) + 0.0845 \quad \textbf{(3.9)}$$

$$\chi = \left(1 - 0.4\frac{V_g}{4A_c\sqrt{f_c'}}\right) \quad \textbf{(3.10)}$$

Parameter χ is the reduction factor accounting for gravity loads; c_1 and c_2 are the column dimensions in the bending direction and normal to the bending direction, respectively. The terms l_1 and l_2 represent span lengths in bending direction and in direction transverse to l_1, respectively, both measured from center to center of the columns. In Equation 3.10, V_g is the direct shear force due to gravity load only, A_c is the area of slab critical section and f_c' is the compressive concrete strength. The expression for the exterior connections has a similar form, which may be found elsewhere (Luo and Durrani, 1995b). For the flat-slab structure under consideration, both α_i and α_e were calculated and then the average of these two values was taken as the effective width used in the model. This value is 2.85 m.

For the determination of the width of the concealed beam, or the slab-beam, there are several different considerations. In one of the early studies, considering the experimental and analytical results, Tsuboi and Kawaguchi (1960) stated that the slab-beam width could be approximated as

$$2b_e \approx 0.58\text{-}0.61*(2a) \quad \textbf{(3.11)}$$

where b_e is the effective width and 2a is the width of the panel. A different expression is given by the Mexico Building Code (1987) as

$$b_{eff} = c + 3h \quad \textbf{(3.12)}$$

where c is the column dimension in the direction perpendicular to the analysis and h is the slab depth. The Greek Code for Reinforced Concrete Structures (1999) states that in the presence of lateral loads, the slab beam width is taken as

$$b_{eff} = b_o + 2h_s \quad \textbf{(3.13)}$$

where b_o is the column width in the direction of interest and h_s is the slab depth. Finally in ACI 318-99, Clause 13.5.3 states "*This section is concerned primarily with slab systems without beams……all reinforcement resisting the part of the moment to be transferred to the column by flexure should be placed between lines that are one and one-half the slab or drop panel thickness, 1.5h, on each side of the column…..*". Hence ACI defines a region of the slab which has special flexural reinforcement and which is like a beam concealed within the slab thickness with a width of

$$b_w = c + 2*(1.5h) \quad \textbf{(3.14)}$$

Considering all the above recommendations, the width of the slab beam is taken as 100 cm. for the first three stories and 90 cm for the top two stories. A typical slab-beam section from the first story of the building is illustrated in Figure 3.8.

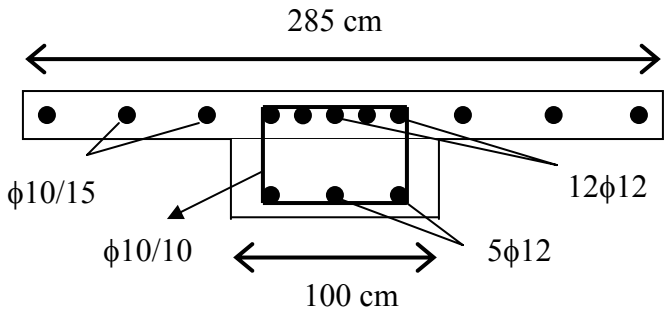

Figure 3.8 Typical Slab-Beam Section of the Flat-Slab Building

Unreinforced Masonry (URM) Infill Panels

Flat-slab structures typically have low lateral stiffness which makes them vulnerable to severe damage during earthquakes of even moderate intensity. The main concern in a flat-slab construction is to avoid progressive collapse as a result of punching failure and to control the excessive lateral drift. The punching failure is prevented by introducing adequate reinforcement at slab-column connections and by adjusting the slab depth against shear failure. The latter issue is handled by placing unreinforced masonry infills, which have high in-plane stiffness to control the lateral drift.

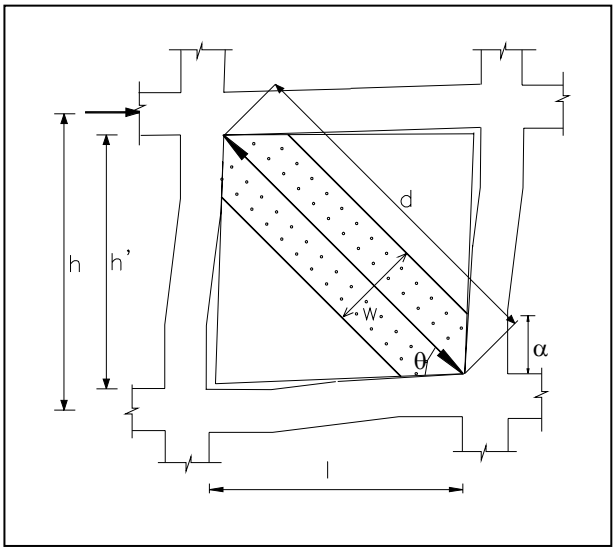

Figure 3.9 Masonry Infill Frame Subassemblage

Masonry infill walls can significantly affect seismic behavior of a frame, so they should be included in the analytical model. At low levels of lateral force, the frames and infill walls act in a fully composite fashion. However, as lateral force levels increase, the frames attempt to deform in a flexural mode while the infill attempts to deform in a shear mode. As a result, the frames and infills separate at the corners on the tension diagonal and a diagonal compression strut on the compression diagonal develops as shown in Figure 3.9. After separation, the effective width of the diagonal strut is less than that of the full panel (Paulay and Priestley, 1992). Eigenvalue, pushover and nonlinear time history analyses should be based on the structural stiffness after

separation. This can be achieved by modeling the infilled frame as an equivalent diagonally braced frame, where masonry infill walls are represented by diagonal compression struts.

The behavior of masonry infill frames has been extensively studied since the 1960s. Holmes (1961) proposed that the strength and stiffness of an infill frame can best be modeled by using diagonal compression struts with modulus of elasticity and thickness equal to that of the actual infill material, and width equal to one-third of the diagonal length of the infill panel. Later, experimental studies of Stafford Smith (1966, 1969 and 1978) showed that the diagonal stiffness and strength of a masonry infill wall depends not only on its dimensions and physical properties but also on its length of contact with the surrounding frame, which is governed by the relative stiffness of the infill and frame. Smith proposed a simple equation for calculating length of contact, α

$$\frac{\alpha}{h} = \frac{\pi}{2\lambda h} \qquad \textbf{(3.15)}$$

where λh is a non-dimensional parameter that represents the relative stiffness of the frame with respect to the infill. λ is expressed as:

$$\lambda = \sqrt[4]{\frac{E_m\, t\, \sin 2\theta}{4 E_s\, I_c\, h'}} \qquad \textbf{(3.16)}$$

where E_m, t and h' are Young's modulus, thickness and height of infill respectively. E_s, I_c and h are Young's modulus, moment of inertia and height of the column, and θ is the slope of the infill diagonal to the horizontal.

In Smith's study, graphs of λh versus equivalent strut width are given for various length/height proportions of infills. Using these, one can estimate equivalent strut width for a masonry infill wall, which is typically between 1/10 and 1/4 of the length of the infill diagonal. Mainstone (1971) provided the following empirical formulation in terms of λh for equivalent strut width:

$$w = 0.175\left(\lambda h\right)^{-0.4} d \qquad \textbf{(3.17)}$$

Here d is the length of the infill diagonal and λh is as given above. This formulation is also recommended by FEMA 273 (1997). Later similar studies, which were based on evaluating the experimental behavior of masonry infilled frames to obtain formulations of strength and equivalent stiffness, were carried out by Klingner and Bertero (1978), Bertero and Brokken (1983) and Zarnic(1990). In a more recent study, Madan et al. (1997) proposed a hysteretic model for simulating masonry infill panels in nonlinear analysis of infilled frames. This model was based on the equivalent diagonal strut approach suggested by Saneinejad and Hobbs (1995).

Three distinct failure modes can be categorized for masonry infill walls: sliding shear failure, compression failure of diagonal strut, and diagonal tensile cracking. However the latter does not constitute a failure condition on its own, as higher lateral forces can be supported without considerable change in stiffness until compression type of failure occurs. In the study conducted by Stafford-Smith and Carter (1969), graphs of $R_c/(f_c'ht)$, $R_s/(f_{bs}'ht)$, $R_t/(f_t'ht)$ versus λh are given for various length/height proportions of infills. R_c, R_{bs}, R_t are the diagonal loads that cause compression, shear and diagonal cracking failures of the infill, respectively, and f_c', f_{bs}', f_t' are the compressive, bond shear, tensile strengths of the infill wall, respectively. Paulay and Priestley (1992) proposed the following equation for calculating diagonal compression failure force:

$$R_c = \frac{2}{3}\frac{\pi}{2\lambda} t f_c^{'} \sec\theta \qquad \textbf{(3.18)}$$

and the following equation for calculating diagonal shear failure force:

$$R_{bs} = \frac{f_{bs}}{l^{'} - \mu_f\left(h/l^{'}\right)} dt \qquad \textbf{(3.19)}$$

where l′ is the distance between centre lines of columns and μ_f is the coefficient of friction. Alternative formulations of limit strength were proposed by Saneinejad and Hobbs (1995) including others.

In this study, masonry infill walls are modeled as diagonal struts. The stiffness properties of the infill are obtained by using Equations 3.16 and 3.17. The equivalent strut width is calculated as 73 cm, approximately 11% of the length of the infill diagonal. To obtain the strength of a masonry infill wall, it is necessary to find the most probable failure mode, the one giving the lowest strength from Equations 3.18 and 3.19, being the most probable mode of failure. Then this value is divided by the effective area of the infill. For the case study building, the strength of the masonry infill is calculated as 3 MPa. The elastic modulus, E_m, of masonry is taken as 8250 MPa, in accordance with Paulay and Priestley (1992) and FEMA 307 (1999).

Material and Section Properties

The concrete is modeled by the nonlinear concrete model with constant (active) confinement modeling in ZEUS-NL. The concrete model is illustrated in Figure 3.10. There are four parameters of the model: compressive strength, f_c, tensile strength, f_t, crushing strain, ε_{co} and confinement factor. This model is based on the research conducted by Mander et al. (1988). A constant confining pressure is assumed, considering the maximum transverse pressure from confining steel. This is introduced on the model through a constant confinement factor, used to scale up the stress-strain relationship throughout the entire strain range. The rules governing the cyclic behavior of the model were further improved by Martinez-Rueda and Elnashai (1997) to enable the prediction of continuing cyclic degradation of strength and stiffness. It also ensures better numerical stability under large displacement analysis (Elnashai et al., 2002).

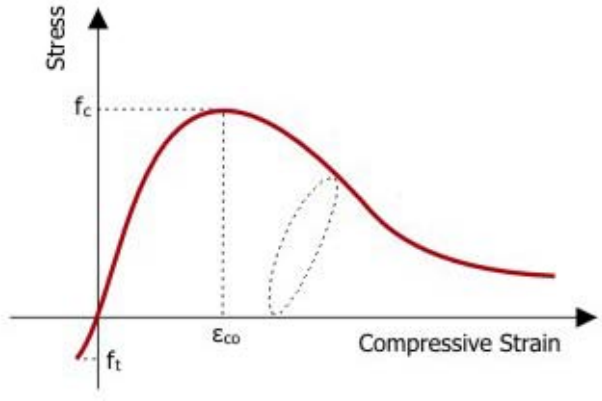

Figure 3.10. Nonlinear Concrete Model (CON2) in ZEUS-NL.

There are several expressions for the calculation of the confinement factor available in the literature, based on analytical as well as experimental data. In this study, the simple relationship proposed by Park et al. (1982) is employed.

$$K = 1 + \frac{\rho_w f_{yw}}{f_c} \qquad \textbf{(3.20)}$$

In the above equation, ρ_w is the volumetric ratio of the transverse reinforcement, f_{yw} is the nominal hoop strength and f_c is the unconfined uniaxial concrete strength. For the case study building, the confinement factor values range between 1.18-1.37 depending on the amount of lateral reinforcement of the corresponding column or the slab-beam.

As it will be explained in the following sections, the compressive strength of concrete is considered as a random variable in fragility analysis of the case study flat-slab building. However, mean material properties can be employed for the reference structural model. The compressive strength of concrete is obtained by the approximate formulation $f_{cm}=f_{ck}+8$ in MPa, i.e. $f_{cm}=35.6$ MPa. The mean tensile strength of concrete is calculated as $f_{ctm}=0.30\ f_{ck}^{2/3}=2.75$ MPa (Limniatis, 2001). Unconfined concrete strain at peak stress is considered as being equal to 0.002.

Steel is modeled with bilinear elasto-plastic model with kinematic strain-hardening in ZEUS-NL. The illustration of the steel model is represented in Figure 3.11. Three parameters are required for the model: elastic modulus of steel, E_s, yield strength of steel, f_y and the strain-hardening parameter μ. In this study, the elastic modulus is considered as 200 kN/mm^2. The yield strength of steel is also a random variable to be used in fragility analysis, but the mean value can be obtained from the approximate formulation $f_{ym}=1.15f_{yk}$, i.e. $f_{ym}=475$ MPa. Strain-hardening parameter μ plays an important role, since the steel reinforcement is the part which maintains the ductility of reinforced concrete members. In reinforced concrete, the strength of the reinforcement bars should continue to increase post-yield with increasing strain, such that sections adjacent to the critical one can sustain moments beyond the elastic limit and a sufficient plastic hinge length can be developed along the member (Penelis and Kappos, 1997). On the

other hand, an upper bound should also be established to avoid excessive strain-hardening, which may cause overstrength in beam members. The strain-hardening parameter μ is considered as 0.01.

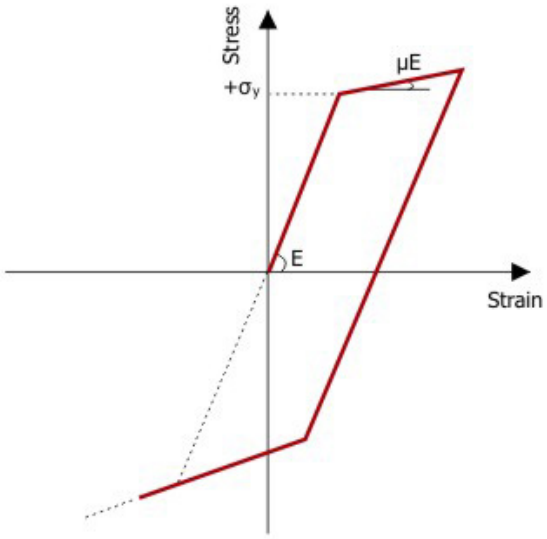

Figure 3.11 Stress-strain Relationship of Steel Used in the Model

Element Formulation

The case study flat-slab building is modeled as a 2-D planar frame. The structural members that constitute the frame are namely the slab-beams, columns and the struts. The cubic elasto-plastic beam-column element of ZEUS-NL is utilized for all of the members (Figure 3.12). According to the formulation of this beam-column element, transverse displacements along the element length in the Eulerian system are expressed by a cubic function, thus enabling an accurate representation of local geometric non-linearities. The calculated element parameters are first transformed and then assembled to the global level, effectively accommodating large displacements and P-δ effects. Exact numerical integration is performed at two Gauss sections per element. Fiber analysis at each Gauss section is employed in the monitoring of direct stresses and strains, based on the specified material constitutive relationships. Shear stresses and strains are not accounted for. In general, the selected element type is considered to accurately model the spread of inelasticity across reinforced concrete sections.

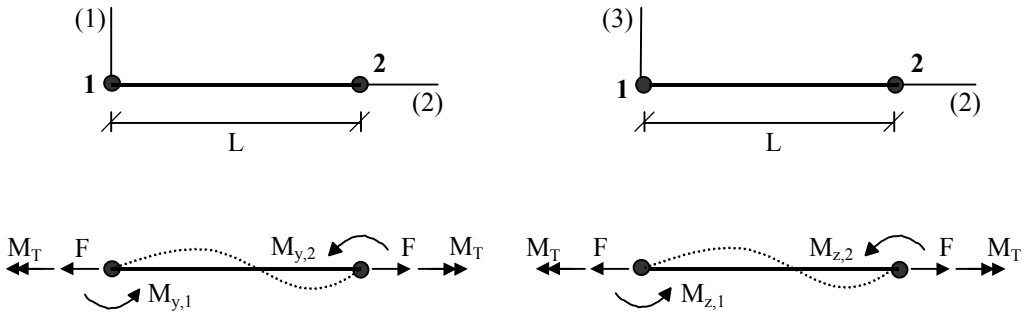

Figure 3.12 The Cubic Elasto-plastic Beam-column Element in ZEUS-NL

A finer mesh is required to model the structural elements in order to account for the distribution of inelasticity throughout the length. Consequently, beams are modeled with four elements whereas columns with three elements in the analytical model of the case study building. An additional consideration regarding the selection of the element lengths involves the desired position of the monitoring sections. The location of two Gauss points per element is set at

$$\xi = \pm\sqrt{3}\,\frac{L}{6} \qquad \textbf{(3.21)}$$

where ξ is measured from the center point of the element length L. For accurate monitoring of stresses and strains at the sections of interest, end elements of beams are dimensioned such that the location of a Gauss point coincides with the face of the column. The lengths of the column end elements are also adjusted such that the Gauss point is located at the underside of the slab-beams.

Compressions struts are modeled using cubic elasto-plastic elements with a bilinear material model for the infill properties that have been discussed in the previous paragraphs. Referring to Figure 3.11 again, modulus of elasticity (E in the figure) is taken as 8250 MPa, and the strength on the infill (σ_y in the figure) is taken as 2 MPa. To simulate the pin joint behavior at the ends of each strut, there exists a 3-D joint element in ZEUS-NL with uncoupled axial, shear and moment

actions (Elnashai et al., 2002). For the complete definition of joint, four nodes are required (Figure 3.13). *Nodes 1* and *2* are the end nodes of the element and must be initially coincident. *Node 3* is only used to define the x-axis of the joint whereas *Node 4* is required to define the x-y plane, together with the already defined x-axis. After deformation, the orientation of the joint x-axis is determined by its initial orientation and the global rotations of *Node 1*.

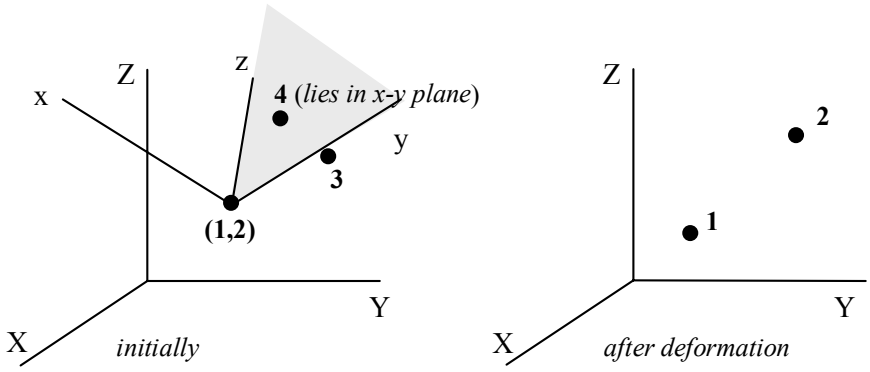

Figure 3.13 3-D Joint Element in ZEUS-NL

The force-displacement characteristics for the axial force (F_x), shear forces (F_y and F_z) and the moments (M_x, M_y and M_z) are determined by the curves included in ZEUS-NL libraries. There are three different curves: elastic linear (LIN), tri-linear symmetrical elasto-plastic (SMTR) and tri-linear asymmetrical elasto-plastic (ASTR). In order to model the pin behavior for the strut members of the case study building, elastic linear curve is employed with very high values for F_x, F_y and F_z relative to M_x, M_y and M_z, thus enabling axial deformations only.

For dynamic analysis, masses in each floor are lumped at the beam column joints. Distributed mass elements are not employed in order to enhance computational efficiency. The mesh configuration and mass distribution of the flat-slab model is shown in Figure 3.14. The small squares show the node locations and the big squares symbolize the lumped masses on the floors.

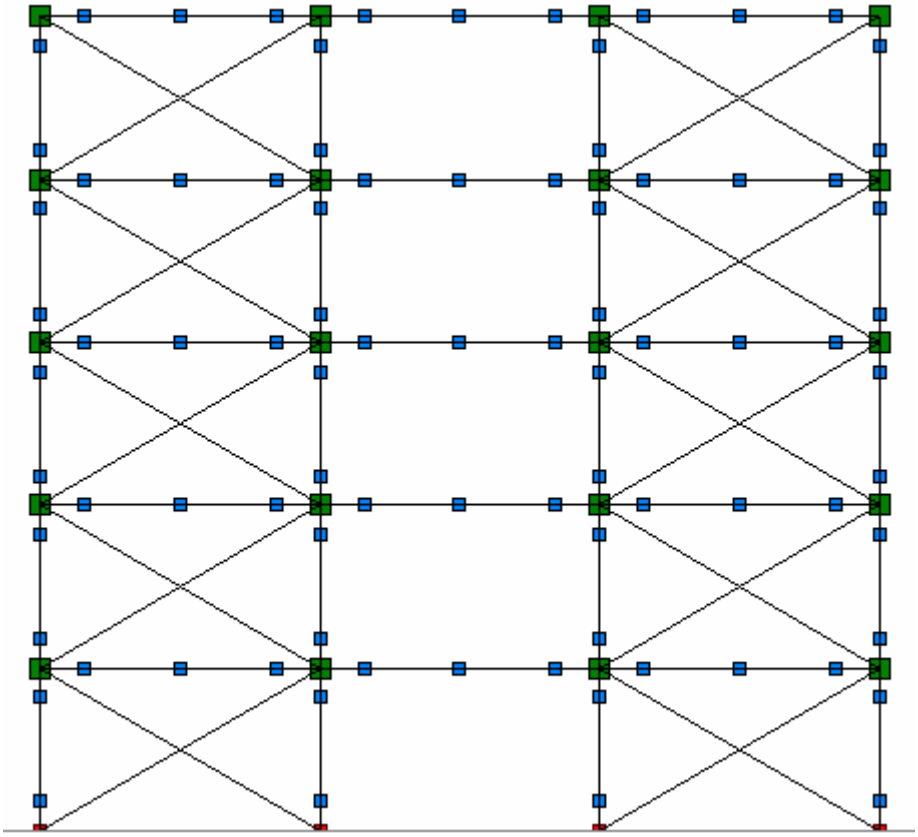

Figure 3.14 Mesh Configuration of the Flat-Slab Model in ZeusNL

3.2.4 Selection of Ground Motion Records

The seismic hazard is the main source of uncertainty in the risk assessment of building structures. It is difficult to determine a single parameter that best characterizes earthquake ground motions. Therefore numerous parameters can be used to relate the ground motions to the level of damage sustained by the structure. The most commonly used parameters are the peak ground acceleration (PGA) and the spectral pseudo-acceleration (S_a). In HAZUS Earthquake Loss Estimation Methodology, spectral displacement (S_d) is the hazard parameter used for constructing the vulnerability curves in the case of structural damage and non-structural damage to drift sensitive components and S_a is the hazard parameter used for constructing the vulnerability curves in the case of non-structural damage to acceleration sensitive components. The effect of magnitude, distance and local soil conditions on the ground motion characteristics

can also be employed in the modeling of uncertainty. The relevance of such factors may be assessed depending on the aims of the conducted research.

Since the current study focuses on the effects of the ground motion variability on the building response, there should be a compromise between the number of ground motions selected and the robustness of the analysis. Bazzuro and Cornell (1994) suggested that five to seven input motions are sufficient for the evaluation of seismic risk. Similarly, in the Uniform Building Code (UBC, 1997), it is suggested that maximum response from time-history analyses with a minimum of three real input motions may be used for design whereas the mean response parameters may be adopted if seven or more motions are used. Finally, Dymiotis et al. (1999) states that three ground motions are sufficient if appropriate choices of records and scaling are made. Taking all of these into consideration, 10 ground motions are selected with a single criterion; the compatibility of the elastic spectra of these ground motions with the code spectrum used in the seismic design of the building as discussed before. The selected ground motions and related characteristics are listed in Table 3.1. The table shows that all the records were taken on soft rock which is consistent with the site class D of the employed code spectra. Three records are from two well-known US earthquakes and the remaining records are from Mediterranean and Middle Eastern countries, where flat-slab construction constitutes a significant portion of the building stock. Magnitudes of the selected ground motion records vary in a range between 5.5 and 7.8, peak ground acceleration (PGA) values between 0.09g and 0.15g, and maximum spectral pseudo-acceleration values ($S_{a,max}$) between 0.302g and 0.454g, respectively. The comparison of the elastic spectra (5% damping) of the ground motion records with the NEHRP spectra (Site Class D) is shown in Figure 3.15. In terms of spectral response, the selected records seem to be in good agreement with the hazard level used in design.

Table 3.1 Characteristics of the Selected Ground Motions

	Location	Comp	Earthquake	Country	Date	M_s	PGA	PGV	$S_{a,max}$
							(g)	(m/s)	(g)
GM1	Buia	NS	Friuli Aftershock	Italy	9/15/1976	6.1	0.109	0.108	0.327
GM2	Boshroyeh	N79E	Tabas	Iran	9/16/1978	7.3	0.102	0.111	0.339
GM3	Cassino Sant'Elia	EW	Lazio Abruzzo	Italy	5/7/1984	5.8	0.114	0.079	0.395
GM4	Gukasian	NS	Spitak	Armenia	12/7/1988	5.8	0.147	0.108	0.395
GM5	Hayward-Muir School	90	Loma Prieta	USA	10/17/1989	7.1	0.139	0.13	0.454
GM6	Tonekabun	EW	Manjil	Iran	6/20/1990	7.3	0.089	0.091	0.302
GM7	L.A.- 15 Story Govt. Off. Bldg.	270	Northridge	USA	1/17/1994	6.7	0.139	0.129	0.362
GM8	El Segundo - 14 Story Off. Bldg.	90	Northridge	USA	1/17/1994	6.7	0.131	0.115	0.362
GM9	Castelmuovo-Assisi	EW	Umbro-Marchigiano	Italy	9/26/1997	5.5	0.110	0.109	0.405
GM10	Yesilkoy Airport	NS	Marmara	Turkey	8/17/1999	7.8	0.089	0.113	0.366

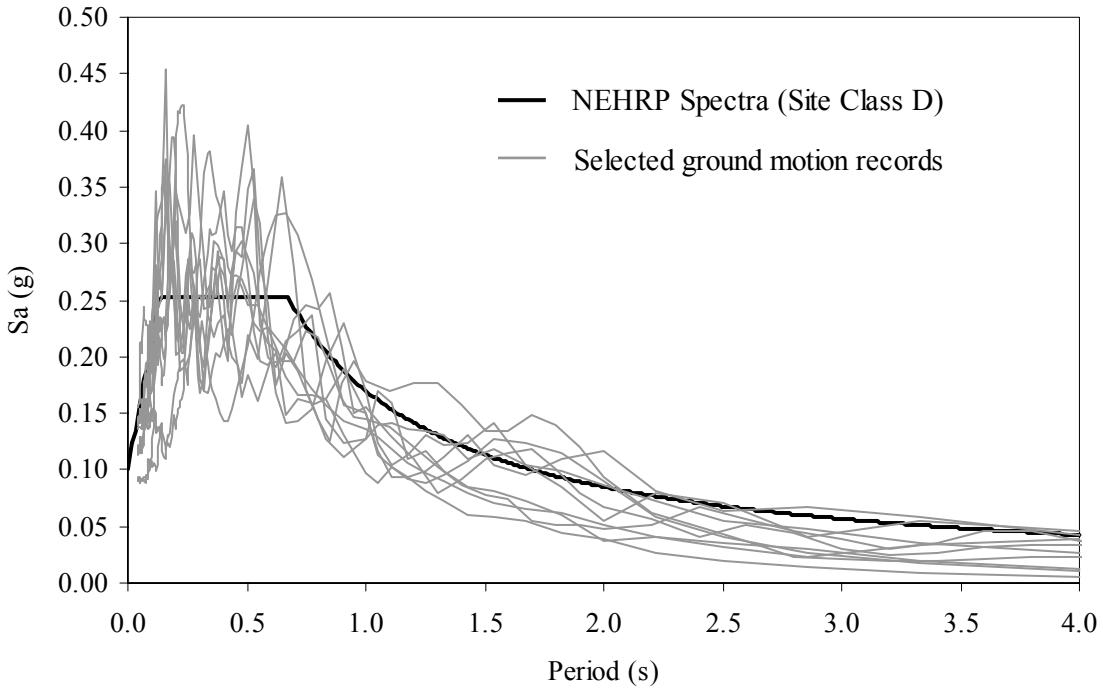

Figure 3.15 Comparison of Elastic Spectra (5% Damping) with the NEHRP Design Spectra

3.2.5 Preliminary Evaluation of Seismic Response

Before conducting nonlinear dynamic analyses to evaluate the seismic vulnerability of the flat-slab structure, it is necessary to assess the preliminary structural behavior through eigenvalue and non-linear static (pushover) analyses. Eigenvalue analysis gives inside to the general characteristics of the building whereas push-over analysis is a powerful tool to observe the capacity and the performance levels of the structure.

Eigenvalue Analysis

Eigenvalue analysis is performed to identify the dynamic characteristics of the system. Knowledge of the structural periods for free undamped vibrations provides a very good insight into the behavior of structures. During inelastic response, the softening of the structure due to yielding results in an increase of these periods, a phenomenon commonly referred to as 'period elongation' (Limniatis, 2001).

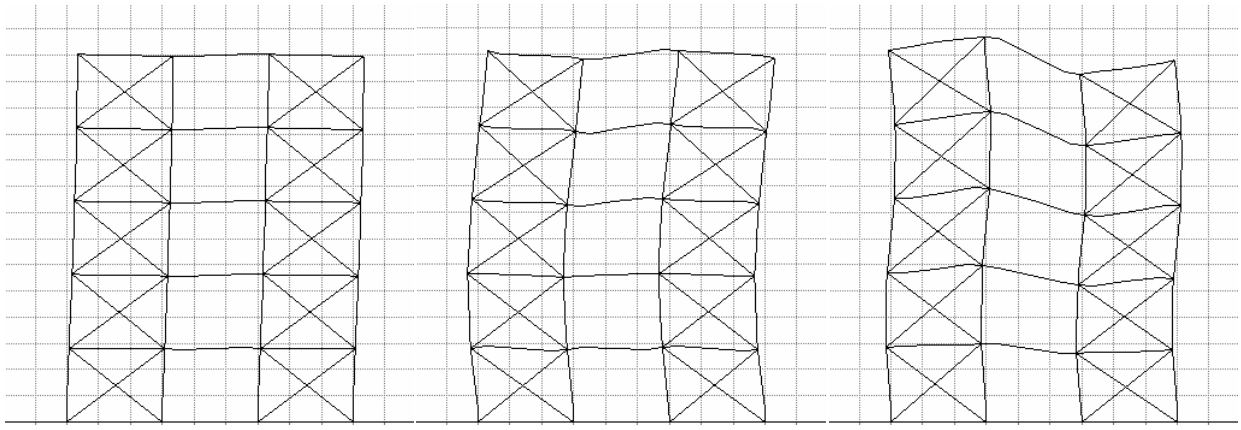

Figure 3.16 Mode Shapes of the 2-D Flat-Slab Model with Infill Panels

The first three natural periods of the structure is obtained as T=0.38, 0.13 and 0.08 seconds, respectively. The periods are significantly affected by the infill panel stiffness. These will fail at low levels of drift, hence the response periods will be elongated as discussed below. The mode

shapes for the first three modes are shown in Figure 3.16. The natural vibration periods seem quite reasonable for mid-rise concrete frames. The eigenvalue analysis is also conducted for the case with no infill walls, i.e. bare frame for the sake of comparison. The first three natural periods of vibration of this structure are 0.98, 0.30 and 0.15 seconds, respectively. The mode shapes of the bare frame are illustrated in Figure 3.17. The fundamental period of the bare flat-slab frame is long for such a 5-story building. The calculated period should typically belong to concrete frames with 9-10 stories. The results also indicate that the flat-slab system is flexible, and the addition of the infill walls produces a significant stiffness increase in the system.

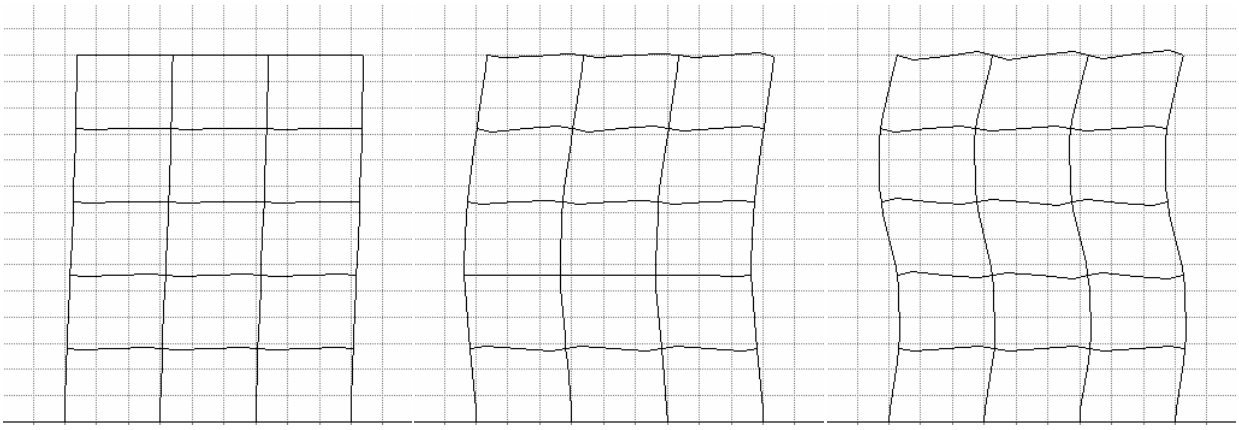

Figure 3.17 Mode Shapes of the 2-D Flat-Slab Model without Infill Panels (Bare Frame)

Pushover Analysis

The static pushover analysis is a relatively simple solution to the complex problem of predicting force and deformation capacity imposed on structures and their elements (Krawinkler, 1996). In other words, the method can be viewed as an analysis process that accounts in an approximate manner for the redistribution of internal forces occurring when the structure is subjected to inertia forces that can no longer be resisted within the elastic range of structural behavior. The method is based on many assumptions that may provide misleading results in some cases. However if the push-over analysis is applied with good judgment, it can provide useful information that cannot be obtained from elastic static or dynamic analysis procedures.

The static pushover analysis is carried out using ZEUS-NL. Three types of control are available in the program: load control, response control and automatic response control. The control scheme of the case study building is composed of two phases: one load control phase and one automatic response control phase. In the first phase, the load factor is directly incremented and the global structural displacements are determined at each load factor level. An inverted triangular distribution is employed for the lateral loading. Force-controlled analysis is chosen in order to identify the structural deficiencies of the frame, such as soft stories. In the second phase, the program automatically chooses a new Degree of Freedom (DOF) whenever convergence difficulties arise during the analysis. The chosen node is the one having the highest rate of nominal tangential response (Elnashai et al., 2002). The main reason of employing automatic control in the second phase is for a better identification of the response in the descending branch of the pushover curve.

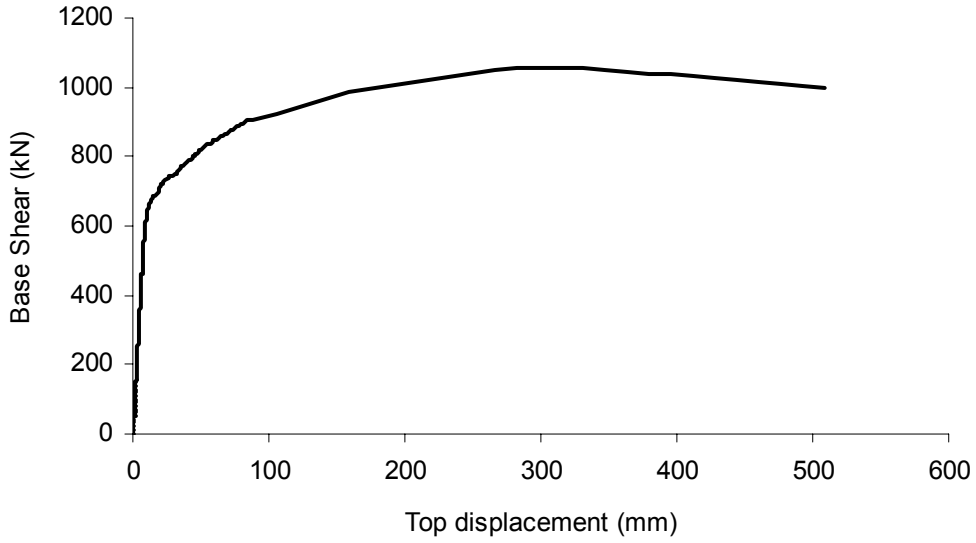

Figure 3.18 Pushover Curve of the Infilled Flat-Slab Frame

The pushover curve of the infilled flat-slab model is shown in Figure 3.18. The frame can sustain a lateral load of 1056 kN (0.25% of the weight of the frame). The deformed shape of the frame at the end of the pushover analysis can be seen in Figure 3.19. The figure reveals that the local

deformation demand in the first three stories is very high. The results indicate a maximum interstory drift ratio of approximately 5% in the first storey. The total drift in the frame at the end of the pushover analysis is 508 mm or 3.63%. The plastic hinge propagation is shown in Figure 3.20. The plastic hinges are concentrated at the first three stories, which is in accordance with the large drifts experienced by the same stories. The first plastic hinges are formed at the beam ends of the first two stories, followed by the ones formed at the first story columns.

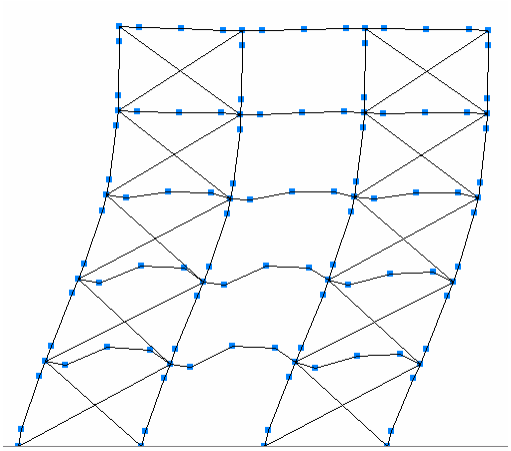

Figure 3.19 Deformed Flat-Slab Model at the End of the Pushover Analysis

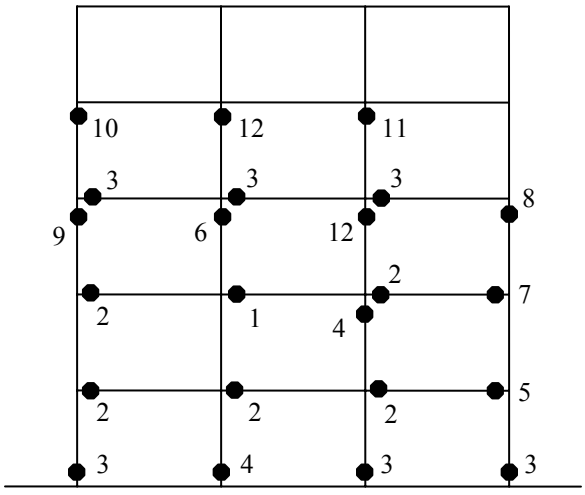

Figure 3.20 Plastic Hinge Formation Sequence of the Flat-Slab Model

3.2.6 Determination of Limit States

Limit states, or in other words the performance levels, play a significant role in the construction of the fragility curves. Well-defined and realistic limit states are of paramount importance since these values have a direct effect on the fragility curve parameters. This is especially true for special systems like flat-slab structures, for which the identification of limit states is highly dependent on the characteristics of the structure. It may be misleading to employ the performance levels defined for regular concrete frames in the case of flat-slab buildings without regarding the inherent flexibility of these structures. Rigorous definitions are required for the limit states of flat-slab buildings.

Separate limit state criteria are appropriate for the assessment of structural response with respect to the global and local levels. For the global level, the most accepted criterion used is the interstory drift. The advantage of this quantity is that it is easy to measure during the analysis and has physical meaning that is well-understood. Interstory drift values for different limit states have also been suggested by seismic codes and guidelines. The relationship between the desired seismic performance and the maximum transient drift ratio for the framed structures recommended by SEAOC (1995) is shown in Table 3.2. The values suggested by FEMA 273 (1997) are given in Table 3.3 for concrete frames and walls.

Table 3.2 Performance Levels and Damage Descriptions Based on Drift (SEAOC, 1995)

Performance level	**Building Damage**	**Transient Drift (%)**
Fully operational	Negligible	ID < 0.2%
Operational	Light	0.2 % < ID < 0.5 %
Life safe	Moderate	0.5 % < ID < 1.5 %
Near collapse	Severe	1.5 % < ID < 2.5 %
Collapse	Complete	2.5 % < ID

Interstory drift ratio is the most commonly used parameter in the literature for the determination of the limit states. Sozen (1981) suggested that an interstory drift of 2% may be set as the

collapse limit for three-quarters of reinforced concrete buildings. At values in excess of this limit, P-δ effects are significant and lead to reduced lateral load resistance causing failure.

Table 3.3 Structural Performance Levels Recommended by FEMA 273 (1996)

Performance Level	**Interstory Drift**	
	Concrete Frames	**Concrete Walls**
Immediate Occupancy	1 % transient, negligible permanent	0.5 % transient, negligible permanent
Life Safety	2 % transient, 1 % permanent	1 % transient, 0.5 % permanent
Collapse Prevention	4 % transient or permanent	2 % transient or permanent

Ghobarah et al. (1998) suggested five damage levels for performance evaluation. An ultimate interstory drift for collapse prevention of 5.6 % has been adopted, whereas a limit of 3% was associated with repairable damage. Dymiotis et al. (1999) derived a statistical distribution for the critical interstory drift using experimental results obtained from the literature. The study utilized data from tests conducted using shaking tables, pseudo-dynamic, monotonic and cyclic loading. It was concluded that the ultimate drift of 3% lies in the lower tail of the statistical distribution. The mean interstory drift values obtained from the distribution were 4.0 and 6.6 for near failure and failure, respectively.

Limniatis (2001) stated that interstory drift ratios of 1% and 3% are commonly suggested for reinforced concrete buildings, corresponding to the attainment of the serviceability and ultimate limit states, respectively. However, there may be some deviations from these values based on the structural system under consideration. According to Limniatis, since flat-slab buildings are known to behave in a more flexible manner to earthquake excitation, it is reasonable to expect increased drift values. Above discussions reveal that the drift values suggested for global limit states show a high scatter, especially for the ultimate or collapse limit state (2-6.6%).

Local criteria are traditionally related with member curvature at yield and ultimate states. Ultimate curvature may either correspond to an ultimate compressive concrete strain or an ultimate tensile strain of the steel fibers. Identification of yield curvature is typically obtained from the first yield of either top or bottom reinforcement in tension for the member under consideration. Other suggested criteria for the attainment of ultimate local failure include buckling of longitudinal reinforcement bars and fracture of confining hoops.

Considering the above discussions it will be appropriate to define the limit states for the case study flat-slab building in global sense, particularly in terms of interstory drift ratio since the behavior and the failure modes of flexible flat-slab structures are governed by deformation. This observation is also verified by Kappos (1991) on the assessment of a flexible 10-story frame structure, as opposed to a similar, but stiff, hybrid structure where local criteria prevailed.

For the determination of performance levels of the flat-slab structure, local limit states of members in an individual story are obtained and mapped on to the story shear vs. story drift curve of that story. Then these performance points are employed to obtain the limit states of the story in terms of interstory drift. This process is repeated for each story and the performance levels of the most critical story are considered as the global limit states of the structure.

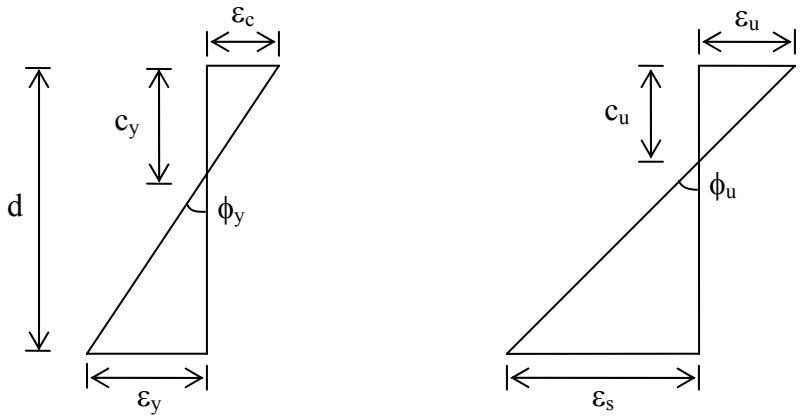

$$\phi_y = \frac{\varepsilon_y}{d - c_y} \qquad \phi_u = \frac{\varepsilon_u}{c_u}$$

Figure 3.21 Strain Diagram at **a)** Yield and **b)** Ultimate Curvature

Local limit states are considered in terms of yield and ultimate curvatures. As discussed above, yield criterion is established at the curvature value when the longitudinal reinforcement starts to yield whereas the ultimate criterion is established at the curvature value when the strain of extreme fiber of concrete reaches its ultimate value, ε_{cu} (Figure 3.21). In the figure, c_y and c_u are the neutral axis depths at yield and ultimate states, respectively. After the local limit states of each member at a specific story are obtained, they are mapped into the story shear vs. drift curve of the same story. This is clearly illustrated in Figure 3.22a for the first story of the flat-slab model considered. In the figure, hollow rectangular marks represent the failure of the diagonal struts used to simulate the infill panels, solid circular marks (gray in color) denote the local yield criterion and hollow triangular marks represent local ultimate criterion. The yield and ultimate limit state occurrences on the structural members of the first story are illustrated on two different sketches (Figure 3.22b and c). Considering the story shear vs. story drift curve, it is observed that the infill panels fail one after the other at a small drift level of 3.5 mm. After the failure of the infill panels, the stiffness is significantly reduced. At a drift level of 25-30 mm, yield limit state is reached at the left end of three beams (Y1) and after that at the bottom end of three first story columns (Y2). Two more yield limit states (Y3, Y4) occur at a drift level of approximately 60 mm, in addition to exceedence of ultimate state in one of the beams (U1). At a drift level of 100 mm, the ultimate limit state is exceeded in three columns (U2). Hence considering this limit state scenario and verifying that the most critical story drifts take place in the first story, the limit states assigned to the flat-slab frame under consideration in terms of interstory drift are shown in Table 3.4.

Table 3.4 Limit States and the Corresponding Interstory Drift Ratios for the Flat-Slab Structure

Limit State	Interstory Drift (mm)	Interstory Drift Ratio (%)
Slight	3.5	0.1
Moderate	28.4	1.0
Extensive	56.1	2.0
Complete	96.9	3.5

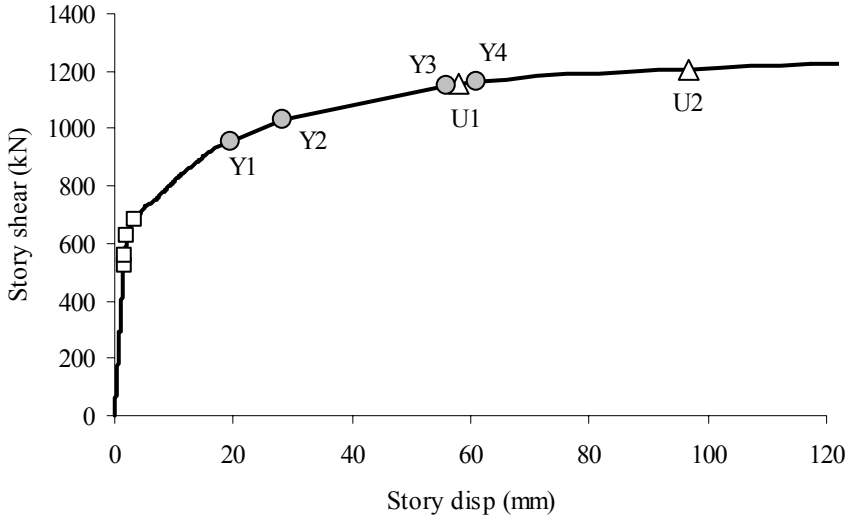

a) Story Shear vs. Story Drift Curve

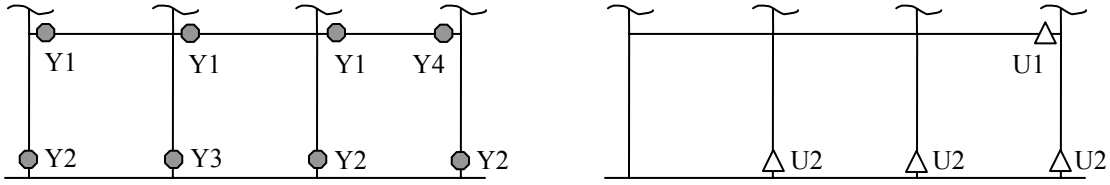

b) Yield Limit State

c) Ultimate Limit State

Figure 3.22 Mapping from Local Limit States to Global Limit States

3.2.7 Material Uncertainty

One of the main sources that control the response uncertainty of a reinforced concrete structure is the inherent variability of material strengths of concrete members. This randomness can be modeled based on the laboratory test data. Generally, the mean and standard deviation are employed to describe the statistical variation of the material properties. Normal or lognormal distributions are commonly used for convenience. In this study, the yield strength of steel and compressive strength of concrete has been chosen as the random variables.

Yield Strength of Steel (f_y)

Variations in the strength of steel have been studied by some researchers in the past. In 1972, Alpsten suggested an extreme value distribution Type I or a lognormal distribution for yield strength of steel. Ellingwood (1977) modeled the variability of the steel yield strength by a lognormal probability distribution. Mirza and MacGregor (1979) reviewed published and unpublished data on the variability of the mechanical properties of reinforcing steel. The data which they gathered were taken from various references (Bannister, 1968; WJE and Associates, 1970; ASTM Task Group, 1972; Allen, 1972) and showed that the coefficient of variation (COV) for the yield strength of reinforcing bars was generally in the order of 1%-4% for individual bar sizes and 4%-7% overall for data derived from one source. When data were taken from many sources, COV increased to 5%-8% for individual sizes and 8%-12% overall. This clearly indicates the significance of selecting samples from different batches and sources. Mirza and McGregor tried to fit normal, lognormal, beta type statistical distributions to the available test data. Normal distribution seemed to correlate well in the range from about the 5^{th} to the 95^{th} percentile (in terms of cumulative frequency function) but differed from the data for low and high probabilities out of this range. Lognormal distribution seemed to be a better fit because of the positive skewness of the data, but it did not show any improvement over normally distributed values at low and high probabilities. On the other hand, beta distribution seemed to correlate well with the entire distribution range of yield strength test data of Grade 40 and Grade 60 reinforcing bars. In their study, the mean values and coefficient of variation for the selected data were found to be 337 MPa and 10.7 % for Grade 40 and 490 MPa and 9.3 % for Grade 60 Bars.

In 1998, Ghobarah et al. stated that the main source of uncertainty in the member capacity comes from the variation between the specified strength and the actual material strength and used a lognormal distribution for the yield strength of steel with a mean value of 473 MPa and COV of 9.3 %. Dymiotis et al. (1999) selected yield strength of steel as one of the random variables in order to assess the seismic reliability of RC frames, with a mean value of f_{yk} + 40 (MPa) and COV of 6 %, where f_{yk} is the characteristic value for yield strength of concrete. In another study to derive deformation-based vulnerability functions of RC bridges, Elnashai et al.(2000) used normal distribution for the yield stress of the reinforcement for B500 steel with an average value of 550 MPa and COV of 5.2%.

Taking all of these into account, a lognormal distribution is assumed for the yield strength of steel in this study. The mean and COV of are taken as 475 MPa and 6 %, respectively. Hence the lognormal mean and standard deviation parameters take the values of 6.161 and 0.06, respectively by employing the following conversion formulae

$$\xi^2 = \ln\left(1 + \frac{\sigma^2}{\mu^2}\right) \tag{3.22}$$

$$\lambda = \ln \mu - \frac{1}{2}\xi^2 \tag{3.23}$$

where μ and σ are the normal distribution mean and standard deviation parameters whereas λ and ξ are the lognormal distribution mean and standard deviation parameters.

Concrete Strength (f_c)

The consensus among the researchers (Julian, 1955; Ang and Cornell, 1974; Ellingwood, 1977; Mirza et al., 1979) is to employ normal distribution to characterize the variability of concrete strength. Mirza et al. suggested that the mean and standard deviation of compressive strength of concrete can be predicted by

$$f_m = 0.675\, f_c^{'} + 1100 \le 1.15\, f_c^{'} \quad (\text{psi}) \tag{3.24}$$

$$V^2 = V_{c,real}^2 + V_{in-situ}^2 + V_R^2 \tag{3.25}$$

where f_c' is the design compressive strength of concrete, $V_{c,real}$ is COV of the concrete strength in the structure with respect to cylinder strength, $V_{in\text{-}situ}$ is COV of the concrete strength in the structure with respect to the in-situ strength and V_R is COV of the concrete strength in the structure due to a variable loading rate. Luo et al (1995) calculated the mean and standard deviation values for 3000 psi (20.69 MPa) concrete by using Equations 3.24 and 3.25 as 3125 psi (21.55 MPa) and 469 psi (3.23 MPa), respectively.

Ghobarah et al. (1998) proposed a normal distribution for the representation of the variability in concrete strength. Based on various studies, they also stated that COV of the concrete compressive strength can be taken as 15% which represents average quality control. Dymiotis et al. (1999) suggested that the mean value of concrete strength may be calculated by f_{ck}+8 (MPa) and COV may be taken as 18%.

Considering above discussions, a normal distribution is employed to represent the variability of concrete strength. For a characteristic concrete strength value of 30 MPa, the mean value is calculated as 35.8 MPa and COV is taken as 15%.

3.2.7.1 Sampling Methods

One of the most important issues for the assessment of structural reliability is the generation of the random variable values, or so called the sampling methods. Many methods have been proposed in the literature and among these; Monte Carlo Method has been the most popular simulation method for estimation of structural reliability. Although this method is a powerful tool, it has the disadvantage of considering a very large sample size in order to achieve the required accuracy. This may not be feasible since it will require a very large computational expense in most of the cases. Therefore some alternative approaches have been developed in order to reduce the sample size. One such method, developed by McKay et al. (1979) is the Latin Hypercube Sampling Method. This is a technique that provides a constrained sampling scheme instead of random sampling according to the direct Monte Carlo Method. This method has been applied to many computer simulations (Iman et al., 1981.a and b; Iman and Conover, 1982; Ayyub and Lai, 1989; Wyss and Jorgensen, 1998).

Basics of Latin Hypercube Sampling Method

Latin Hypercube Sampling selects n different values from each k random variables $X_1,\ldots..,X_k$ in the following manner: The range of each variable is divided into n non-overlapping intervals on the basis of equal probability of occurrence (hence the area of each interval under the density function should be equal to the probability value of P(X)=1/n). This is illustrated in Figure 3.23

in the case of a normal distribution and for a sample size of n=5. Since n=5, the probability density function should be divided into five portions of equal probability P(X)=0.20 (Figure 3.23.b). These interval limits can easily be determined from the cumulative distribution function (Figure 3.23.a).

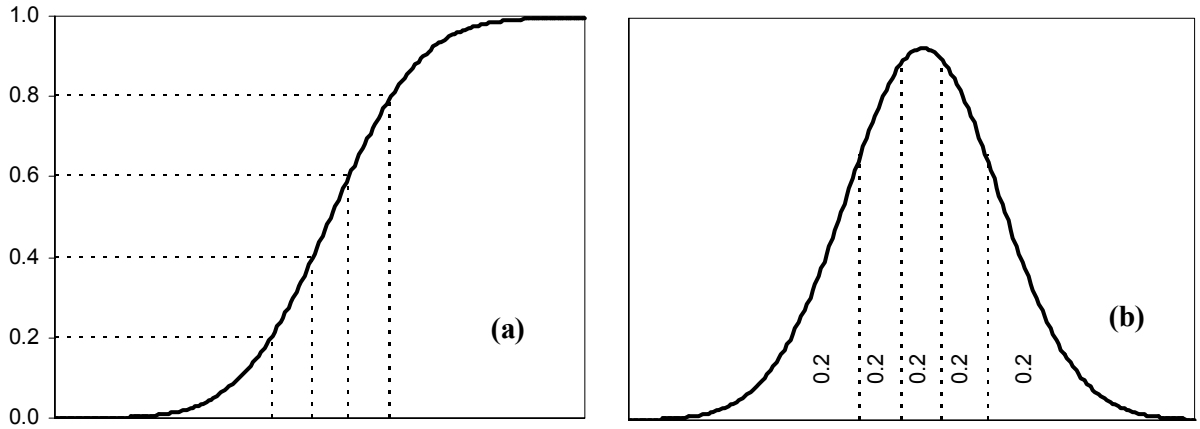

Figure 3.23 a) Cumulative Distribution, **b)** Density Function Divided into 5 Intervals of Equal Probability.

Then n different values (between 0 and 1) in n non-overlapping intervals are randomly selected for each random variable, i.e. one value per interval is generated. Next step is to convert these random variables into cumulative probabilities for each of the n intervals by linear transformation.

$$P_m = \left(\frac{1}{n}\right) U_m + \left(\frac{m-1}{n}\right) \qquad \textbf{(3.26)}$$

In this formulation, m is an integer counter between 1 and n corresponding to the interval numbers, U_m is the random number generated between 0 and 1 and P_m is the cumulative probability value for the m^{th} interval obtained from the randomly generated number. Equation 3.26 shows that only one generated value falls into each of the n intervals since

$$\left(\frac{m-1}{n}\right) < P_m < \frac{m}{n} \qquad \textbf{(3.27)}$$

It should also be noted that (m-1)/n and m/n are the lower and the upper bound for the m^{th} interval, respectively.

After the random values (P_m's) are obtained for each interval, these values are used with the inverse distribution function to produce the specific values to be employed in the final Latin Hypercube Sample.

$$X_{k,m} = F_X^{-1}(P_m) \qquad \textbf{(3.28)}$$

In this formulation, $X_{k,m}$ is the m^{th} value generated for the k^{th} random variable and F_x^{-1} is the inverse cumulative distribution function of that specific random variable.

Finally, the values generated for each random variable are paired together. To achieve this, random permutation of n numbers corresponding to n generated values is used for each variable. Then grouping is accomplished by associating those different random permutations. For illustration, consider two random variables X_1 and X_2 with a sample size of 5. Hence the random permutation sets for these variables are as follows:

Permutation Set No.1 (3, 1, 5, 2, 4)
Permutation Set No.2 (2, 4, 1, 3, 5)

By using the respective positions within these permutation sets as interval numbers for X_1 (Set 1) and X_2 (Set 2), the pairing of intervals presented in Table 3.5 may be formed.

Thus on computer run number 1, the input vector is formed by selecting the generated value of X_1 from the interval number 3 and pairing this value with the specific value of X_2 selected from the interval number 2. The vectors for the other four runs are constructed in the same order.

Table 3.5 Pairing of the Generated Values of X_1 and X_2 Based on Interval Numbers

Computer Run No	Interval No. for X_1	Interval No. for X_2
1	3	2
2	1	4
3	5	1
4	2	3
5	4	5

3.2.7.2 Treatment of Material Uncertainty in This Study

In this study, two random variables were selected to model the material variability: yield strength of steel reinforcement, f_y, and compressive strength of concrete, f_c. The variability in the yield strength of steel reinforcement in beams and columns are treated separately. The two random variables are denoted as $f_{y,b}$ and $f_{y,c}$, respectively. A lognormal distribution is assumed for steel reinforcement with a mean of 475 MPa and and a COV of 6 % (Figure 3.24.a). Similarly, a normal distribution is assumed for the concrete strength. The mean is 35.8 MPa and the COV is 15% (Figure 3.24.b).

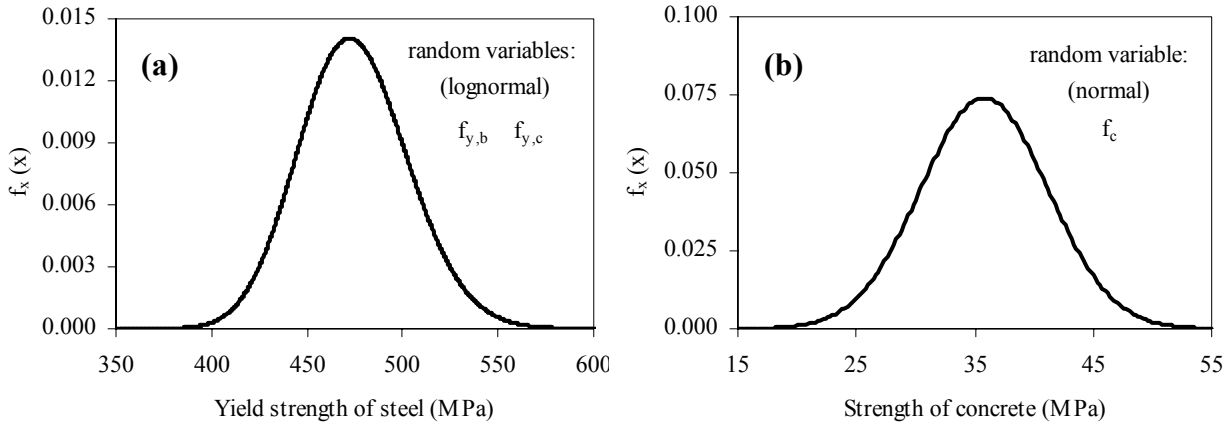

Figure 3.24 Probability Density Function for **a)** Yield Strength of Steel, **b)** Strength of Concrete.

The next issue is to determine the sample size in order to quantify the material uncertainty. The sample size is extremely important in terms of computational expense since making a small increase in the sample size can add a huge number of dynamic analyses. Elnashai et al (2000) used a sample size of both 30 and 40 to model the variability of f_y and f_c, the random variables in their study to obtain the deformation based vulnerability functions for RC bridges. This study showed that the average and the standard deviation values of these two sets were very close to each other, or in other words, they were insensitive to the sample size. In the same manner, a sample size of 30 is assumed for each random variable (f_c, $f_{y,b}$ and $f_{y,c}$) which is used to define the material uncertainty in this study.

For each dynamic run, a set of values corresponding to random variables is required for input. The grouping of these values is determined by using the Latin Hypercube Sampling Method. Again, 30 random numbers between 0 and 1 are generated for each variable. Then each distribution is divided into 30 parts of equal probability and one sample taken from each interval by using Equation 3.26 with n=30. Next, the inverse functions of the corresponding cumulative distributions (lognormal for $f_{y,b}$ and $f_{y,c}$ and normal for f_c) are used to obtain the generated values of the random variables. Grouping of each random variable is performed by associating a random permutation of the 30 samples.

Table 3.6 presents the numerical implementation of the above procedure for the random variable f_c, concrete strength. The first column represents the interval number (also the sample size). The second column shows the 30 random numbers generated between 0 and 1. The third column gives the cumulative probability values for each interval obtained by employing Equation 3.26. The values in the fourth column are obtained by using the inverse normal cumulative distribution function for the values obtained in the third column. The last column ranks of each sample obtained by random permutation. This process is repeated for the other two variables (for which the values are not shown in this report) and the final set of input variables are obtained by matching the ranks (i.e. the values ranked no.1 are matched, the values ranked no.2 are matched until all the values are ranked and matched). Table 3.7 shows the ranked values. Each row in this table represents a set of input variables for a dynamic analysis which should be repeated for each

Table 3.6 Generating Samples for the Random Variable f_c

Interval number	Random numbers generated btw. 0 and 1	Values obtained by Equation 5	Values obtained by inverse CDF	Rank by rand. perm.
1	0.667	0.022	25.005	18
2	0.029	0.034	26.021	25
3	0.750	0.092	28.656	2
4	0.520	0.117	29.417	15
5	0.997	0.167	30.604	19
6	0.368	0.179	30.862	9
7	0.099	0.203	31.344	21
8	0.920	0.264	32.411	24
9	0.596	0.287	32.773	20
10	0.347	0.312	33.162	23
11	0.482	0.349	33.722	16
12	0.946	0.398	34.415	10
13	0.130	0.404	34.499	13
14	0.295	0.443	35.033	30
15	0.399	0.480	35.530	4
16	0.360	0.512	35.961	27
17	0.025	0.534	36.261	1
18	0.278	0.576	36.829	29
19	0.578	0.619	37.430	22
20	0.602	0.653	37.918	5
21	0.103	0.670	38.164	8
22	0.392	0.713	38.820	26
23	0.814	0.760	39.601	6
24	0.713	0.790	40.139	17
25	0.504	0.817	40.651	3
26	0.654	0.855	41.486	14
27	0.751	0.892	42.435	12
28	0.855	0.928	43.665	7
29	0.841	0.961	45.287	28
30	0.486	0.983	47.169	11

Table 3.7 Input Variables that Characterize the Material Variability in this Study

	f_c (Mpa)	$f_{y,b}$ (MPa)	$f_{y,c}$ (MPa)
1	36.261	508.749	462.132
2	28.656	468.045	452.461
3	40.651	444.097	460.928
4	35.530	480.063	473.853
5	37.918	505.134	491.337
6	39.601	421.481	458.102
7	43.665	481.744	499.861
8	38.164	457.339	478.300
9	30.862	498.705	465.854
10	34.415	464.414	487.329
11	47.169	490.016	474.434
12	42.435	461.128	468.784
13	34.499	451.368	484.062
14	41.486	435.662	481.121
15	29.417	439.656	498.398
16	33.722	485.895	519.568
17	40.139	450.282	470.075
18	25.005	469.428	509.851
19	30.604	426.740	434.525
20	32.773	488.061	551.975
21	31.344	456.307	450.232
22	37.430	520.268	445.022
23	33.162	517.502	505.151
24	32.411	472.860	492.751
25	26.021	464.272	427.977
26	38.820	551.175	415.895
27	35.961	495.899	515.650
28	45.287	474.031	442.222
29	36.829	494.513	455.912
30	35.033	478.144	481.937
MAX	**47.169**	**551.175**	**551.975**
MIN	**25.005**	**421.481**	**415.895**

ground motion record and intensity of that record. The table altogether constitutes the material variability used to derive the fragility curves of flat-slab structures in this study.

3.2.8 Seismic Analysis

In this study, nonlinear time-history analysis is employed to evaluate the seismic response of the flat-slab structure and to derive the fragility curves. While this method is the most tedious way, it is the most accurate way of assessing the vulnerability of structures.

Since the case study structure is complicated and it is composed of many beam, column and strut elements, the computation time becomes a serious issue. Hence the number of the time-history analysis to be performed plays a significant role in the feasibility of the fragility analysis. In the current analyses, thousands of time-history runs have to be performed to derive a set of fragility curves, which becomes very time consuming to do one by one. At this point, an important feature of the ZEUS-NL software, Z-BEER (Elnashai et al, 2002), is used. In this utility, hundreds of dynamic analyses can be made while automatically filtering and extracting the required response parameters from the gigabytes of output data.

Elastic spectral displacement (S_d) is employed as the hazard parameter for constructing the vulnerability curves of the flat-slab structure. For this purpose, the displacement spectra of the selected ground motions are constructed as observed in Figure 3.25. The vertical dotted line in the figure denotes the elastic period belonging to the flat-slab structure under consideration. The scaling procedure is based on the S_d values at this specific period. On the average, the S_d value corresponding to this period is approximately 10 mm. After conducting dynamic analysis, it is observed that the interstory drift values are in the range of 0.14%-0.22% when S_d is equal to 10 mm. This corresponds to none to slight damage in terms of the limit states determined for the case study building. The values of S_d decided to be included in the vulnerability analysis are shown in Table 3.8:

Table 3.8 Spectral Displacement Values Used for Defining the Intensity of the Ground Motion

Intensity	1	2	3	4	5	6	7	8	9	10	11
Sd (mm)	2.5	5	10	20	30	35	40	50	60	70	80

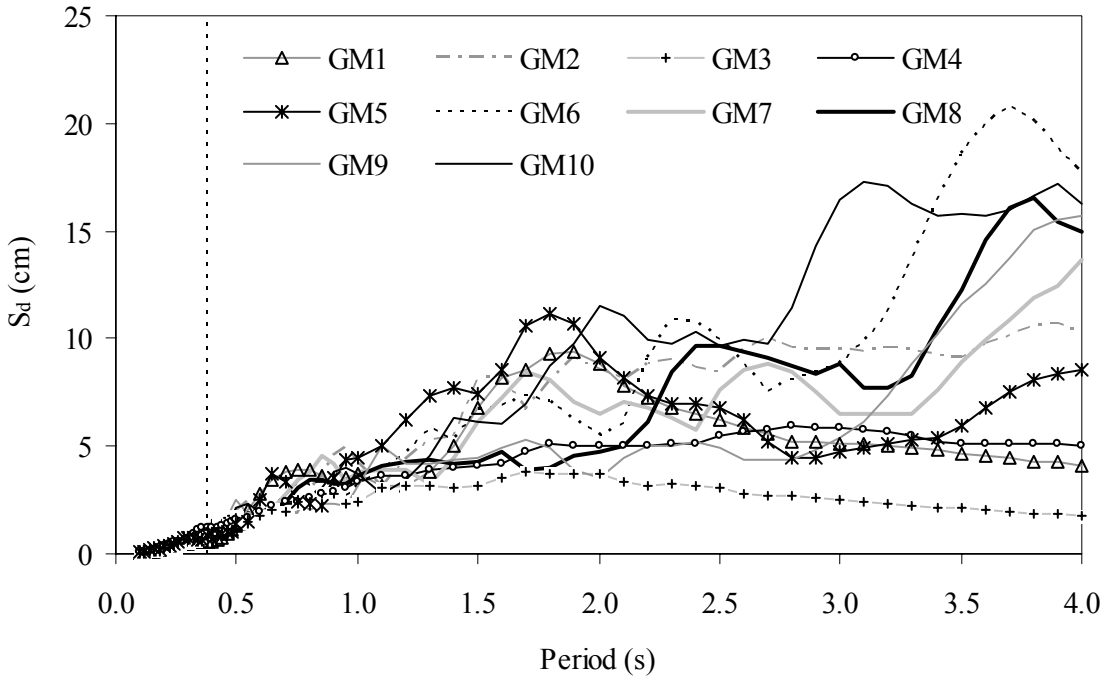

Figure 3.25 Displacement Spectra (ξ=5%) of the Selected Ground Motions

The amplification factors are calculated by dividing the spectral displacement by the spectral displacement of the original ground motion record. Then these amplification factors are used in the input section of the structural analysis program in order to scale the ground motion. Dynamic analyses are conducted by subjecting the flat-slab structure to the ground motion records given in Table 3.1 at each of the above intensity levels (employing the corresponding amplification factor).

3.2.9 Construction of the Fragility Curves

After the completion of the 3300 nonlinear time-history analyses, a huge amount of response data is accumulated. The response statistics are assessed in terms of interstory drift. Damage vs. motion relationship of the flat-slab structure is given in Figure 3.26. The y-axis represents the interstory drift in mm and the x-axis represents the spectral displacement in mm. Each vertical line of scattered data corresponds to an intensity level. There exists 330 data points (corresponding to each of the ground motion record for each material simulation) at each intensity level. It is observed that the maximum interstory drift values increase as the ground motion intensity increases. The horizontal lines in the figure represent the limit states considered in this study in terms of interstory drift. From bottom to top, these are the limits for Slight, Moderate, Extensive and Complete damage, respectively. The drift values of the limit states can be obtained from Table 3.4.

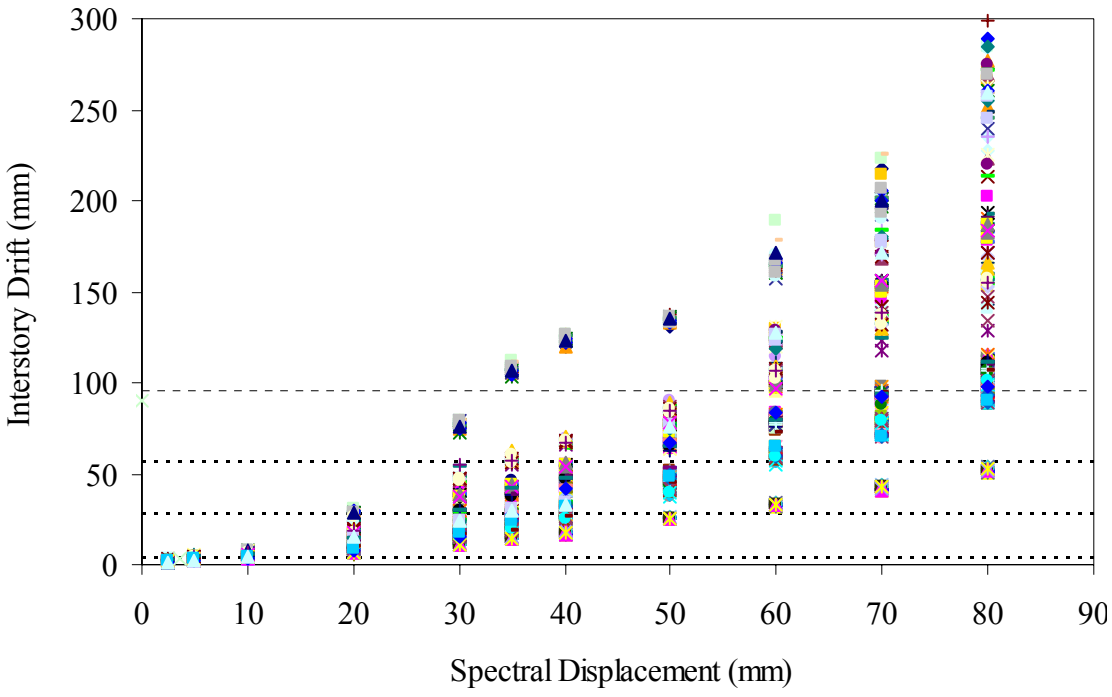

Figure 3.26 Damage vs. Motion Relationship for the Flat-Slab Structure

Table 3.9 Statistical Normal and Lognormal Distribution Parameters for Each Intensity Level

Dist.	Spectral Displacement (mm)										
Param.	2.5	5	10	20	30	35	40	50	60	70	80
μ	1.863	3.144	5.026	13.650	29.347	38.277	46.896	66.637	88.826	113.982	145.513
σ	0.509	0.713	1.218	6.600	19.251	25.927	29.202	28.794	35.784	48.687	78.201
λ	0.586	1.121	1.586	2.509	3.200	3.456	3.684	4.114	4.411	4.652	4.853
ξ	0.268	0.224	0.239	0.458	0.598	0.614	0.572	0.414	0.388	0.409	0.504

A statistical distribution is fitted to the data in each intensity level (on each vertical line). The normal and lognormal parameters (mean and standard deviation) are calculated for each of these S_d intensity levels (Table 3.9). In the table, μ and σ are the mean and the standard deviation of the normal distribution; λ and ξ are the mean and standard deviation of the lognormal distribution.

At each intensity level (for each statistical distribution), the probability of exceeding each limit state is calculated. For illustration purposes, the statistical distribution for S_d=30 mm and 60 mm are shown in Figure 3.27. LS1, LS2, LS3 and LS4 represent the limit states for Slight, Moderate, Extensive and Complete Damage, respectively. The lognormal mean and standard deviation values are also given in the figure. The probability of exceedence of a certain limit state is obtained by calculating the area of the lognormal distribution over the horizontal line of that limit state. Hence, the following values are obtained for S_d=30mm and 60mm:

For S_d=30 mm,

P (S_d > LS1) = 0.999

P (S_d > LS2) = 0.404

P (S_d > LS3) = 0.083

P (S_d > LS4) = 0.011

For S_d=60 mm,

P (S_d > LS1) = 1.000

P (S_d > LS2) = 0.997

P (S_d > LS3) = 0.839

P (S_d > LS4) = 0.338

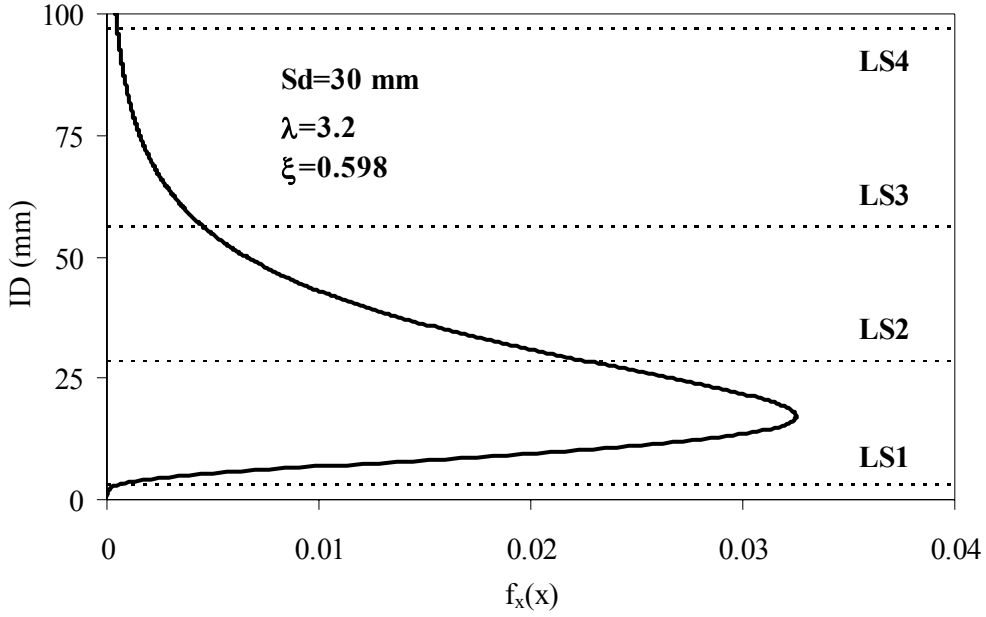

a) S_d=25 mm

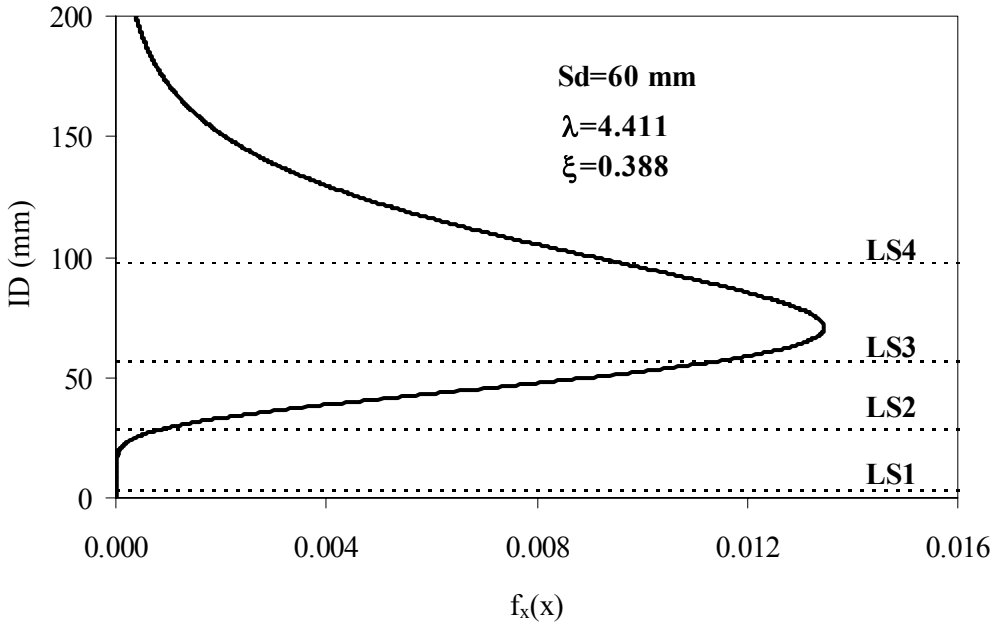

b) S_d=50 mm

Figure 3.27 Lognormal Statistical Distributions for Two Different Levels of Seismic Intensity

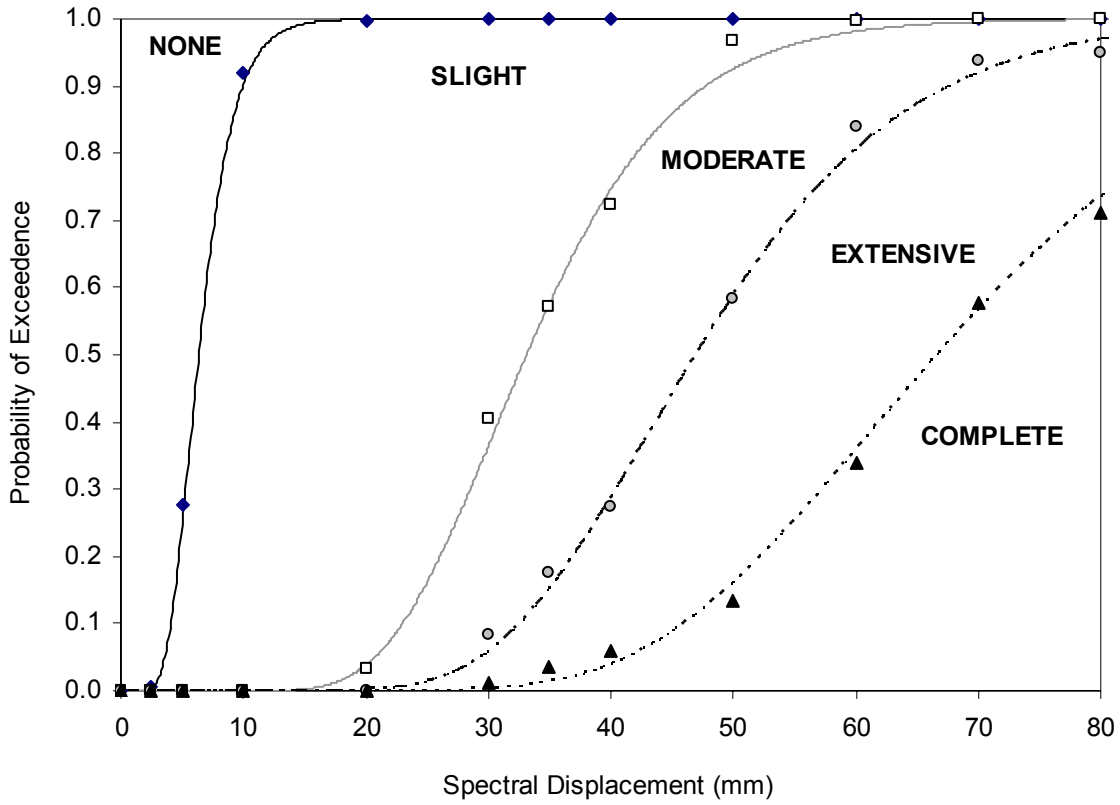

Figure 3.28 Vulnerability Curves for the Flat-Slab Structure

After calculating the probability of exceedence of the limit states for each intensity level, the vulnerability graph can be constructed by plotting this data vs. spectral displacement (scatter data in Figure 3.28). As the final step, a statistical distribution can be fitted to these data points, to obtain the vulnerability curves. In this study, a lognormal fit is assumed for the vulnerability data. The mean and standard deviation parameters of the curves are given as follows:

LS1 (None to Slight Damage):	$\mu = 6.76,$	$\sigma = 2.44$
LS2 (Slight to Moderate Damage):	$\mu = 34.49,$	$\sigma = 10.03$
LS3 (Moderate to Extensive Damage):	$\mu = 48.94,$	$\sigma = 14.24$
LS4 (Extensive to Complete Damage):	$\mu = 69.55,$	$\sigma = 20.60$

Finally, Figure 3.28 represents the fragility curves of the flat-slab structure. The curves get flatter as the limit state shifts from slight to complete. This is due to the nature of the statistical distribution of the response data. The variability of the interstory drift at high ground motion intensity levels is much more pronounced relative to the variability at low intensity levels. Hence small variations in low intensity cause significant differences in the limit state exceedence probabilities. This indicates the high sensitivity of the structure to changes in seismic demand. The steep shape of the slight limit state curve is due to the flexibility of the flat-slab structures and infill panel stiffness and strength.

3.2.10 Comparison of Flat-Slab Structures with Framed Structures

The fragility curves of flat-slab structures are unique since they have not been developed before by any researcher. Therefore, it is not possible to verify these curves by comparing them with the ones from other studies. Instead an indirect approach is employed for this verification. Accordingly, the mean fragility curves of a very similar framed structure is developed using the same methodology. Then the developed fragility curves are compared with the existing fragility curves of framed structures.

In order to develop the mean fragility curves for the framed structure, modifications are made in the previous analytical model. The slab-beams are replaced by conventional beams of size 30 cm x 60 cm in size and a longitudinal reinforcement ratio ρ around 1.5%. The columns and the infill walls are kept the same as the original flat-slab model. There are two reasons for developing the mean fragility curves only: The first reason is based on the observation that the variability in ground motion is much more pronounced than the material variability while conducting the fragility study of flat-slab structures. Therefore mean response statistics will not be very misleading when compared to the results obtained by considering the material variability. The second reason is that the consideration of the material variability increases the number of simulations significantly. It is not feasible to make another 3300 time-history analyses for comparison purposes only. Therefore, the fragility analysis of the framed structure is conducted with the mean values of random variables, the yield strength of steel (f_y=475 MPa) and the

compressive strength of concrete (f_c=35.8 MPa) and 130 simulations are sufficient to complete the analysis with these values. The mean fragility curves derived for framed structures are shown in Figure 3.29 along with the fragility curves previously obtained flat-slab structures. It is clear that the flat-slab structure is more vulnerable to seismic hazard and will sustain more damage than the typical framed structure developed for this study throughout the entire range of its seismic response. This is an expected outcome due to the inherent flexibility of flat-slab structures under seismic action.

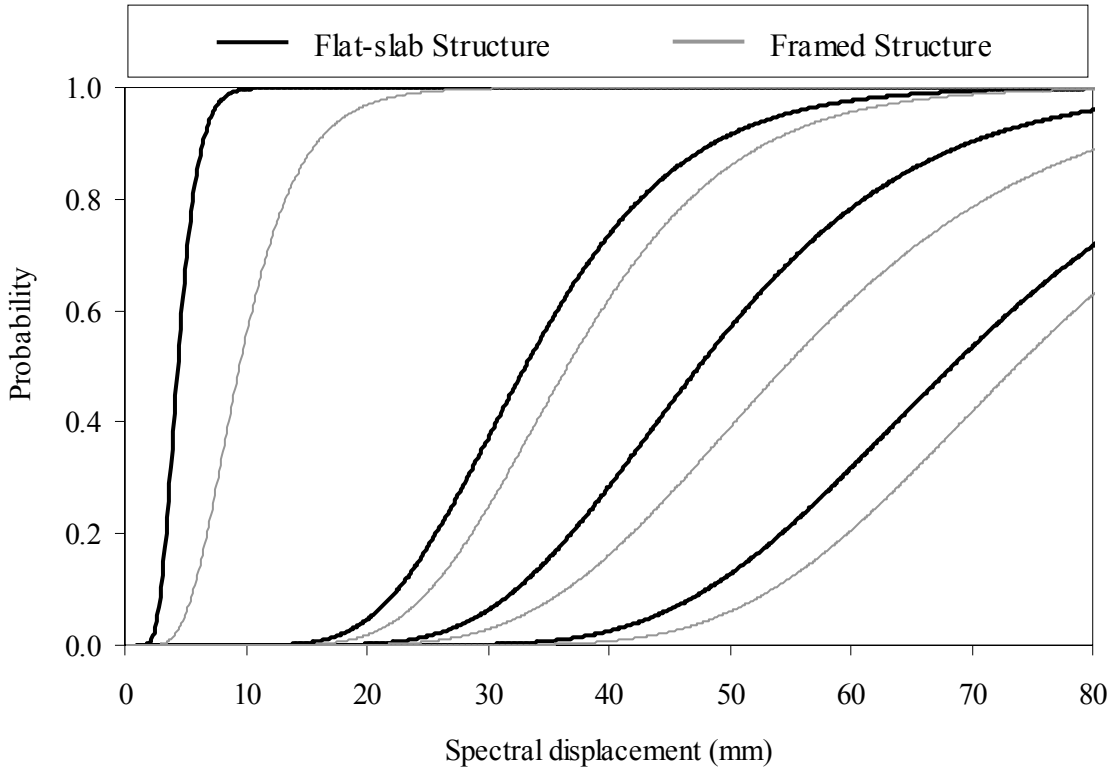

Figure 3.29 Comparison of Fragility Curves for Flat-slab and Framed Structures

It is also interesting to observe that the difference between the flat-slab structure and the framed structure is much more pronounced at the lower limit states. This is mainly due to the reason explained previously. Small variations at low levels of seismic intensity can create amplified effects on the fragility curves whereas even large variations at high levels of seismic intensity

may not be that much reflected on the curves. The analysis results indicate that the difference in story drift values between two types of structures is small for low intensity levels and gets larger as the seismic intensity level increases. However, an opposite trend is observed for the fragility curves.

Next, the fragility curves derived for framed structures are compared with the curves from the literature. However this cannot be accomplished with the current form of these curves, i.e. it is not possible to find fragility curves where spectral displacement at the fundamental period is used as the hazard parameter. Therefore the fragility curves for framed structures are reconstructed after employing spectral acceleration instead of spectral displacement. This is accomplished by a simple conversion of the spectral values and then matching the converted values with the corresponding response (interstory drift) values. The spectral acceleration based fragility curves are shown in Figure 3.30.

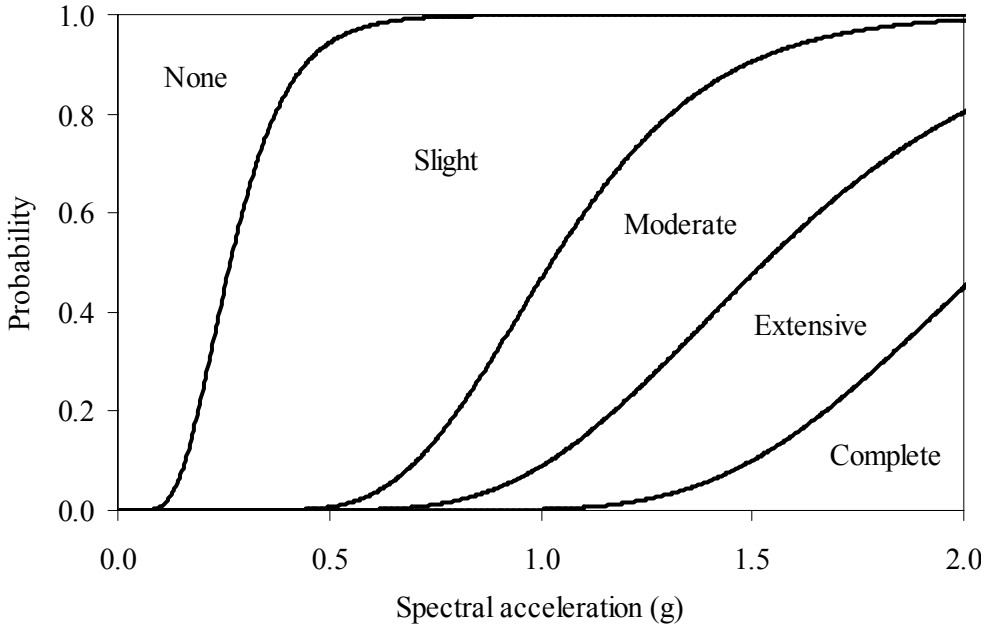

Figure 3.30 Acceleration-based Fragility Curves for the Framed Structure

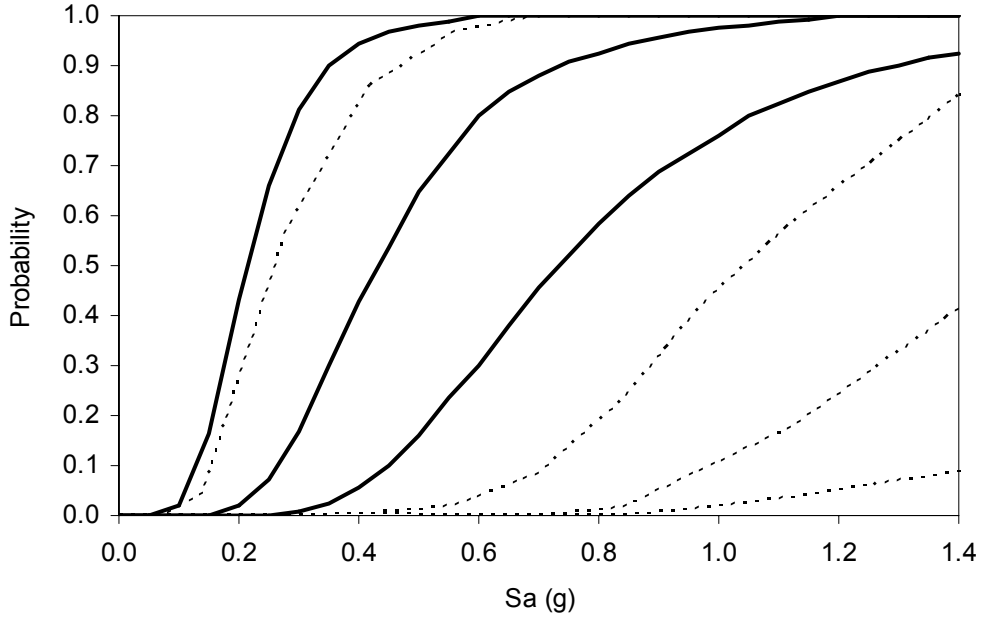

Figure 3.31 The Comparison of the Study Curves (dotted) with the Curves Developed by Hwang and Huo (solid)

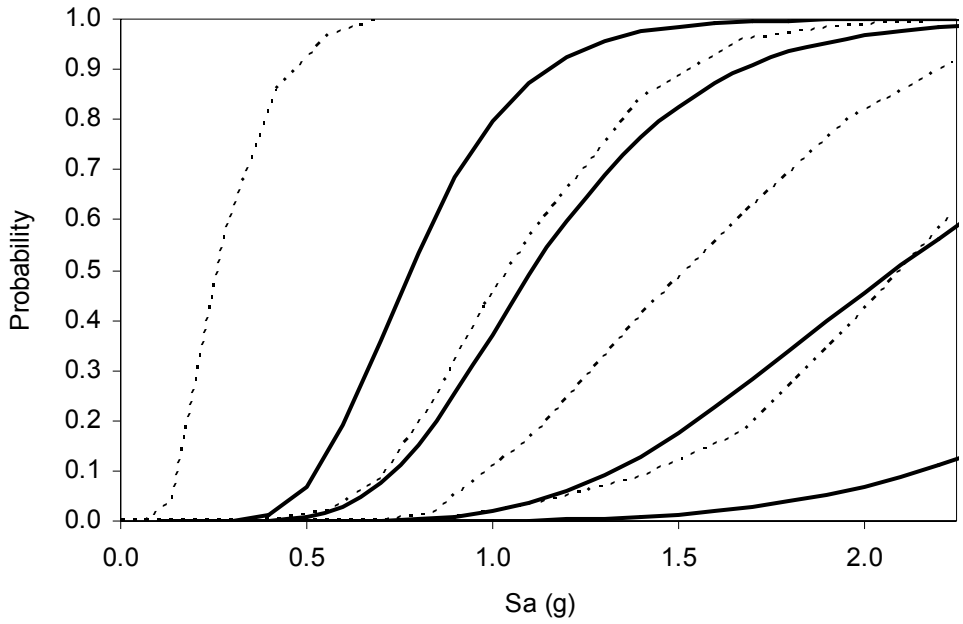

Figure 3.32 The Comparison of the Study Curves (dotted) with the Curves Developed by Singhal and Kremidjian (solid)

The next two figures, Figures 3.31 and 3.32, show the comparison of the curves obtained for framed structures with the ones present in the literature. These curves belong to Hwang & Huo (1997) and Singhal and Kremidjian (1997), respectively and they were presented before (Figure 2.1 and 2.3) for demonstration purposes. For simplicity, let us call these curves as HH curves and SK curves, respectively. It is observed that the study curves have a better match with SK curves than with HH curves. The study curves seem to sustain more damage in the case of SK curves whereas the opposite is true when compared with the HH curves. Table 3.10 gives a comparison about the fragility curve characteristics of these different studies. As seen, ground motion selection is quite different. There are also some differences in the characterization of the hazard and damage parameters. Quantification of the limit states for SK and HH curves is given in Section 2.2 whereas the values defined for this study are given in Table 3.4. It should be kept in mind that the quantification of the limit states significantly affects the development of the fragility curves.

Table 3.10 Fragility Curve Characteristics

	Derived Curves	**SK Curves**	**HH Curves**
Structure	RC Frame	RC Frame	RC Frame
Ground Motion	Actual, From various earthquakes	Synthetic (for West US region)	Synthetic (Memphis-close to NMSZ)
Analysis	Time-history	Time-history	Time-history
Random Variables	f_c, f_y	f_c, f_y	f_c, f_y
Damage Parameter	Interstory Drift	Park & Ang Index	Interstory Drift
Hazard Parameter	$S_d(T_1)$	$S_a(T_1)$	$S_a(T_1)$ and PGA
Limit States	4	4	3

The observed discrepancy between the curves cannot be prevented since there is no consensus about the derivation of fragility curves and every researcher uses a unique methodology to develop these curves. In other words, the resulting curves are strongly dependent on the choices made for the analysis method, structural idealization, characterization of seismic hazard and employed damage parameters. These choices have been seen to cause significant discrepancies

in the vulnerability predictions by different researchers for the same location, even in the cases where the same structure and seismicity are considered (Priestley, 1998). Hence it can be concluded that although differences exist, the fragility curves derived for the flat-slab structure are more or less in the same range with the ones available in the literature, and difference are justifiable on grounds structural response characteristics.

The next step is to implement the fragility curves of the flat-slab structure into HAZUS and to employ them in earthquake loss estimation analyses. HAZUS-compatible fragility curves for flat-slab structure are investigated in detail in the second part of the report. The resulting fragility curves seem to be in agreement with the built-in HAZUS fragility curves of similar reinforced concrete structural forms.

PART II

LOSS ESTIMATION ANALYSIS OF FLAT-SLAB STRUCTURES

4. HAZUS EARTHQUAKE LOSS ESTIMATION METHODOLOGY

For the purpose of mitigating short term consequences, social and economic impacts from earthquakes, The Federal Emergency Management Agency (FEMA), together with the National Institute of Building Sciences (NIBS) has developed HAZUS (stands for "Hazards U.S."), a standard, nationally-applicable methodology for assessing earthquake risk. HAZUS was first released in 1997, followed by three subsequent releases. The latest version is tentatively scheduled to be released in the summer of 2003. With each new edition, significant enhancements have been added to increase the capabilities of HAZUS.

HAZUS operates on a Pentium class personal computer with Windows 98, 2000 or NT installed on it. It further requires additional user investment for a Geographic Information System (GIS) software. HAZUS works on two different GIS platforms: ArcView and MapInfo.

The discussion related with the pros and cons of the HAZUS methodology in this report refer to the Service Release 2 (SR2) version of HAZUS99 Software. There can be some changes and enhancements in future releases, related with the stated features and limitations of the methodology. However, these are beyond the scope of this report.

4.1 Features of HAZUS Methodology

HAZUS methodology deals with nearly all aspects of the built environment and a wide range of different types of losses. It can be utilized at multiple levels of resolution to accommodate not only budget constraints, but also varying levels of user expertise. In other words, the methodology permits estimates to be made at several levels of sophistication, based on the level of data input into the analysis. The better and more complete the inventory information, the more meaningful the results.

A nationally applicable scheme is developed for the methodology, which includes standard methods for inventory data collection based on census tract areas; using database maps of soil

types; ground motion and ground failure; classifying occupancy of buildings and facilitie; classifying building structure type; describing damage states; developing building damage functions; grouping; ranking and analyzing lifelines; using technical terminology and providing output.

HAZUS software uses GIS technologies for displaying and manipulating inventory, and allows losses and consequences to be portrayed on both spreadsheets and maps. The GIS technology provides a powerful tool for displaying the outputs and enables the visualization of the results of different earthquake scenarios.

The framework of the methodology includes each of the components shown in Figure 4.1: Potential Earthquake Science Hazard (PESH); Inventory, Direct Physical Damage; Induced Physical Damage; Direct Economic/Social Loss and Indirect Economic Loss. Modules are independent with the output of some modules acting as input to others. In general, each of the components are required for loss estimation. However the degree of sophistication and associated costs vary greatly with the user and the application.

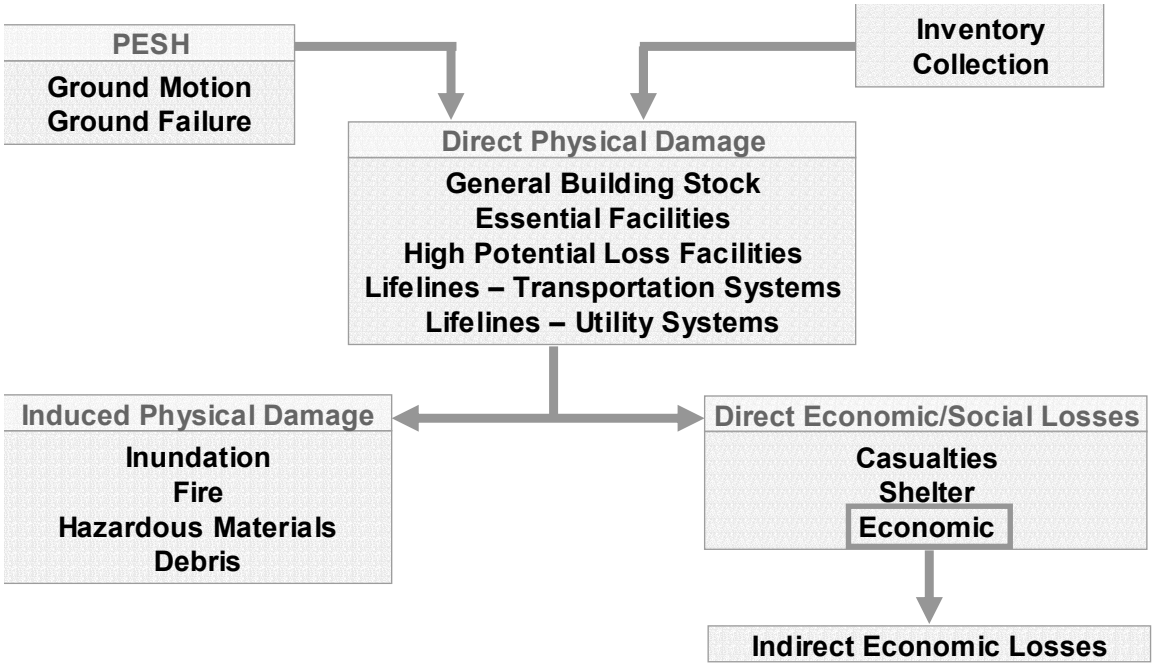

Figure 4.1 Components of the HAZUS Earthquake Loss Estimation Methodology

The most important feature of the HAZUS methodology is its modular nature. This modularity gives an enormous flexibility to the methodology and enables the addition of new modules (or improvement of existing ones) without reworking the entire methodology. Improvements may be made to adapt modules to local or regional needs or to incorporate new models and data. Hence locally developed inventories and other data that more accurately reflect the local environment can be substituted resulting in higher accuracy in predicting the earthquake losses. Another advantage of the modular nature of HAZUS is that it enables users to limit their studies to selected losses. Such a limited study may be desirable for a variety of reasons, including budget and inventory constraints, or the need to obtain answers to specific problems. The modularity also permits logical evolution of the methodology as research progresses and the state-of-the-art advances.

Three levels of analysis can be employed with HAZUS. These levels require from the simplest to the most detailed input options based on the needs of the user. The definitions of these levels are somewhat arbitrary and have no distinct boundaries between them. These three levels can be listed as follows:

Level 1 (Default Data Analysis): This is the simplest type of analysis. It requires the minimum amount of information which is already available in HAZUS and the minimum effort by the user. The user can run a loss estimation analysis by using the following steps:
a) Define the study region: The study region can be a combination of states, counties, cities or even census tracts. Each study region has its own characteristics that can be edited or modified independently from other study regions.
b) Define a scenario earthquake: The user must identify the earthquake characteristics in order to run the loss analysis. There are several options available to define a scenario earthquake in HAZUS. The characterization of hazard can be deterministic, probabilistic or user supplied information. The deterministic hazard can further be classified as a historical epicenter event (from HAZUS database of 3500 events), a source event (involving the selection of desired fault source from HAZUS database of Western US faults), or an arbitrary event, which is simply defined by its epicenter location and magnitude. This is the most appropriate option to be used with default type analysis since it requires minimum input information (Figure 4.2).

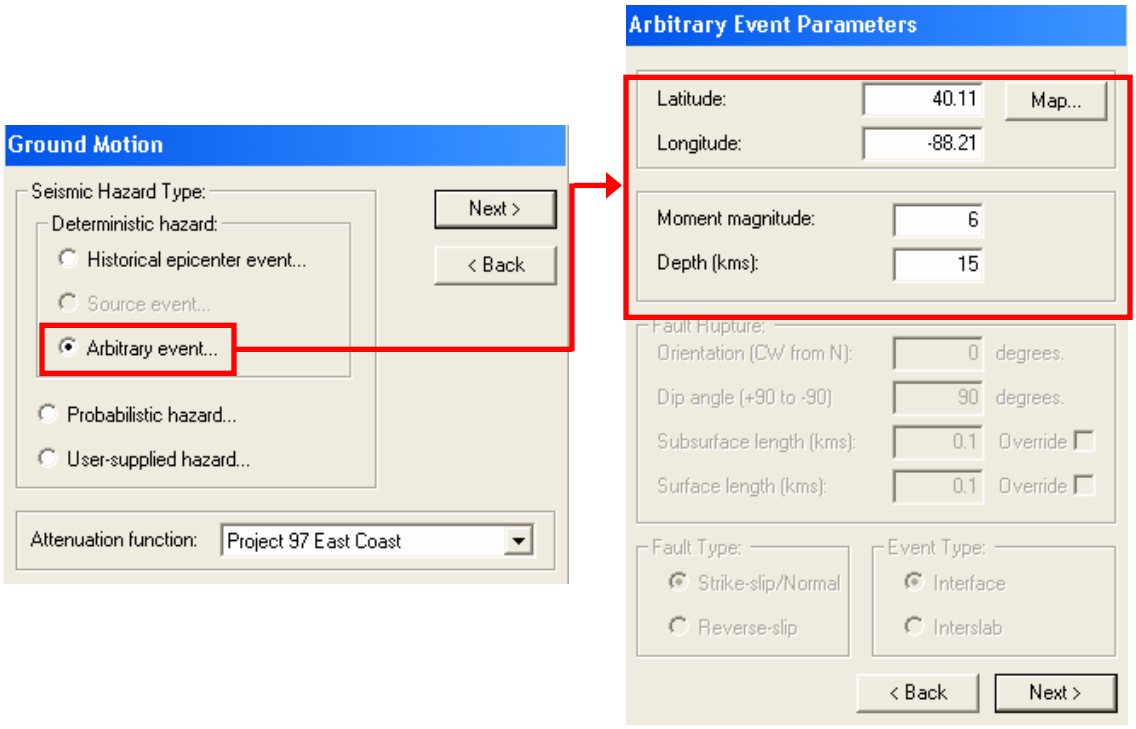

Figure 4.2 The Simplest Way of Defining Scenario Earthquake in HAZUS

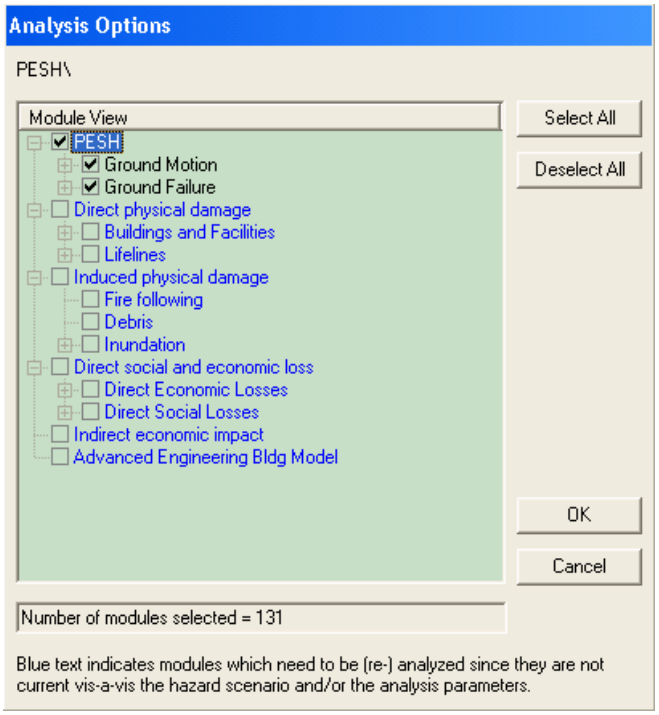

Figure 4.3 "Analysis Options" Menu in HAZUS

c) Run the analysis: Once the study region and the scenario earthquake are defined, the user can run the analysis by selecting the desired analysis options from the "Analysis Options" window. An important thing to remember is that the PESH Module, in which the user defines the hazard, must be selected in every loss estimation analysis. The selection of other modules is optional and depends on the choices of the users (Figure 4.3).

d) Obtain the results: The outputs of HAZUS modules can be presented either in a tabular or a graphical form. Three types of output are available: the thematic map of results, the table of results by census tract and the summary table of results by county or whole region. The different forms of output presentation provide an enormous flexibility to the user in assessing and reporting the loss estimation results (Figure 4.4).

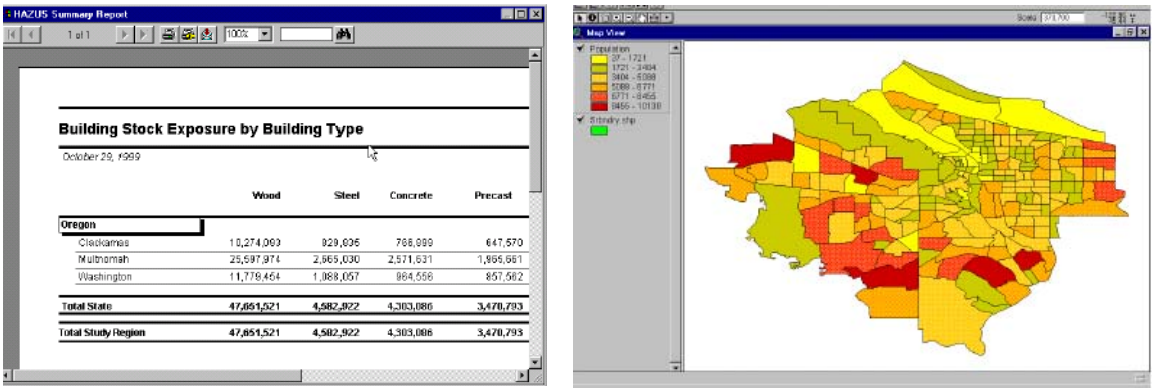

Figure 4.4 Output Options of HAZUS; **a)** Summary Reports, **b)** Thematic Maps

The loss estimates obtained by using the "Default Data Analysis" will be crude and will only be appropriate as initial loss estimates to determine whether more detailed analyses are required. Furthermore, some components of the methodology, requires a more detailed inventory than the default one supplied by HAZUS, and cannot be used at this level of analysis. The detailed information related with the default data analysis is provided in the HAZUS User Manual (National Institute of Building Sciences, 1999a)

Level 2 (User-Supplied Data Analysis): The User Supplied Data Analysis requires a more detailed inventory data and much more effort by the user when compared to Level 1 type of analysis. As more complete data is provided by the user, there will be significant improvements

in the quality and the accuracy of the results. For instance, the user may improve the loss estimation by introducing soil or liquefaction maps, enhancing the inventory by local data, preparing a detailed inventory for all essential facilities and modeling the economy of the study region in detail, etc. The technical background required to run a 'Level 2' analysis is detailed in the HAZUS Technical Manuals (National Institute of Building Sciences, 1999b).

Level 3 (Advanced Data and Models Analysis): The Advanced Data and Models Analysis constitutes the most advanced level of earthquake loss estimation methodology. It incorporates results from engineering and economic studies using methods not available in the HAZUS Methodology. An extensive participation of technical expert knowledge is required to perform a detailed analysis and to assess the damage and loss estimates. Although the quality and the detail of the results depend upon the user's effort, they are significantly improved when compared with Level 1 and 2 analyses.

In this level of analysis, the user can utilize the Advanced Engineering Building Module-AEBM (National Institute of Building Sciences, 1999c) of HAZUS to use building specific damage and loss functions in great detail. This module is included in version HAZUS99 SR-2. The flowchart of AEBM is given in Figure 4.5. AEBM analysis begins with the creation of the study region and the definition of the scenario earthquake, just like the regular analysis. AEBM has two different components; AEBM Inventory and Profile. The AEBM Inventory involves general information about the building to be analyzed; such as location (longitude and latitude), size, number of occupants, and replacement and loss of function costs. The AEBM Profile involves information about occupancy class and building type, seismic design level, building quality and other structural characteristics, including building specific damage and loss parameters like structural and non-structural fragility curve medians and betas, casualty ratios and repair cost ratios.

Each building to be analyzed has a unique AEBM Inventory and Profile. A single AEBM Profile can be linked to a number of AEBM Inventories to evaluate a group of similar buildings. Hence it is possible to conduct earthquake loss estimation analysis of any specific type of building or a group of buildings not available in the HAZUS' database by developing case-specific damage and loss parameters through pushover and vulnerability analyses.

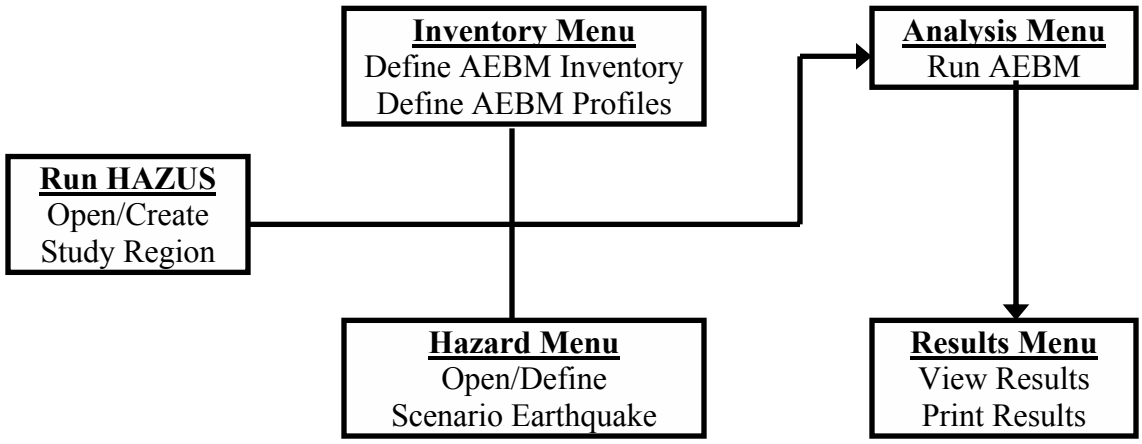

Figure 4.5 Flowchart of the HAZUS AEBM

4.2 Limitations of HAZUS Methodology

There are limitations in the HAZUS Methodology that users should be aware of in addition to its features. This section focuses on the limitations of HAZUS in the current version (Service Release-2).

The first limitation of the hazard module is the high uncertainty related to the characteristics of ground motion in the Eastern U.S. Conservative treatment of this uncertainty can lead to an overestimation of losses in this area, both for scenario events and when using probabilistic ground motion. Hence it is not possible to know how well HAZUS estimates the losses for the Central and Eastern U.S. The second limitation points out the overestimation of the losses from small magnitude (less than magnitude of 6.0) earthquakes. It is also difficult to quantify the extent of this overestimation. Furthermore, consequences of earthquakes with magnitudes less than 6 and higher than 7.5 are not quite reliable, according to the HAZUS User Manual, since the implications of very short and very long durations of ground motions upon damage are poorly understood. Other limitations concerning the hazard module are that the duration effects of ground motions are not explicitly considered in the loss estimation methodology and the modeling capabilities for aftershocks are very limited.

Moreover, HAZUS assumes that all locations have the same soil conditions. The default value used by HAZUS is Class D for all sites according to NEHRP Provisions (FEMA, 1997). In order to account for the effects of the local soil conditions, the user should provide a soil map for HAZUS, with the required format.

Default inventories of HAZUS can be obtained from publicly available databases and are aggregated on a county or census tract scale. These inventories are generally imperfect representations of the corresponding communities since they involve many assumptions and generalizations. Many of the databases are out of date, inaccurate or do not capture data characteristics of a specific community that may have a wide variety of ages, sizes, shapes and structural systems of buildings constructed using different seismic design codes.

The HAZUS Methodology is most accurate when applied to a class of buildings or facilities, and least accurate when applied to a particular building or facility. However, AEBM provides the ability to assess the performance and to estimate losses associated with individual buildings. In addition, the results for non-structural damage are not quite reliable since the coefficients for non-structural damage are based upon less complete data than that of structures.

HAZUS also does not include damage and loss estimates for nuclear power plants or dams. These structures are so complex that estimating the losses would require a very detailed study. Therefore, HAZUS restricts the treatment of these facilities to mapping them in the study region. Furthermore, the accuracy of losses associated with lifelines may be less than for losses associated with the general building stock.

Pilot and calibration studies have as yet not provided an adequate test concerning the possible extent and effects of landsliding and the performance of water systems.

Casualty results are crude estimates since data are not available for all building types and the coefficients for casualty estimates are based primarily upon damage from earthquake events that occurred in suburban areas at times of the day when people were generally not occupying commercial structures.

The methodology calculates the potential exposure to flood or fire following the earthquake in terms of the fraction of a geographical area that may be flooded or burned, but does not have methods for rigorous calculation of damage or loss due to flooding or fire. Consequently, these two potential contributors to the total loss are not included in the estimates of economic loss, casualties, or loss of shelter.

The indirect economic loss module is new and experimental. While the output from the pilot studies has generally been credible, this module requires further testing.

4.3 Uncertainty in HAZUS Methodology

HAZUS Earthquake Loss Estimation Methodology is composed of four basic steps. These are:

- Definition of the earthquake hazard,
- Definition of the inventory characteristics,
- Estimation of earthquake damage sustained by the inventory,
- Calculation of Losses (Economic and/or Social).

Uncertainties are inherent in all stages of the methodology. They arise partly from the incomplete scientific knowledge concerning earthquakes and their effect upon buildings and facilities. They also result from the approximations and simplifications that are necessary for comprehensive analysis. Incomplete or inaccurate inventories of the built environment, demographics and economic parameters add to the uncertainty. In general, the limited amount of scientific information, the lower quality data and the limited engineering information results in greater variability of the expected losses. As stated by Whitman et al (1997), losses estimated using HAZUS for a specific earthquake scenario should be regarded as being uncertain by a factor of two, and in some cases even greater.

4.3.1 Sources of Uncertainty and Error

There are many factors that contribute to the uncertainty in the results of the HAZUS Methodology. The most significant ones are listed below:

Ground Motion: The highest uncertainty in any earthquake loss estimation methodology comes from the earthquake itself. Due to its probabilistic nature, no one can ever predict how a "scenario earthquake" will truly affect a region. The magnitude and the location of the earthquake, the associated faulting of the ground motions and landsliding will not be precisely as anticipated. This is especially true for the Central and Eastern Regions, where the past earthquake data is not sufficient and the hazard itself is poorly understood. Hence the results of an earthquake loss study should not be looked upon as a "prediction", but rather as an indication of what the future may hold. HAZUS Methodology is not an exception to this.

Default Inventory Data: The estimated losses in HAZUS are very sensitive to the characteristics of the inventory. In fact, it is nearly impossible to develop a perfect inventory for a specific region. There generally exists an enormous database of various types of buildings and facilities of different sizes, shapes, and structural systems constructed over decades because of the diverse seismic design codes. Any outdated information including population, square footage of the buildings, etc. can be a serious source of error in the estimation process. Inaccurate or incomplete geographical (GIS) data, especially for engineering structures like dams, bridges, nuclear facilities, etc. can be another pitfall for the methodology.

Interpretation of damage/loss parameters: Due to the complexity of the inventory data, a great deal of uncertainty exists concerning the structural resistance of most buildings and other facilities. Moreover, there is no sufficient data from past earthquakes or laboratory experiments to permit precise definitions of damage based on existing ground motions even for specific buildings. To deal with such complexity and the lack of data, subjective classifications or decisions must take place. Eventually, these are considered as potential sources of error. In HAZUS, there are qualitative definitions for damage states; hence the meaning of slight, moderate, extensive and complete damage can vary from one expert to another.

Additional uncertainty is due to the approximations and the simplifications that are used in the analytical modeling and in the analyses that are performed to determine damage parameters. A typical example is the employment of a simplified nonlinear static procedure (Capacity Spectrum Method) to calculate the damage state medians of HAZUS fragility curves.

Furthermore, many parameters in the HAZUS Loss Modules depend on data from local or national resources, from previous studies and also from expert opinion. Therefore these parameters have a significant degree of uncertainty. Regional cost multipliers used to calculate building repair costs, in the Direct Economic Losses Module, or the Casualty Rates used while calculating the casualties in the Direct Social Losses Module, are good examples of such loss parameters.

Incidental errors: This is not a common source of error, and it may be originated from mismatch between database information or spatial information, employment of wrong ID numbers for facilities, etc.

4.3.2 Treatment of Uncertainty

HAZUS does not explicitly include a treatment for uncertainty. The results obtained will be the mean (or average) values of losses, and do not include ranges that would help the user to assess the confidence intervals of results. However it is possible to examine the variability of the model by performing a sensitivity analysis.

In the sensitivity analysis, an input parameter is changed and the others are kept constant, and then the sensitivity of the results to the change is evaluated. If the results vary to a great extent, this means that the model is very sensitive to this input parameter, so the value used in loss estimation should be selected very carefully. If the results are not affected too much by the change in the value of the input parameter, then it is not practical to determine the exact value of the corresponding input parameter.

The following is a list of the parameters used in the sensitivity analysis within the HAZUS methodology:

- The magnitude of the scenario earthquake,
- The attenuation relationship,
- The mix of construction quality levels (inferior, code, superior),
- Fragility Curve Parameters (median and lognormal standard deviation parameters of damage states of building structure types),
- The repair and replacement costs,
- The type of economy in the Indirect Economical Losses Module,
- The unemployment Rate in the Indirect Economical Losses Module.

There are examples of such sensitivity analyses in the literature. For instance, the research recently conducted by Grossi (2001) includes a sensitivity analysis of the HAZUS methodology and the interaction of the uncertainty with the effects of mitigation and insurance. Parameters used in the sensitivity analysis include earthquake recurrence, ground motion attenuation, soil classification, and the exposure and fragility of residential structures. In the study, Oakland, California was used as the study region. Several conclusions were drawn from the study. First, it is stated that the earthquake loss estimation process seems to be very uncertain. Depending on the parameters and models chosen to be used in an analysis, there is almost a difference of 3 in the average annual loss. Considering the study region, the largest range of uncertainty, or in other words, the most influential parameter in estimating losses is the attenuation relationship. Other factors in the order of importance are listed as: earthquake recurrence, exposure, fragility before mitigation, soil classification and fragility after mitigation.

Another way of dealing with uncertainty in HAZUS is to enhance the inventory data. Obviously the quality and the uncertainty of the results are directly related to the detail of the inventory and the economic and demographic data provided. It is possible to obtain crude estimates of losses with the default inventory data. On the other hand, the uncertainties resulting from the inventory data can be reduced and the most accurate results can be obtained if the inventory data is enhanced by accommodating the characteristics of the associated study region.

As stated in the HAZUS Technical Manual, the methodology has been tested against the judgment of experts and, to the extent possible, against records from several past earthquakes. However limited and incomplete data about actual earthquake damage precludes complete calibration of the methodology. When a real earthquake occurs, the damage observed on the ground is absolute and should replace the predicted results. This is called ground-truthing the results in HAZUS. This feature allows the HAZUS user to feed in the real observed data so that the analysis results are significantly refined. If available, this is an effective way of reducing the uncertainties in the methodology.

It is also important to understand the dependency of modules and parameters within the HAZUS methodology. As the dependency of parameters increases, the uncertainty of results increases, too.

Finally, some of the important HAZUS parameters that need to be enhanced to reduce the uncertainty in loss estimation are listed as follows:

- *Inventory parameters:* Square footage in General Building Stock (update to latest data), Demographics (update to latest census), accurate and complete inventory for Essential Facilities (choose proper building type).
- *Hazard Parameters:* Attenuation functions, soil effects (soil type), earthquake magnitude, landslide effects (maps), liquefaction effects (maps).
- *Building Damage Functions:* Capacity curve parameters (yield and ultimate performance values), fragility curve parameters (fragility medians and betas).
- *Casualty parameters (Social Losses):* Casualty rates.
- *Shelter Parameters (Social Losses):* Shelter modification factors.
- *Economic Parameters (Economic Losses):* Cost Modifiers, building interruption factors, long term impact (number of employees, type of economy, reconstruction priorities).

4.4 Building-Related Modules in HAZUS

HAZUS consists of many modules to estimate the damage to all kinds of civil engineering structures and the corresponding wide range of social and economic losses. However, this study is based on the assessment of the vulnerability of a special building type; the flat-slab structures. Therefore, only the modules related with the damage and loss characteristics of building structures are discussed in the following sections. The investigated modules are shown as gray boxes in Figure 4.6. Hence direct physical damage to general building stock due to ground shaking will be investigated and then the relationship between the damage and estimations of casualties, direct and indirect economic losses will be assessed.

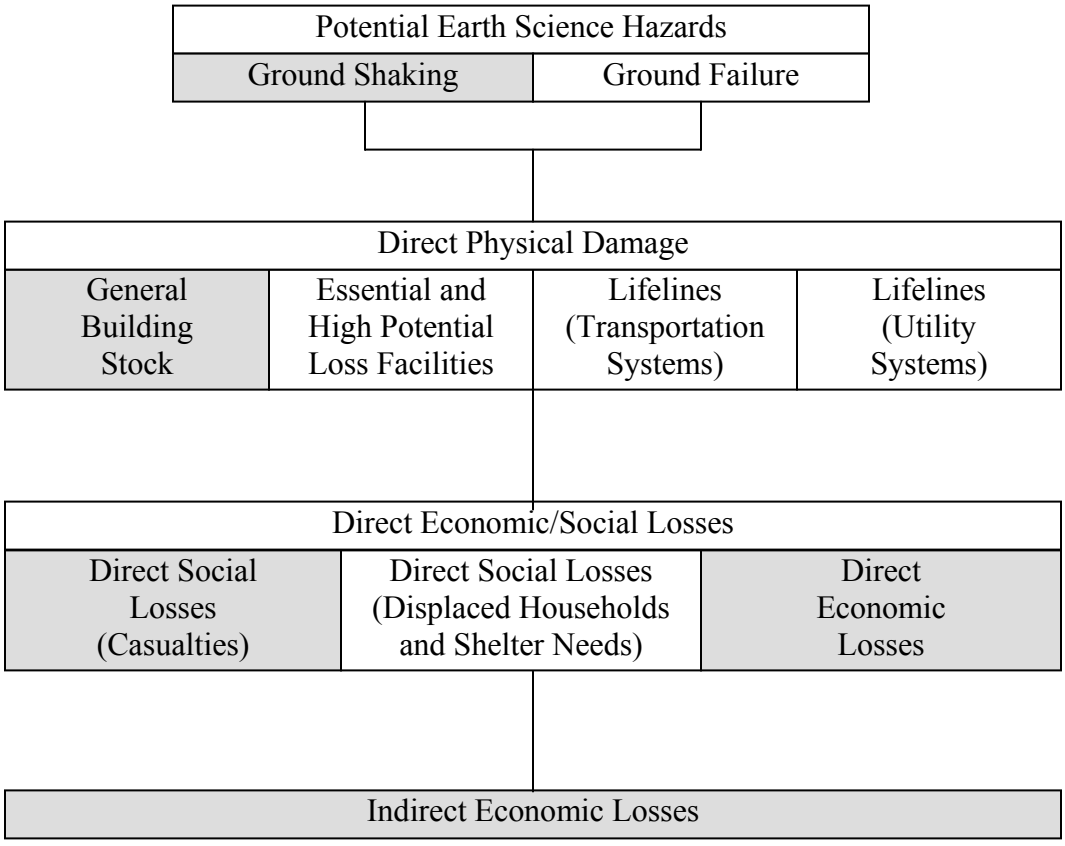

Figure 4.6 Investigated HAZUS Modules in the Study

4.5 HAZUS Damage Modules

The damage functions in the modules estimate the probability of discrete states of structural and non-structural building damage that are used as inputs to the estimation of building losses, including economic loss, casualties and the loss of function. The functions use quantitative measures of ground shaking (and ground failure) and analyze model building types in a similar manner to the engineering analysis of a single structure.

In HAZUS, damage is divided into two parts: direct physical damage and induced physical damage. Direct physical damage is used to estimate damage to buildings and lifelines. In this report, the damage specific to the general building stock is investigated. General building stock represents typical buildings of a given model building type designed to withstand either High-Code, Moderate-Code or Low-Code seismic standards, or not seismically designed (referred to as Pre-Code buildings). Buildings are classified both in terms of their use or occupancy class, and in terms of their structural system or model building type. Damage is predicted based on model building type since the structural system is considered as the key factor in assessing the overall building performance, loss of function and casualties. Thirty-six model building types are used to classify buildings within the overall categories of wood, steel, concrete, masonry and mobile homes. All of these types are listed in Table 4.1. Hence model building type is a function of the building height. Typical building heights in the table are used to determine the capacity curve properties. The buildings are described as low-rise (LR), moderate-rise (MR) and high-rise (HR). Occupancy class is important in determining economic loss since the building value is primarily a function of building use. There are 7 general and 28 specific occupancy classes as listed in Table 4.2. General occupancy classes are identified as residential, commercial, industrial, agriculture, religion/non-profit, and government/education. The building inventory data relate model building type and the occupancy class on the floor area as illustrated in Figure 4.7. This figure has been prepared for presentation purposes, hence it only includes limited number of categories for occupancy type and the model building type, and the values are arbitrary. In HAZUS, the information about the distribution of the total floor area of the model building types for each occupancy class is available for a given geographical area.

Table 4.1 HAZUS Model Building Types

No	Label	Description	Height			
			Range		Typical	
			Name	Stories	Stories	Feet
1	W1	Wood, light frame (<5000 sq.ft.)		All	1	14
2	W2	Wood (>5000 sq.ft.)		All	2	24
3	S1L		LR	1-3	2	24
4	S1M	Steel Moment Frame	MR	4-7	5	60
5	S1H		HR	8+	13	156
6	S2L		LR	1-3	2	24
7	S2M	Steel Braced Frame	MR	4-7	5	60
8	S2H		HR	8+	13	156
9	S3	Steel Light Frame		All	1	15
10	S4L	Steel Frame with Cast-in-Place	LR	1-3	2	24
11	S4M	Concrete Shear Walls	MR	4-7	5	60
12	S4H		HR	8+	13	156
13	S5L	Steel Frame with Unreinforced	LR	1-3	2	24
14	S5M	Masonry Infill Walls	MR	4-7	5	60
15	S5H		HR	8+	13	156
16	C1L		LR	1-3	2	20
17	C1M	Concrete Moment Frame	MR	4-7	5	50
18	C1H		HR	8+	12	120
19	C2L		LR	1-3	2	20
20	C2M	Concrete Shear Walls	MR	4-7	5	50
21	C2H		HR	8+	12	120
22	C3L	Concrete Frame with Unreinforced	LR	1-3	2	20
23	C3M	Masonry Infill Walls	MR	4-7	5	50
24	C3H		HR	8+	12	120
25	PC1	Precast Concrete Tilt-Up Walls		All	1	15
26	PC2L	Precast Concrete Frame with	LR	1-3	2	20
27	PC2M	Concrete Shear Walls	MR	4-7	5	50
28	PC2H		HR	8+	12	120
29	RM1L	Reinforced Masonry Bearing Walls	LR	1-3	2	20
30	RM1M	/w Wood or Metal Deck Diaphragms	MR	4+	5	50
31	RM2L	Reinforced Masonry Bearing Walls	LR	1-3	2	20
32	RM2M	/w Precast Concrete Diaphragms	MR	4-7	5	50
33	RM2H		HR	8+	12	120
34	URML	Unreinforced Masonry Bearing	LR	1-2	1	15
35	URMM	Walls	MR	3+	3	39
36	MH	Mobile Homes		All	1	12

Table 4.2 HAZUS Building Occupancy Classes

Label	Occupancy Class	Example Descriptions
	Residential	
RES1	Single Family Dwelling	House
RES2	Mobile Home	
RES3	Multi Family Dwelling	Apartment/Condominium
RES4	Temporary Lodging	Hotel/Motel
RES5	Institutional Dormitory	Group Housing, Jails
RES6	Nursing Home	
	Commercial	
COM1	Retail Trade	Store
COM2	Wholesale Trade	Warehouse
COM3	Personal & Repair Services	Service Station/Shop
COM4	Professional/Technical Services	Offices
COM5	Banks	
COM6	Hospital	
COM7	Medical Office/Clinic	
COM8	Entertainment & Recreation	Restaurants/Bars
COM9	Theaters	
COM10	Parking	Garages
	Industrial	
IND1	Heavy	Factory
IND2	Light	Factory
IND3	Foods/Drugs/Chemicals	Factory
IND4	Metals/Mineral Processing	Factory
IND5	High Technology	Factory
IND6	Construction	Office
	Agriculture	
AGR1	Agriculture	
	Religion/Non-Profit	
REL1	Church/Non-Profit	
	Government	
GOV1	General Services	Office
GOV2	Emergency Response	Police/Fire Station/EOC
	Education	
EDU1	Grade Schools	
EDU2	Colleges/Universities	Does not include group housing

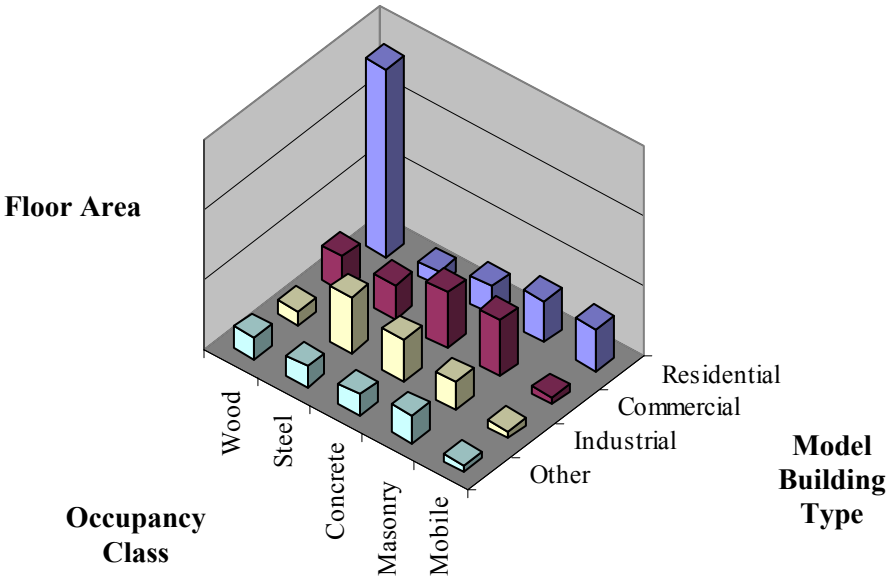

Figure 4.7 Example of Mapping between Occupancy Class and Building Type

4.6 Building Damage due to Ground Shaking

There are two sets of curves used in HAZUS to estimate damage to buildings resulting from ground shaking: (1) capacity curves and (2) fragility curves. HAZUS capacity curves are plots of the building's lateral load resistance (in terms of spectral acceleration) as a function of lateral displacement (in terms of spectral displacement). In HAZUS, a unique capacity curve is defined for each specific building type and seismic design level.

HAZUS fragility curves predict the probability of reaching or exceeding either Slight, Moderate, Extensive or Complete damage states for a given level of spectral displacement (structural) or spectral acceleration (non-structural). The probability of being in a particular state of damage and the input used to predict building related losses are calculated as the difference between fragility curves. More detailed information about HAZUS capacity and fragility curves are provided in the following sections.

4.6.1 Capacity Curves

The capacity curves are defined by two points in HAZUS: yield capacity (D_y, A_y) and ultimate capacity (D_u, A_u). Up to the yield capacity, the building capacity curve is assumed to be linear with stiffness based on an estimate of the expected period of the building. From yield to the ultimate point, the capacity curve transitions in slope from an essentially elastic state to a fully plastic state. The capacity curve is assumed to remain plastic past the ultimate point (Figure 4.8). The following formulations are used for these two points:

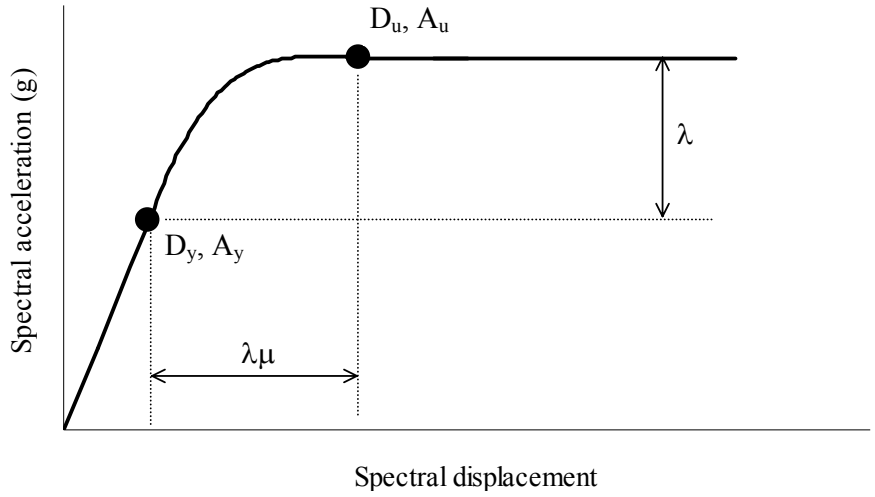

Figure 4.8 Example Building Capacity Curve and Control Points

$$A_y = C_s \gamma / \alpha_1 \quad \textbf{(4.1.a)}$$

$$D_y = 9.8 A_y T_e^2 \quad \textbf{(4.1.b)}$$

$$A_u = \lambda A_y \quad \textbf{(4.2.a)}$$

$$D_u = \lambda \mu D_y \quad \textbf{(4.2.b)}$$

C_s is the design strength coefficient and approximately corresponds to the lateral force design requirements of current seismic codes. It is a function of the building's seismic zone location and other factors including the site soil condition, the type of lateral load resisting system and the

building period. An example of design strength values are given in Table 4.3 for selected building types. Gray boxes indicate the types that are not permitted by current seismic codes.

Table 4.3 Example Building Capacity Parameters - C_s

Building Type	Seismic Design Level			
	High-Code	Moderate-Code	Low-Code	Pre-Code
W1	0.200	0.150	0.100	0.100
S1L	0.133	0.067	0.033	0.033
S1M	0.100	0.050	0.025	0.025
S1H	0.067	0.033	0.017	0.017
C2L	0.200	0.100	0.050	0.050
URML			0.067	0.067

T_e is the expected elastic fundamental mode period of the building. It is a function of building type and height. α_1 is the fraction of the building weight effective in the pushover mode, whereas α_2 is the fraction of the building height at the elevation where pushover mode displacement is equal to spectral displacement. γ and λ are overstrength factors relating true yield strength to design strength and ultimate strength to yield strength, respectively. Finally μ symbolizes the ductility ratio relating ultimate displacement to λ times the yield displacement. Tables 4.4 and 4.5 demonstrate some example values for these parameters for the selected model building types.

4.6.2 Demand Spectrum

In order to obtain the building response necessary to construct the corresponding fragility curves, the demand spectrum of ground shaking should be determined. The demand spectrum is based on the 5% damped response spectrum at the building's site reduced for effective damping when effective damping exceeds the 5% damping level of the input spectrum. The standard spectrum shape consists of two primary parts: (1) a region of constant spectral acceleration at short periods and (2) a region of constant spectral velocity at long periods. Short period spectral acceleration, S_s, is defined by 5% damped spectral acceleration at a period of 0.3 seconds. The constant

spectral velocity region has spectral acceleration proportional to 1/T and is anchored to the 1-second, 5% damped spectral acceleration, S_1. The amplification of ground shaking to account for local site conditions is based on the soil factors of the NEHRP Provisions. These provisions define a standardized site geology classification scheme and specify soil amplification factors; i.e., F_A for the acceleration domain and F_V for the velocity domain. Figure 4.9 shows an example of 5% damped response spectra with the aforementioned parameters.

Table 4.4 Example Building Capacity Parameters – T_e, α_1, α_2, γ and λ

Building Type	Height to Roof (ft)	Period, Te (seconds)	Modal		Overstrength	
			α_1	α_2	γ	λ
W1	14	0.35	0.75	0.75	1.50	3.00
S1L	24	0.50	0.75	0.75	1.50	2.50
S1M	60	1.08	0.75	0.75	1.25	2.00
S1H	156	2.21	0.65	0.60	1.10	2.00
C2L	20	0.35	0.75	0.75	1.50	2.50
URML	15	0.35	0.50	0.75	1.50	2.00

Table 4.5 Example Building Capacity Parameters – μ

Building Type	Seismic Design Level			
	High-Code	Moderate-Code	Low-Code	Pre-Code
W1	8.0	6.0	6.0	6.0
S1L	8.0	6.0	5.0	5.0
S1M	5.3	4.0	3.3	3.3
S1H	4.0	3.0	2.5	2.5
C2L	8.0	6.0	5.0	5.0
URML			3.3	3.3

HAZUS simulates the inelastic response by modifying the elastic system properties by using the effective stiffness and damping characteristics of the building. Effective stiffness properties are based on secant stiffness and effective damping properties based on the combined viscous and hysteretic measures of dissipated energy. Hence the demand spectrum is in the form of elastic response divided by the amplitude-dependent damping reduction factors (i.e., R_A at periods of

constant acceleration and R_V at periods of constant velocity) as shown in Figure 4.9. Spectrum reduction factors are a function of the effective damping of the building, β_{eff}. Effective damping is the sum of the elastic damping term β_E and the hysteretic damping term, β_H associated with post-yield, inelastic response. The elastic damping term is assumed to be a constant, so it is independent of the amplitude. The hysteretic damping term is dependent on the amplitude of post-yield response and is based on the area enclosed by the hysteresis loop at peak response displacement and acceleration. It is also dependent on a degradation factor, κ, which defines the fraction of the area used to determine hysteretic damping.

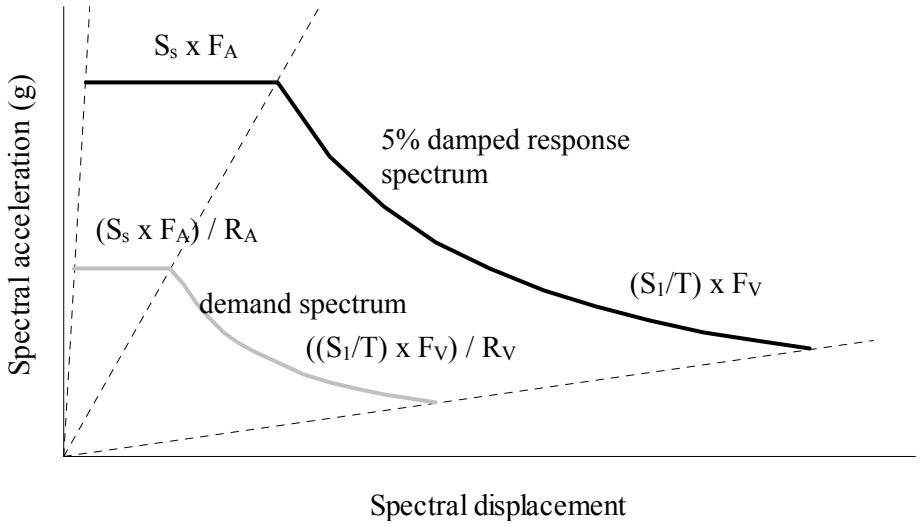

Figure 4.9 5% Damped Response Spectra

4.6.3 Determination of Peak Building Response

The demand curve intersects the building capacity curve at the point of peak response displacement, D, and acceleration, A (Figure 4.10). These performance values are used with vulnerability curves to estimate the damage state variables. At this point it should be mentioned that the peak values obtained by applying this method are open to discussion due to the differences between static and dynamic response. Although nonlinear static approaches are simple and easy to implement, they also lack accuracy when compared to elaborate dynamic time-history analysis.

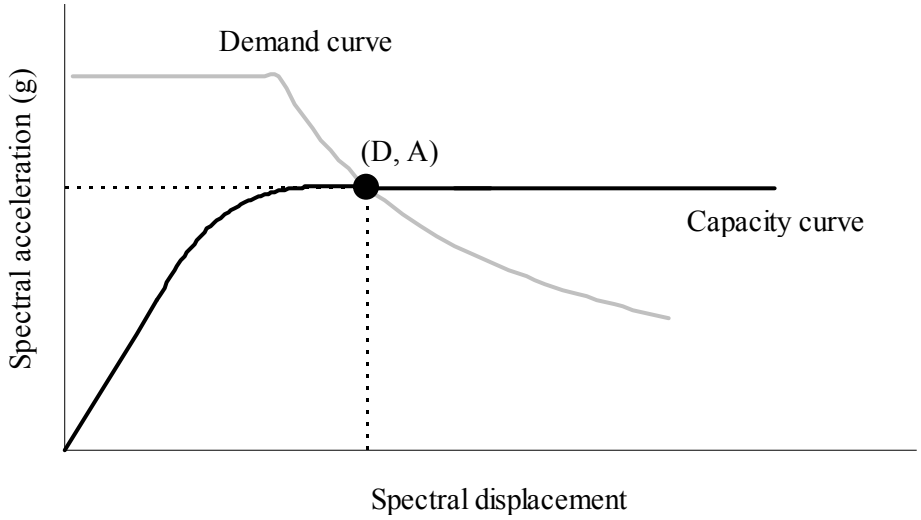

Figure 4.10 Determination of Peak Building Response from Demand and Capacity Curves

4.6.4 Fragility Curves

Building fragility curves in HAZUS are lognormal functions that describe the probability of reaching or exceeding structural and non-structural damage states, given the deterministic (median) estimates of spectral response. These curves take into account the variability and uncertainty associated with the capacity curve properties, damage states and ground shaking. Each fragility curve is defined by a median value of the demand parameter (spectral displacement or acceleration) that corresponds to the threshold of that damage state and by the variability associated with that damage state.

The fragility curves distribute damage among Slight, Moderate, Extensive and Complete damage states. For any given value of spectral response, discrete damage state probabilities are calculated as the difference of the cumulative probabilities of reaching, or exceeding successive damage states. Discrete damage state probabilities are then used as inputs to the calculation of various types of building related loss. Figure 4.11 provides an example of discrete damage state probabilities for three levels of earthquake ground shaking. The terms “weak”, “medium” and

"strong" are used here for simplicity; in the actual methodology, only quantitative values of spectral response are employed.

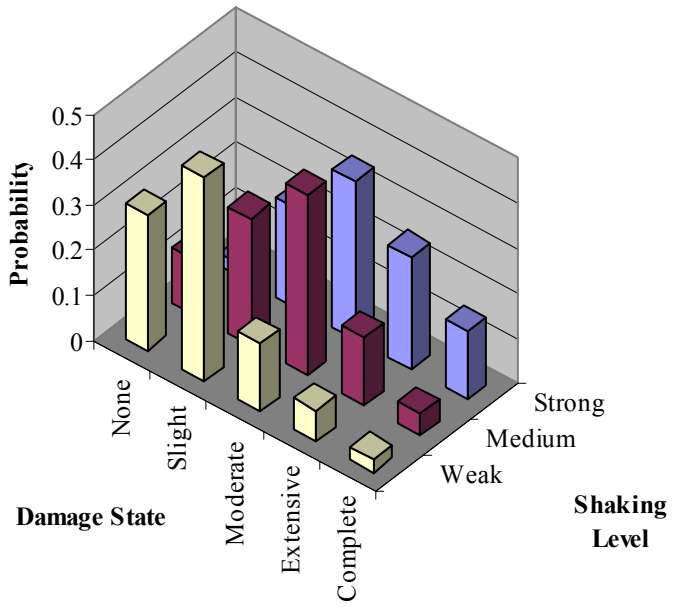

Figure 4.11 Example Discrete Damage State Probabilities

Each fragility curve is characterized by the median and the lognormal standard deviation (β) values of the Potential Earth Science Hazard (PESH) demand. Different PESH parameters are used for different types of damage. Spectral displacement is the PESH parameter used for structural damage and non-structural damage to drift-sensitive components. Spectral acceleration is employed for calculating non-structural damage to acceleration sensitive components. The built-in median and beta parameters of HAZUS are tabulated according to the type of damage and design level. For example, Table 4.6 presents structural fragility curve parameters for the High-Code seismic deign level and for selected building types only. The same tabular form is also valid for non-structural damage to drift and acceleration sensitive components (Tables 4.7 and 4.8, respectively). Note that the PESH parameter employed in Table 4.8 is the spectral acceleration and that the median values are independent of the model building type (always in constant value).

Table 4.6 Structural Fragility Curve Parameters - High- Code

Building Type	Spectral displacement (inches)							
	Slight		Moderate		Extensive		Complete	
	Median	Beta	Median	Beta	Median	Beta	Median	Beta
W1	0.50	0.80	1.51	0.81	5.04	0.85	12.60	0.97
S1L	1.30	0.80	2.59	0.76	6.48	0.69	17.28	0.72
S1M	2.16	0.65	4.32	0.66	10.80	0.67	28.80	0.74
S1H	3.37	0.64	6.74	0.64	16.85	0.65	44.93	0.67
C2L	0.72	0.81	1.80	0.84	5.40	0.93	14.40	0.81
URML								

Table 4.7 Non-structural Drift Sensitive Fragility Curve Parameters - High- Code

Building Type	Spectral displacement (inches)							
	Slight		Moderate		Extensive		Complete	
	Median	Beta	Median	Beta	Median	Beta	Median	Beta
W1	0.50	0.85	1.01	0.88	3.15	0.88	6.30	0.94
S1L	0.86	0.81	1.73	0.85	5.40	0.77	10.80	0.77
S1M	2.16	0.71	4.32	0.72	13.50	0.72	27.00	0.80
S1H	4.49	0.72	8.99	0.71	28.08	0.74	56.16	0.77
C2L	0.72	0.87	1.44	0.88	4.50	0.97	9.00	0.99
URML								

Table 4.8 Non-structural Acceleration Sensitive Fragility Curve Parameters - High- Code

Building Type	Spectral acceleration (g)							
	Slight		Moderate		Extensive		Complete	
	Median	Beta	Median	Beta	Median	Beta	Median	Beta
W1	0.30	0.73	0.60	0.68	1.20	0.68	2.40	0.68
S1L	0.30	0.67	0.60	0.67	1.20	0.68	2.40	0.67
S1M	0.30	0.67	0.60	0.68	1.20	0.67	2.40	0.67
S1H	0.30	0.68	0.60	0.67	1.20	0.67	2.40	0.67
C2L	0.30	0.69	0.60	0.67	1.20	0.66	2.40	0.64
URML								

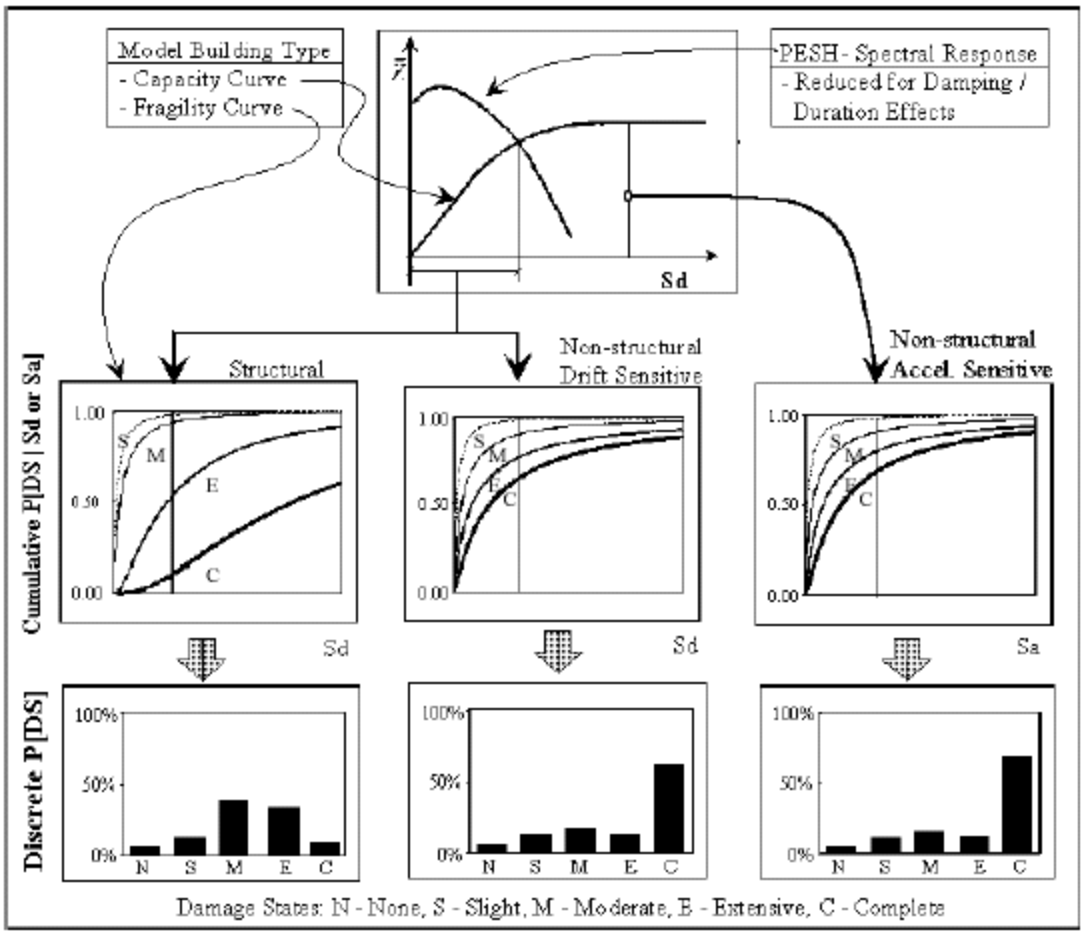

Figure 4.12 Example Building Damage Estimation Process

Hence structural and nonstructural fragility curves can be constructed for spectral displacement or acceleration defined by the intersection of capacity and demand curves (or simply by using the tabular values supplied by HAZUS). Then cumulative probabilities are differenced to obtain discrete probabilities of being in each of the damage states. This process is schematically shown in Figure 4.12. Discrete probabilities obtained are then employed in the estimation of loss parameters.

4.6.5 Uncertainty of HAZUS Fragility Curves

The level of uncertainty involved in the derivation of HAZUS Fragility Curves deserves special concern since it is directly related to the main goal of this study, i.e. the development of fragility curves to be used within the HAZUS Methodology.

HAZUS fragility curves are characterized by the median and the lognormal standard deviation (β) values of seismic demand. The lognormal standard deviation is generally expressed in terms of the randomness and uncertainty components of variability (Kennedy et al., 1980). Since it is not practical to consider these two components separately, a combined random variable term is used in order to develop the composite best-estimate fragility curve.

In general, the total variability of each damage state is modeled by the combination of the following three contributors to damage variability:

- Uncertainty in the damage state threshold
- Variability in the capacity properties of the model building type of interest
- Uncertainty in response due to the spatial variability of ground motion demand

Each of these contributors is assumed to be lognormally distributed random parameters. Analytically, the total variability of each structural damage state, $\beta_{T,ds}$, is defined as

$$\beta_{T,ds} = \sqrt{\left(\text{CONV}\left[\beta_C, \beta_D, \overline{S}_{d,Sds}\right]\right)^2 + \left(\beta_{M,ds}\right)^2} \qquad \textbf{(4.3)}$$

where β_C, and β_D are the lognormal standard deviation parameters that describe the variability of the capacity curve and the demand spectrum, respectively. The other term, $\beta_{M,ds}$, is the lognormal standard deviation parameter that describes the uncertainty in the estimate of the median value of the threshold of structural damage state, ds. The variability of the building response depends jointly on demand and capacity. The function "CONV" in the above equation represents a complex process of convolving probability distributions of the demand spectrum and the capacity curve, respectively. The convolution process produces a surface that describes the

probability of each demand/capacity intersection point when the median demand spectrum is scaled to intersect the median capacity curve at a given amplitude of response. Discrete values of the probabilistic surface are summed along a line anchored to the damage state median of interest to estimate the probability of reaching or exceeding the median value given building response at the intersection point. This process is repeated for other intersection points to form a cumulative description of the probability of reaching or exceeding the damage state of interest. A lognormal function is fit to this cumulative curve yielding an estimate of the lognormal standard deviation of the combined effect of demand and capacity variability on building fragility.

The lognormal parameter $\beta_{M,ds}$ is assumed to be mutually independent of capacity and demand, so its contribution to total variability is achieved by employing the Square-Root-Sum-of-the-Squares (SRSS) method.

4.7 HAZUS Loss Modules

Building loss functions of HAZUS can be assumed as the second part of an integral two-step process in which estimates of building damage (i.e., probability of damage state) are transformed into estimates of various types of loss. In this report, the following loss modules are investigated: Direct Social Losses (Casualties), Direct and Indirect Economic Losses.

4.7.1 Direct Social Losses (Casualties)

This module provides a methodology for estimating casualties directly caused by structural or non-structural damage although non-structural casualties are not directly derived from non-structural damage but instead are derived from structural damage output.

Severity levels of the casualties are determined by a four level injury scale. Each level is listed in Table 4.9 with the corresponding description.

Table 4.9 Injury Classification Scale

Injury Severity Level	Injury Description
Severity 1	Requires basic medical help w/o hospitalizing
Severity 2	Requires greater degree of medical care w/ hospitalizing
Severity 3	Poses an life threatening condition if not treated immediately
Severity 4	Instantaneously killed or mortally injured

The input requirements of the module are as follows:

Scenario time definition: The methodology provides information necessary to produce casualty estimates for three times a day. The following time options are provided:

a) Earthquake striking at 2 am (*night time scenario*)

b) Earthquake striking at 2 pm (*day time scenario*)

c) Earthquake striking at 5 pm (*commute time scenario*)

These scenarios are expected to generate the highest casualties for the population at home, the population at work/school and the population during rush hour, respectively.

Data supplied by other modules: Other modules supply population distribution data, inventory data (building stock distribution) and damage state probabilities. The default values embedded in the methodology are the best estimates and they are provided at the census tract level.

Data specific to casualty module: First it should be kept in mind that it is not quite possible to figure out the actual casualty rates by this methodology. However by forecasting the approximate number of casualties and injuries, the methodology supplies useful information to regional emergency medical authorities just after an earthquake. Default casualty rates defined by the methodology are as follows:

Indoor casualty rates:

- Casualty rates by model building type for slight, moderate and extensive structural damage.
- Casualty rates by model building type for complete damage without structural collapse.

- Casualty rates by model building type for complete damage with structural collapse.
- Collapse rates by model building type for complete structural damage state.

Outdoor casualty rates:

- Casualty rates by model building type for slight, moderate, extensive and complete structural damage.

Table 4.10 Indoor Casualty Rates for Complete Structural Damage (with Collapse)

No	Building Type	Casualty Severity Level			
		Severity 1 (%)	Severity 2 (%)	Severity 3 (%)	Severity 4 (%)
1	W1	40	20	3	5
2	S1L	40	20	5	10
3	S1M	40	20	5	10
4	S1H	40	20	5	10
5	C2L	40	20	5	10
6	URML	40	20	5	10

Table 4.11 Collapse Rates for Complete Structural Damage

	Model Building Type	Probability of Collapse Given a Complete Damage State
1	W1	3%
2	S1L	8%
3	S1M	5%
4	S1H	3%
5	C2L	13%
6	URML	15%

Tables 4.10 and 4.11 give examples of indoor casualty rates by model building type for complete structural damage with collapse and collapse rates by model building type for complete structural damage, respectively.

4.7.2 Earthquake Casualty Model

Casualties caused by a postulated earthquake can be modeled by developing a tree of events leading to their occurrence. The earthquake related casualty event tree begins with an initiating event (earthquake scenario) and follows the possible course of events leading to the loss of life or injuries. Each branch of the tree is assigned a probability of occurrence. Evaluation of the branching probabilities constitutes the main effort in the earthquake casualty modeling.

For example, the expected number of occupants killed in a building during a given earthquake can be simulated with an event tree as shown in Figure 4.13. Assuming that all the branching probabilities are known or inferred, the probability of an occupant being killed can be calculated as follows:

$$P_{killed} = P_A*P_E + P_B*P_F + P_C*P_G + P_D*(P_H*P_J + P_I*P_K) \quad \textbf{(4.4)}$$

The expected number of occupants killed is a product of the number of occupants of the building at the time of earthquake and the probability of an occupant being killed.

$$EN_{occupants\ killed} = N_{occupants} * P_{killed} \quad \textbf{(4.5)}$$

The ‘Number of occupants’ data, or in other words, the population distribution data is provided in tabular form for different groups of population and for three times of day (2:00 am, 2:00 pm, 5:00 pm) for each census tract. There are two multipliers associated with each entry in the table. The second multiplier indicates the fraction of a population component present in an occupancy for a particular scenario time. The first multiplier then divides that population component into indoors and outdoors. The part of this tabular data related with the indoor population is given in Table 4.12.

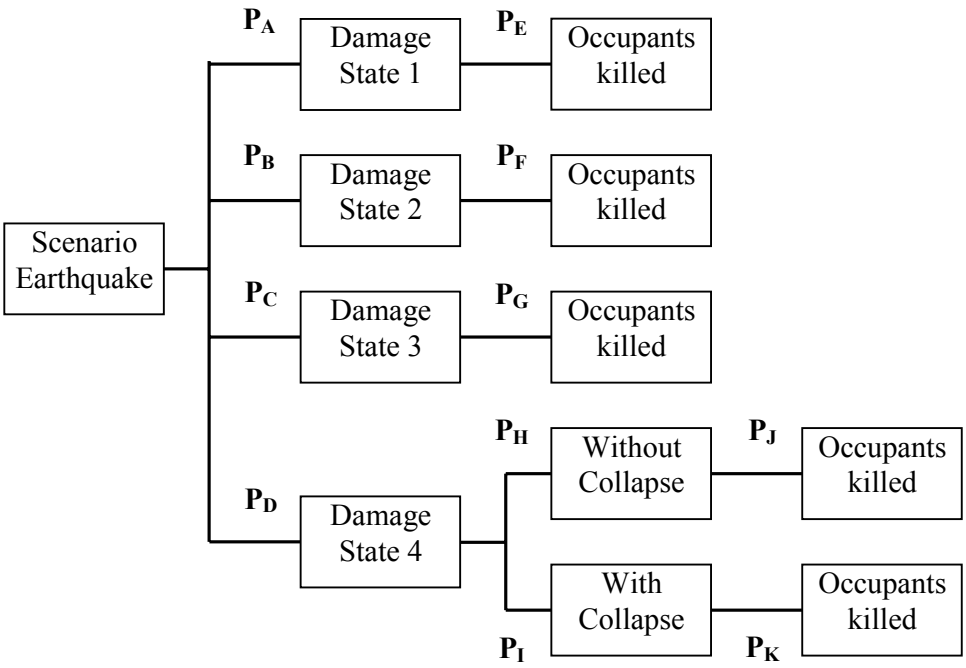

Figure 4.13 Example Casualty Event Tree Model

Table 4.12 Default Relationships for Estimating Population Distribution

Distribution of People in Census Tract			
Occupancy	**2:00 AM**	**2:00 PM**	**5:00 PM**
Indoors			
Residential	(0.999)0.99(NRES)	(0.70)0.75(DRES)	(0.70)0.5(NRES)
Commercial	(0.999)0.02(COMW)	(0.99)0.98(COMW)+ (0.80)0.20(DRES)+ 0.80(HOTEL)+ 0.80(VISIT)	0.98[0.50(COMW)+ 0.10(NRES)+ 0.70(HOTEL)]
Educational		(0.90)0.80(AGE_16)+ 0.80(COLLEGE)	(0.80)0.50(COLLEGE)
Industrial	(0.999)0.10(INDW)	(0.90)0.80(INDW)	(0.90)0.5(INDW)
Hotels	0.999(HOTEL)	0.19(HOTEL)	0.299(HOTEL)

where

NRES is the nighttime residential population inferred from census data,

DRES is the daytime residential population inferred from census data,

COMW is the number of people employed in the commercial sector,

INDW is the number of people employed in the industrial sector,
AGE_16 is the number of people 16 years of age and under inferred from census data,
COLLEGE is the number of students on college and university campuses in the census tract inferred from square footage for default values,
HOTEL is the number of people staying in hotels in the census tract inferred from square footage for default values,
VISIT is the number of regional residents who do not live in the study area, visiting the census tract for shopping and entertainment (default is set to zero).

4.7.3 Direct Economic Losses

HAZUS provides estimates for structural and non-structural repair costs caused by building damage and the associated loss of building contents and business inventory. Business interruption and rental income losses are also estimated. Direct economic loss estimates are provided in 1994 dollars in HAZUS99 Release SR-2. Input data for this module consists of building damage estimates from the direct physical damage module. The damage estimates are in the form of probabilities of being in each damage state, for each structural type or occupancy class. These damage state probabilities are then converted to monetary losses using inventory information and economic data.

The next section includes descriptions of the methodologies and tables which explain a number of direct economic loss items derived from estimates of building damage.

4.7.3.1 Building Repair and Replacement Costs

For a given occupancy and damage state, building repair and replacement costs are estimates as the product of the floor area of each building type within the given occupancy, the probability of the building type being in the given damage state, and the repair costs of the building type per square foot for the given damage state, summed over all building types within the occupancy.

$$CS_i = \sum_{ds=2}^{5} CS_{ds,i} \quad \textbf{(4.6)}$$

$$CS_{ds,i} = CI * \sum_{j=1}^{36} FA_{i,j} * PBS_{ds,j} * RCS_{ds,i,j} \quad \textbf{(4.7)}$$

where:

$CS_{ds,i}$ is the cost of structural damage (repair and replacement costs) for damage state ds and occupancy i,

CS_i is the cost of structural damage (repair and replacement costs) for occupancy i,

CI is the regional cost index multiplier,

$FA_{i,j}$ is the floor area of model building type j in occupancy group i based on the total floor area of occupancy i and the distribution of the floor area between model building types,

$PBS_{ds,j}$ is the probability of model building type j being in structural damage state ds,

$RCS_{ds,i,j}$ is the structural repair and replacement costs (per square foot) for occupancy i and model building type j in damage state ds. A part of the tabular values for structural repair costs (dollars / square foot) in moderate damage state are shown in Table 4.13.

The repair costs for model building types within a structural system type are all the same. It should also be noted that damage state 'none' (ds=1) does not contribute to the calculation of the cost of structural damage and thus the summation in Equation 4.6 is from ds=2 to ds=5.

Table 4.13 Structural Repair Costs for Moderate Damage (Dollars per Square Foot)

	Structural System Type						
Occupancy	W1	S1	C1	PC1	RM1	URM	MH
RES1	1.5	1.5	1.5	1.5	1.5	1.5	1.5
COM1	1.5	1.5	1.5	1.5	1.5	1.5	1.5
IND1	0.8	0.8	0.8	0.8	0.8	0.8	0.8
AGR1	0.6	0.6	0.6	0.6	0.6	0.6	0.6
REL1	1.7	1.7	1.7	1.7	1.7	1.7	1.7
GOV1	1.2	1.2	1.2	1.2	1.2	1.2	1.2
EDU1	1.4	1.4	1.4	1.4	1.4	1.4	1.4

A similar calculation is performed for non-structural damage. Non-structural damage is broken down into acceleration and drift sensitive damage. It does not include the damage to contents such as furniture and computers. Non-structural damage costs are calculated as follows:

$$CNSA_i = \sum_{ds=2}^{5} CNSA_{ds,i} \quad \textbf{(4.8)}$$

$$CNSA_{ds,i} = CI * FA_i * PONSA_{ds,i} * RCA_{ds,i} \quad \textbf{(4.9)}$$

$$CNSD_i = \sum_{ds=2}^{5} CNSD_{ds,i} \quad \textbf{(4.10)}$$

$$CNSD_{ds,i} = CI * FA_i * PONSD_{ds,i} * RCD_{ds,i} \quad \textbf{(4.11)}$$

where:

$CNSA_{ds,i}$ is cost of acceleration sensitive non-structural damage for damage state ds and occupancy i,

$CNSA_i$ is the cost of acceleration sensitive non-structural damage for occupancy i,

$CNSD_{ds,i}$ is cost of drift sensitive non-structural damage for damage state ds and occupancy i,

$CNSD_i$ is the cost of drift sensitive non-structural damage for occupancy i,

FA_i is the floor area of occupancy group i (in square feet),

$PONSA_{ds,i}$ is the probability of the occupancy i being in non-structural acceleration sensitive damage state ds,

$PONSD_{ds,i}$ is the probability of the occupancy i being in non-structural drift sensitive damage state ds,

$RCA_{ds,i}$ is the acceleration sensitive non-structural repair and replacement costs (per square foot) for occupancy i in damage state ds (Table 4.14),

$RCD_{ds,i}$ is the drift sensitive non-structural repair and replacement costs (per square foot) for occupancy i in damage state ds (Table 4.15).

To determine the total cost of non-structural damage for occupancy class i (CNS_i), Equations 4.8 and 4.10 must be summed.

$$CNS_i = CNSA_i + CNSD_i \quad \textbf{(4.12)}$$

The total cost of building damage for occupancy class i is the sum of the structural and non-structural damage.

$$CBD_i = CS_i + CNS_i \quad \textbf{(4.13)}$$

Finally, to determine the cost of building damage, Equation 4.13 must be summed over all occupancy classes.

$$CBD = \sum_i CBD_i \quad \textbf{(4.14)}$$

Table 4.14 Acceleration Sensitive Non-structural Repair Costs ($/square foot)

No	Label	Occupancy Class	Acceleration Sensitive Non-structural Damage State			
			Slight	Moderate	Extensive	Complete
1	RES1	Single Family Dwelling	0.3	1.7	5.1	17.0
2	COM1	Retail Trade	0.4	2.2	6.6	22.0
3	IND1	Heavy Industrial Building	0.7	3.7	11.1	37.0
4	AGR1	Agriculture	0.1	0.6	1.8	6.0
5	REL1	Church/Membership Org.	0.8	4.1	12.3	41.0
6	GOV1	Government Services	0.7	3.3	9.9	33.0
7	EDU1	Schools/Libraries	0.5	2.4	7.2	24.0

Table 4.15 Drift Sensitive Non-structural Repair Costs ($/square foot)

No	Label	Occupancy Class	Drift Sensitive Non-structural Damage State			
			Slight	Moderate	Extensive	Complete
1	RES1	Single Family Dwelling	0.6	3.2	16.0	32.0
2	COM1	Retail Trade	0.3	1.4	7.0	14.0
3	IND1	Heavy Industrial Building	0.1	0.6	3.0	6.0
4	AGR1	Agriculture	*	0.1	0.5	1.0
5	REL1	Church/Membership Org.	0.6	2.8	14.0	28.0
6	GOV1	Government Services	0.4	2.2	11.0	22.0
7	EDU1	Schools/Libraries	0.7	3.6	18.0	36.0

It should be noted that the costs related with complete damage correspond to replacement costs since the complete damage state implies that the structure must be replaced. The replacement value of the structure is the sum of the structural and non-structural components. Hence to determine the total replacement cost per square foot for a particular occupancy, the following formulation is employed:

$$RC_i = CI * \left[RCA_{5,i} + RCD_{5,i} + RCS_{5,i} \right] \quad \textbf{(4.15)}$$

$$RCS_{5,i} = \sum_{j=1}^{36} RCMB_{5,i,j} * FA_{i,j} / FA_i \quad \textbf{(4.16)}$$

where:

RC_i is the replacement cost per square foot for occupancy i,

$RCA_{5,i}$ is the acceleration sensitive non-structural repair costs (per square foot) for occupancy i in damage state 5,

$RCD_{5,i}$ is the drift sensitive non-structural repair costs (per square foot) for occupancy i in damage state 5,

$RCS_{5,i}$ is the structural repair costs(per square foot) for occupancy i in damage state 5,

$RCMB_{5,i,j}$ is the structural replacement cost for model building type j in occupancy i in damage state 5.

CI, $FA_{i,j}$ and FA_i were defined previously.

4.7.3.2 Building Contents Losses

Building contents are defined as furniture and equipment that are not an integral part of the structure, computers and other supplies. It is assumed that most content damage is a function of building accelerations. Therefore, acceleration sensitive non-structural damage is considered to be a good indicator of contents damage. The cost of contents damage is calculated as follows:

$$CCD_i = CI * CV_i * \sum_{ds=2}^{5} CD_{ds,i} * RC_{ds,i} \quad \textbf{(4.17)}$$

$$RC_{ds,i} = \sum_{j=1}^{36} PBNSA_{ds,j} * FA_{i,j} * \left(RCA_{5,i} + RCD_{5,i} + RCMB_{5,i,j}\right) \quad \textbf{(4.18)}$$

where:

CCD_i is the cost of contents damage for occupancy i,

CV_i is contents value for occupancy i, expressed as percent of replacement value (Table 4.16),

$CD_{ds,i}$ is the percent contents damage for occupancy i in damage state ds (Table 4.17),

$RC_{ds,i}$ is the replacement cost (in dollars) for occupancy i in damage state ds,

$PBNSA_{ds,j}$ is the probability of model building type j being in non-structural acceleration sensitive damage state ds.

Table 4.16 Contents Value as Percentage of Building Replacement Value

No	Label	Occupancy Class	Contents Value (%)
1	RES1	Single Family Dwelling	50
2	COM1	Retail Trade	100
3	IND1	Heavy Industrial Building	150
4	AGR1	Agriculture	100
5	REL1	Church/Membership Org.	100
6	GOV1	Government Services	100
7	EDU1	Schools/Libraries	100

$FA_{i,j}$, $RCA_{5,i}$, $RCD_{5,i}$ and $RCMB_{5,i,j}$ were previously defined. Table 4.16 provides default contents values for each occupant as a percentage of the replacement value of the facility. The contents damage percentages in Table 4.17 assume that when in a complete damage state, some percentage of contents, set at 15%, can be retrieved.

Table 4.17 Percent Contents Damage

No	Label	Occupancy Class	Acceleration Sensitive Non-structural Damage State			
			Slight	Moderate	Extensive	Complete
1	RES1	Single Family Dwelling	1	5	25	50
2	COM1	Retail Trade	1	5	25	50
3	IND1	Heavy Industrial Building	1	5	25	50
4	AGR1	Agriculture	1	5	25	50
5	REL1	Church/Membership Org.	1	5	25	50
6	GOV1	Government Services	1	5	25	50
7	EDU1	Schools/Libraries	1	5	25	50

4.7.3.3 Business Inventory Losses

There are two main assumptions for this loss model: The first assumption is that the business inventory for each occupancy class is based on annual sales. The second assumption is that, as it was with building contents, acceleration sensitive non-structural damage is a good indicator of losses to business inventory. The business inventory losses are given by the following expressions.

$$INV = INV_7 + INV_8 + \sum_{i=17}^{23} INV_i \qquad \textbf{(4.19)}$$

$$INV_i = FA_i * SALES_i * BI_i * \sum_{ds=2}^{5} PNSA_{ds,i} * INVD_{ds,i} \qquad \textbf{(4.20)}$$

where :

INV_i is the value of inventory losses for occupancy i,

INV is the total value of the inventory losses,

$SALES_i$ is the annual gross sales or production (per square foot) for occupancy i (Table 4.18),

BI_i is the business inventory as a percentage of annual gross sales for occupancy i where i=7,8,17-23 (Table 4.19),

$INVD_{ds,i}$ is the percent inventory damage for occupancy i in damage state ds (Table 4.20).

FA_i and $PONSA_{ds,i}$ were previously defined.

Table 4.18 Annual Gross Sales or Production ($/sq. ft.)

No	Label	Occupancy Class	1990 Output / Employment	Sq. ft. floor space /Employee	Annual Sales ($/ft^2)
		Commercial			
7	COM1	Retail Trade	$24,979	825	30
8	COM2	Wholesale Trade	$38,338	900	43
		Industrial			
17	IND1	Heavy	$220,212	550	400
18	IND2	Light	$74,930	590	127
19	IND3	Foods/drugs/chemicals	$210,943	540	391
20	IND4	Metals/Minerals Processing	$268,385	730	368
21	IND5	High Technology	$73,517	300	245
22	IND6	Construction	$107,739	250	431
		Agriculture			
23	AGR1	Agriculture	$20,771	250	83

Table 4.19 Business Inventory (% of Gross Annual Sales)

No	Label	Occupancy Class	Business Inventory (%)
		Commercial	
7	COM1	Retail Trade	13
8	COM2	Wholesale Trade	10
		Industrial	
17	IND1	Heavy	5
18	IND2	Light	4
19	IND3	Foods/drugs/chemicals	5
20	IND4	Metals/Minerals Processing	3
21	IND5	High Technology	4
22	IND6	Construction	2
		Agriculture	
23	AGR1	Agriculture	8

Table 4.20 Percent Business Inventory Damage

No	Label	Occupancy Class	Acceleration Sensitive Non-structural Damage State			
			Slight	Moderate	Extensive	Complete
		Commercial				
7	COM1	Retail Trade	1	5	25	50
8	COM2	Wholesale Trade	1	5	25	50
		Industrial				
17	IND1	Heavy	1	5	25	50
18	IND2	Light	1	5	25	50
19	IND3	Foods/drugs/chemicals	1	5	25	50
20	IND4	Metals/Minerals Processing	1	5	25	50
21	IND5	High Technology	1	5	25	50
22	IND6	Construction	1	5	25	50
		Agriculture				
23	AGR1	Agriculture	1	5	25	50

4.7.3.4 Building Repair Time / Loss of Function

Loss of function is the time that a facility is not capable of conducting business. This, in general, will be shorter than repair time because a business will rent alternative space while repairs and construction are being completed. The time to repair a damaged building can be divided into two parts: construction and clean-up time (Table 4.21), and time to obtain financing, permits and complete design (Table 4.22). For the lower damage states, the construction time will be close to the real repair time. At the higher damage levels, a number of additional tasks such as decision making, financing, inspection etc. that will increase the actual repair time must be undertaken.

For some businesses, building repair time is largely irrelevant, because alternative space can be rented or they may have spare industrial/commercial elsewhere which can be used. These factors are presented in Table 4.23, which provides multipliers to be applied to the values in Table 4.22 to arrive at estimates of business interruption for economic purposes. The modifiers from Table 4.23 are multiplied by extended building construction times as follows:

$$LOF_{ds} = BCT_{ds} * MOD_{ds} \quad \textbf{(4.21)}$$

Table 4.21 Building Clean-up and Repair Time (Construction) (Time in days)

No	Label	Occupancy Class	Construction Time				
			Structural Damage State				
			None	Slight	Moderate	Extensive	Complete
1	RES1	Single Family Dwelling	0	2	30	90	180
2	COM1	Retail Trade	0	5	30	90	180
3	IND1	Heavy Industrial Building	0	10	30	120	240
4	AGR1	Agriculture	0	2	10	30	60
5	REL1	Church/Membership Org.	0	10	30	120	240
6	GOV1	Government Services	0	10	30	120	240
7	EDU1	Schools/Libraries	0	10	30	120	240

Table 4.22 Building Recovery Time (Time in days)

No	Label	Occupancy Class	Recovery Time				
			Structural Damage State				
			None	Slight	Moderate	Extensive	Complete
1	RES1	Single Family Dwelling	0	5	120	360	720
2	COM1	Retail Trade	0	10	90	270	360
3	IND1	Heavy Industrial Building	0	10	90	240	360
4	AGR1	Agriculture	0	2	20	60	120
5	REL1	Church/Membership Org.	0	5	120	480	960
6	GOV1	Government Services	0	10	90	360	480
7	EDU1	Schools/Libraries	0	10	90	360	480

Table 4.23 Building and Service Interruption Time Multipliers

No	Label	Occupancy Class	Construction Time				
			Structural Damage State				
			None	Slight	Moderate	Extensive	Complete
1	RES1	Single Family Dwelling	0	0	0.5	1	1
2	COM1	Retail Trade	0.5	0.1	0.1	0.3	0.4
3	IND1	Heavy Industrial Building	0.5	0.5	1	1	1
4	AGR1	Agriculture	0	0	0.05	0.1	0.2
5	REL1	Church/Membership Org.	1	0.2	0.05	0.03	0.03
6	GOV1	Government Services	0.5	0.1	0.02	0.03	0.03
7	EDU1	Schools/Libraries	0.5	0.1	0.02	0.05	0.05

where:

LOF_{ds} is loss of function for damage state ds,

BCT_{ds} is building construction and cleanup time for damage state ds (Table 4.22),

MOD_{ds} is the construction time modifiers for damage state ds (Table 4.23).

4.7.3.5 Relocation Expenses

Relocation costs may be incurred while repairs are being made when the level of the building damage is such that the building or portions of the building are unusable. In this model, the following relocation expenses are considered: disruption costs that include the cost of shifting and transferring, and the rental of temporary space.

There are two assumptions in the calculation of the relocation expenses: First, it is unlikely that an occupant will relocate if a building is in damage states of 'None' or 'Slight'. Second, it is assumed that entertainment, theaters, parking facilities and heavy industry will not relocate to new facilities, instead they will resume operation until the repairs or replacements have been completed. Hence relocation costs can be calculated as follows:

$$REL_i = FA_i * \left[\begin{array}{c} (1 - PO_i) * \sum_{ds=3}^{5} \left(POST_{ds,i} * DC_i \right) + \\ PO_i * \sum_{ds=3}^{5} \left(POST_{ds,i} * \left(DC_i + RENT_i * RT_{ds} \right) \right) \end{array} \right] \quad \textbf{(4.22)}$$

where:

REL_i is the relocation cost for occupancy class i (i=1-13 and 18-28),

$POST_{ds,i}$ is the probability of occupancy class I being in structural damage state ds,

DC_i is the disruption costs for occupancy i ($/ft^2, Table 4.24),

RT_{ds} is the recovery time for damage state ds (Table 4.22),

PO_i is the percent owner occupied for occupancy i (Table 4.25),

$RENT_i$ is the rental cost ($/ft^2/day) for occupancy i (Table 4.24).

Table 4.24 Rental Costs and Disruption Costs

No	Label	Occupancy Class	Rental Cost		Disruption Costs
			($/ft^2/month)	($/ft^2/day)	($/ft^2)
1	RES1	Single Family Dwelling	0.50	0.02	0.60
2	COM1	Retail Trade	0.85	0.03	0.80
3	IND1	Heavy Industrial Building	0.15	0.01	N/A
4	AGR1	Agriculture	0.50	0.02	0.50
5	REL1	Church/Membership Org.	0.75	0.03	0.70
6	GOV1	Government Services	1.00	0.03	0.70
7	EDU1	Schools/Libraries	0.75	0.03	0.70

Table 4.25 Percent Owner Occupied

No	Label	Occupancy Class	Percent Owner Occupied
1	RES1	Single Family Dwelling	75
2	COM1	Retail Trade	55
3	IND1	Heavy Industrial Building	75
4	AGR1	Agriculture	95
5	REL1	Church/Membership Org.	90
6	GOV1	Government Services	70
7	EDU1	Schools/Libraries	95

4.7.3.6 Loss of Income

Income losses occur when building damage disrupts economic activity. Income losses are the product of the floor area, income realized per square foot and the expected days of loss of function for each damage state. Proprietor's income losses are expressed as follows:

$$YLOS_i = (1 - RF_i) * FA_i * INC_i * \sum_{ds=1}^{5} POST_{ds,i} * LOF_{ds} \quad \textbf{(4.23)}$$

where:

$YLOS_i$ is the income loss for occupancy class i,

INC_i is the income per day (per square foot) for occupancy class i (Table 4.26),

RF_i is the recapture factor for occupancy class i (see next paragraph).

FA_i, $POST_{ds,i}$ and LOF_{ds} were previously explained. The values of LOF_{ds} should be taken from Equation 4.21.

Table 4.26 Proprietor's Income

No	Label	Occupancy Class	Income		Wages	Employees	Output
			per sq. ft. per year	per sq. ft. per day	per sq. ft. per day	per sq. ft.	per sq. ft. per day
1	RES1	Single Family Dwelling	0.000	0.000	0.000	0.000	0.000
2	COM1	Retail Trade	16.299	0.045	0.156	0.004	0.330
3	IND1	Heavy Industrial Building	66.808	0.183	0.303	0.003	1.281
4	AGR1	Agriculture	61.810	0.169	0.067	0.004	0.632
5	REL1	Church/Membership Org.	35.220	0.096	0.227	0.004	1.264
6	GOV1	Government Services	28.925	0.079	2.180	0.025	0.506
7	EDU1	Schools/Libraries	44.025	0.121	0.284	0.005	2.449

The business related losses from earthquakes can be recouped to some extent by working overtime after the event. Table 4.27 presents a set of recaptured factors for the economic sectors used in the direct loss module. They are deemed appropriate for business disruptions lasting up to three months.

Table 4.27 Recapture Factors

Occupancy	Wage Recapture (%)	Employment Recapture (%)	Income Recapture (%)	Output Recapture (%)
RES1	0	0	0	0
COM1	0.87	0.87	0.87	0.87
IND1	0.98	0.98	0.98	0.98
AGR1	0.75	0.75	0.75	0.75
REL1	0.60	0.60	0.60	0.60
GOV1	0.80	0.80	0.80	0.80
EDU1	0.60	0.60	0.60	0.60

4.7.3.7 Rental Income Losses

Rental income losses include residential, commercial and industrial properties. Rental income losses are calculated only for damage states 3, 4 and 5 since it is assumed that a renter will pay full rent if the property is in the damage state none or slight. Hence,

$$RY_i = (1 - PO_i) * FA_i * RENT_i * \sum_{ds=3}^{5} POST_{ds,i} * RT_{ds} \quad \textbf{(4.24)}$$

where RY_i is the rental income loss for occupancy i. All other terms were previously explained. Hence for PO_i, $RENT_i$ and RT_{ds}, refer to Tables 4.25, 4.24 and 4.22, respectively.

4.7.4 Indirect Economic Losses

Earthquakes may produce dislocations in economic sectors not sustaining direct damage. All businesses are forward-linked (rely on regional customers to purchase their output) or backward-linked (rely on regional suppliers to provide their inputs) and are thus potentially vulnerable to interruptions in their operation. Such interruptions are called indirect economic losses. It should be noted that these losses are not confined to immediate customers or suppliers of damaged enterprises. All of the successive round of customers of customers and suppliers of suppliers are impacted. In this way, even limited earthquake physical damage causes a chain reaction, or ripple effect, that is transmitted through the regional economy.

The Indirect Loss Module is a computational algorithm that utilizes input-output coefficients to reallocate surviving production. The algorithm computes post-event excess demands and supplies. It rebalances the economy by drawing from imports, inventories, and idle capacity when supplies are constrained. It allows for inventory accumulation, production for export (to other regions) and sales to meet reconstruction needs in the event that normal demands are insufficient to absorb excess supplies. The process of reallocation is governed by the amount of imbalance detected in each of the economy's sectors. Rebalancing is accomplished iteratively by

adjusting production proportionately until the discrepancy between supplies and demands is within a tolerable limit. In the HAZUS Technical Manual it is stated that the Indirect Loss Module is new and experimental and still needs considerable refinement. The results obtained from this module will be much more plausible in the future versions of HAZUS software.

5. IMPLEMENTATION OF FLAT-SLAB STRUCTURES IN HAZUS

As it was mentioned previously, the building types available in HAZUS do not contain flat-slab structures specifically. Hence it will be a novel study to implement the derived fragility curves into HAZUS and estimate the earthquake losses in flat-slab structures by making use of the methodology. However, to achieve this, the differences between the two methodologies to develop fragility curves must be fully understood since it will not make sense to compare the sets of curves without knowing the underlying assumptions and the analytical or the empirical tools involved. The work presented in this chapter is an attempt to compare the procedures employed in the derivation of fragility curves of the flat-slab structure with the built-in HAZUS functions and then to implement the derived fragility curves into HAZUS. In the implementation process, the Advanced Engineering Building Module (AEBM) of HAZUS is employed. This module is intended to facilitate site-specific building loss estimation analysis. It allows the user to input building specific data and override the default fragility curves for individual structures. The final part of this section is devoted to the prediction of earthquake losses in flat-slab buildings with comparison to the built-in structural types in HAZUS subjected to different scenario earthquakes in two study regions; Urbana, IL and Shelby County, TN.

5.1 Differences in Methodologies for Constructing Fragility Curves

Since there is not a unique way for developing the fragility curves, each methodology has its own assumptions and procedures, mostly reflecting the goals of that individual study. The same argument is also valid for the methodology of the current study and HAZUS. Therefore, before implementing the derived fragility curves into HAZUS software, one should be aware of the differences between these two methodologies. The most significant ones are:

- Fragility curves in HAZUS are created using a combination of engineering analysis, laboratory and other empirical component data, and the expert opinion of several structural engineers. The use of expert opinion is a factor that weakens the conclusions reached by the study since it lacks a scientific basis. Hence it is highly subjective and

open to discussion. The structural analysis method used in HAZUS is the Capacity Spectrum Method (CSM). On the other hand, the methodology used in this study utilizes the nonlinear time-history analysis, the most elaborate and accurate way of calculating the seismic response, as the computation method.

- In the case of developing category-based fragility curves (i.e. creating fragility functions for an entire class of buildings) such as flat-slab structures, additional sources of uncertainty originating from geometric configuration (number of stories and bays), design details and quality of construction exists. These types of uncertainties are not accounted for in this study. The fragility curves are derived employing one 5-story, 3-bay flat-slab structure only. Although the HAZUS Methodology is a category-based approach, there is not sufficient technical information about the selection of building models in deriving the curves for each building category. On the other hand, different set of curves are constructed in HAZUS differentiated by height (low-, mid- and high-rise), seismic design level (low, moderate and high seismic design) and seismic performance level or quality (code/ordinary, pre-code/inferior and special/superior) within each category. The fragility curves representing the flat-slab structures in this study fit within the HAZUS category of mid-rise construction and moderate seismic design level. The seismic performance of the building can be assumed to be ordinary.

- HAZUS fragility curves represent categories of buildings and are not building specific. According to the HAZUS Technical Manual (National Institute of Building Sciences, 1999b), fragility curves are more reliable as predictors of damage for large, rather than small, population of buildings although they are theoretically applicable to a single building as well as to all buildings of a given type. In contrast with the category based approach of HAZUS, the fragility curves in this study are derived for an individual flat-slab building with a complicated analytical model; hence they are more building-specific.

- A very significant distinction between the two methodologies is that the HAZUS fragility curves are derived based on the damped elastic spectral displacement at the intersection of a pushover curve and the earthquake response spectrum. However the fragility curves

derived in this study are functions of spectral displacement at fundamental period of the building. Because of this period discrepancy, there is not a one-to-one correspondence between the two sets of curves. This difference in definition of the seismic hazard has also been pointed out by Porter et al. (2001). Their study focused on improving the loss estimation methods for wood-frame structures by using a new methodology called the Assembly-Based Vulnerability (ABV). They derived the fragility curves for 19 distinct wood-frame buildings of varying ages, sizes, configuration, quality of construction, retrofit and redesign conditions. The resulting fragility curves give the distribution of damage as a function of spectral amplitude at the fundamental frequency. Hence they used a simple method in order to transform their curves to provide HAZUS-compatible vulnerability functions. A similar approach is also used in this study to obtain HAZUS-compatible fragility curves for flat-slab structures. This is explained in more detail in the next section.

5.2 Procedure for Obtaining HAZUS-compatible Fragility Curves

The above discussion indicates the discrepancy in the interpretation of the hazard parameter used in both methodologies. In this study, the spectral parameter is a function of the fundamental period of the structure whereas in HAZUS it represents the period at the intersection point of a pushover curve and an earthquake response spectrum. Hence a procedure is required to convert the derived curves into the HAZUS format for the sake of developing a comparative basis. The procedure used by Porter et al. (2001) for the derivation of HAZUS compatible fragility curves for wood-frame structures is summarized as follows:

1. Each of the 19 wood-frame buildings used in their study is associated with a HAZUS building type. Since the buildings are mapped into HAZUS classes, the push-over curve of the corresponding HAZUS building type is assumed to represent the wood-frame building under consideration.
2. The ABV analysis is used to obtain the seismic response for each simulation. The response is in terms of the damage factor, which is the repair cost for structural and non-

structural building components, divided by the replacement cost of the entire building. The damage state based on the computed damage factor is determined using Table 5.1, which is based on personal judgment.

3. For each ABV simulation, the spectral displacement at the intersection of the selected pushover curve and the response spectrum of the scaled ground motion used in the ABV analysis is obtained.
4. Employing the damage state data obtained in Step 2 and hazard data (spectral displacement) obtained in Step 3, statistics of the probability of reaching or exceeding each damage state, versus the spectral displacement is compiled and the parameters of the fragility curve are obtained by regression analysis.

Table 5.1 Relationship between the HAZUS Damage States and the Damage Factor

HAZUS Damage States	Damage Factor
Slight	0.1-5%
Moderate	5-20%
Extensive	20-50%
Complete	50-100%

The procedure described above is a simple one with many assumptions. A similar procedure is used in this study to interpret the derived vulnerability functions in the HAZUS-compatible format. However, a simple verification about the re-interpretation of the fragility curves in HAZUS format is presented before explaining the procedure employed to obtain the HAZUS-compatible fragility curves.

CSM is used in the verification process. It is based on the determination of the intersection period of the pushover curve and the earthquake response spectrum in S_a versus S_d (ADRS) format and then the comparison of the derived fragility curves with the ones embedded in HAZUS. This simple verification is supported by two examples in the report.

The first example utilizes mean curves, i.e. a pushover curve obtained with mean material properties and an elastic spectrum obtained by averaging the spectral values of the ground motions used in the study (Table 3.1). The pushover curve, which is in terms of base shear and roof displacement, is converted into a capacity spectrum, which is in terms of spectral acceleration and spectral displacement by using (ATC, 1996)

$$S_a = \frac{V/W}{\alpha_1} \tag{5.1}$$

$$S_d = \frac{\Delta_{roof}}{PF_1 \, \phi_{roof,1}} \tag{5.2}$$

where V is the base shear, W is the dead weight of the building, Δ_{roof} is the roof displacement and $\phi_{roof,1}$ is the amplitude of first mode at roof level. PF_1 is the modal participation factor for the first mode and given by the equation

$$PF_1 = \left[\frac{\sum_{i=1}^{N} \left(w_i \, \phi_{i,1} \right) / g}{\sum_{i=1}^{N} \left(w_i \, \phi_{i,1}^2 \right) / g} \right] \tag{5.3}$$

where w_i/g is the mass assigned to story level i and $\phi_{i,1}$ is the amplitude of the first mode at the same level i. Finally, the parameter α_1 is the modal mass coefficient for the first mode and can be defined as

$$\alpha_1 = \frac{\left[\sum_{i=1}^{N} \left(w_i \, \phi_{i,1} \right) / g \right]^2}{\left[\sum_{i=1}^{N} w_i / g \right] \left[\sum_{i=1}^{N} \left(w_i \, \phi_{i,1}^2 \right) / g \right]} \tag{5.4}$$

The capacity spectrum and the mean elastic spectrum are both illustrated in Figure 5.1.a. The line which is tangent to the initial part of the capacity spectrum is the fundamental period of the flat-slab structure (T=0.38 seconds). The other line which lies between the origin and the intersection

point of the capacity and the demand spectra is the period value (T=0.69 seconds) which is used in the development of the HAZUS fragility functions. The difference between these two interpretations of structural period becomes clearer in Figure 5.1.b. The figure shows the period values and the corresponding spectral displacement values on the mean displacement spectrum, obtained by averaging the spectral displacement values of the ground motions used in the study. The spectral displacement obtained by using the fundamental period, $S_d(T_o)$, is equal to 10 mm whereas the spectral displacement value obtained by using the intersection period, $S_d(T_c)$, is equal to 25 mm. Since $S_d(T_o)$ and $S_d(T_c)$ correspond to the same level of seismic performance (same structural capacity and ground motion intensity), they should address similar values of damage distribution when the corresponding fragility functions are involved. This is illustrated in Figure 5.2. The sets of fragility curves belong to the HAZUS moment resisting frames (Figure 5.2.a) and the flat-slab structure used in this study (Figure 5.2.b), which are functions of spectral displacement at the intersection period and the fundamental period, respectively. The vertical lines on the figures represent the distribution of damage obtained from the same level of seismic intensity, but interpreted in different ways for the fragility curves. Hence HAZUS curves give 92% None-Slight Damage (70% None, 22% Slight) and 8% Moderate Damage whereas the study curves give 100% Slight Damage. The results are not discouraging when considering the vast differences encountered in the development of these two sets of fragility functions.

For the sake of comparison, another case is considered, this time with a scaled ground motion from the set and the inelastic demand spectra to locate the performance point. The selected record is GM7, taken from a 15 story Governmental Office Building in L.A. during the 1994 Northridge Earthquake (Table 3.1). The Capacity Spectrum Method is illustrated in Figure 5.3.a. A bilinear approximation is fitted to the capacity spectrum. The intersection period is obtained by trial and error at a ductility value of approximately 5 for the capacity spectrum and the inelastic demand spectrum. The value of the intersection period is equal to 1.34 seconds. The spectral displacement values corresponding to the intersection period and the elastic fundamental period are shown in Figure 5.3.b using the displacement spectrum of the scaled ground motion record. These are 225 mm and 45 mm, respectively. When the values are inserted into the corresponding fragility curves, a similar damage distribution is obtained (Table 5.2 and Figure 5.4). The results obtained verify that the fragility curves can only be compared after proper

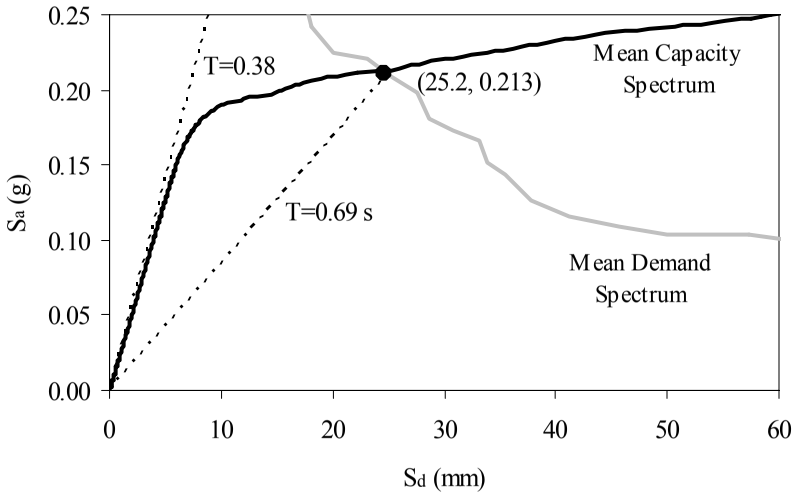

Figure 5.1.a Capacity Spectrum Method with Mean Curves

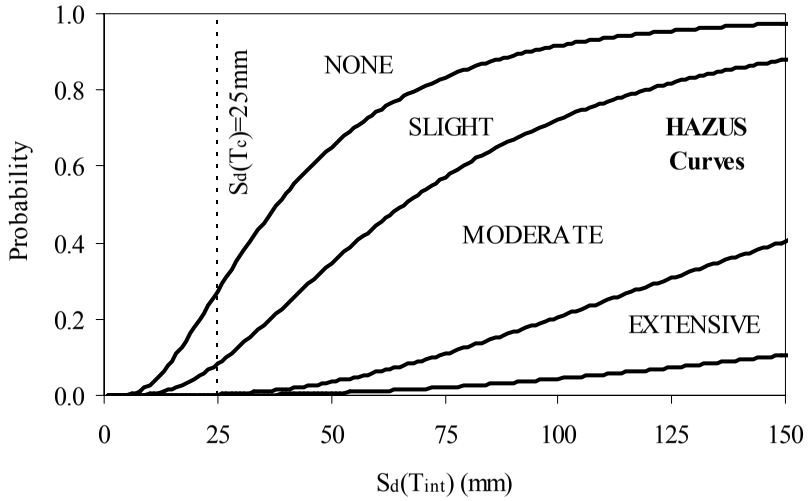

Figure 5.2.a Damage Distribution using HAZUS Curves

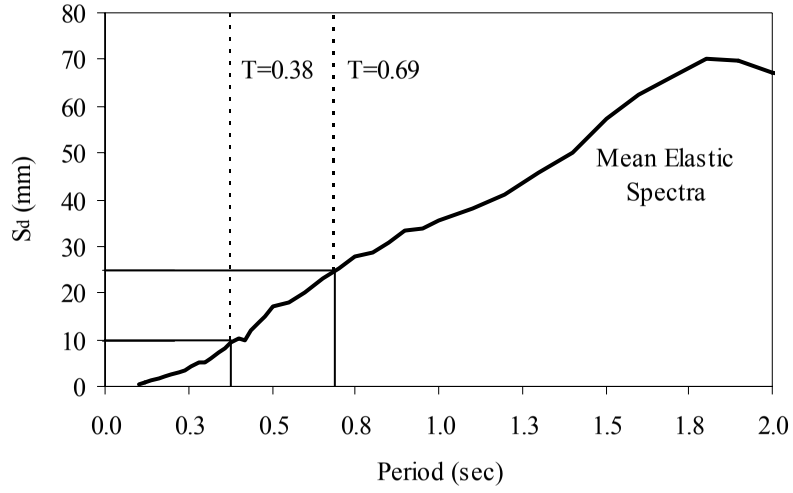

Figure 5.1.b Corresponding Spectral Displacement Values

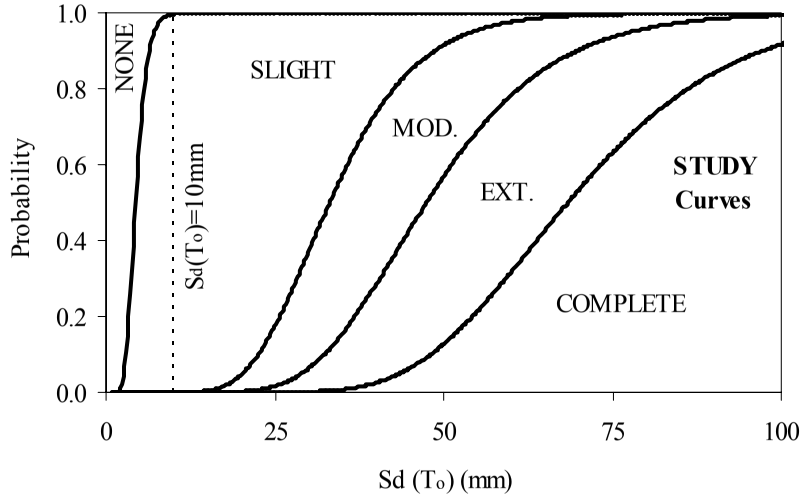

Figure 5.2.b Damage Distribution using Study Curves

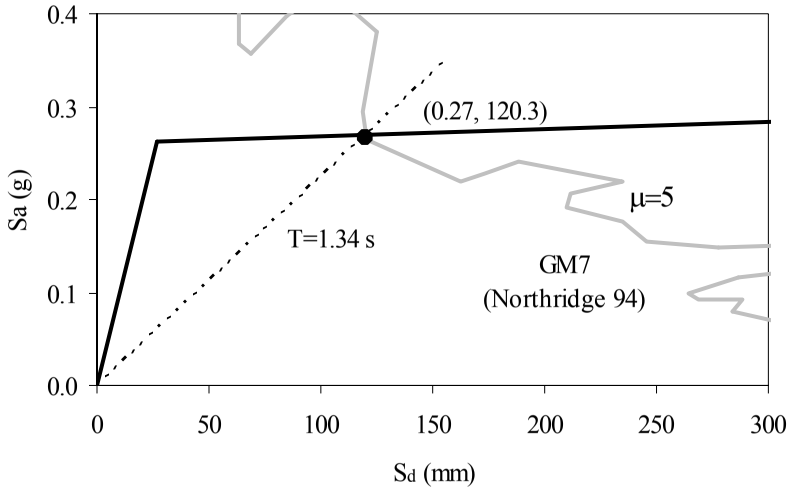

Figure 5.3.a Capacity Spectrum Method with GM7

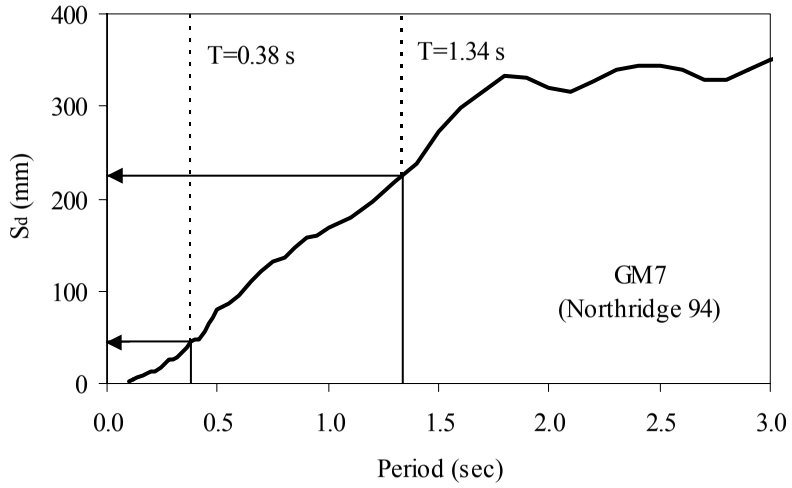

Figure 5.3.b Corresponding Spectral Displacement Values

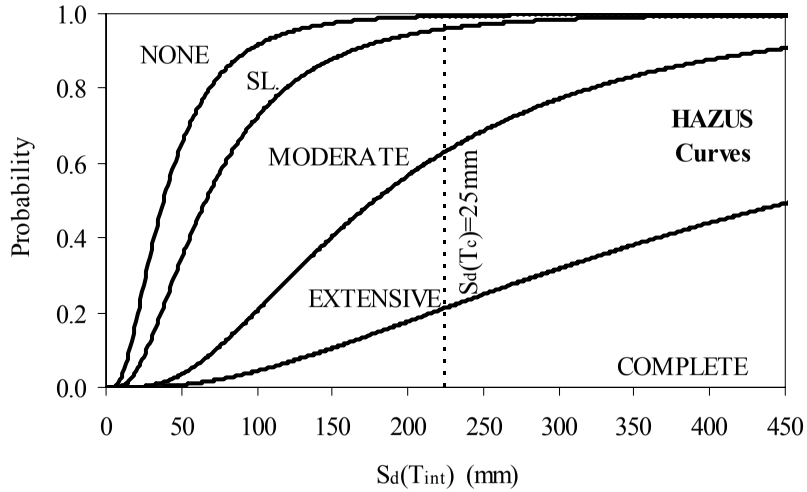

Figure 5.4.a Damage Distribution using HAZUS Curves

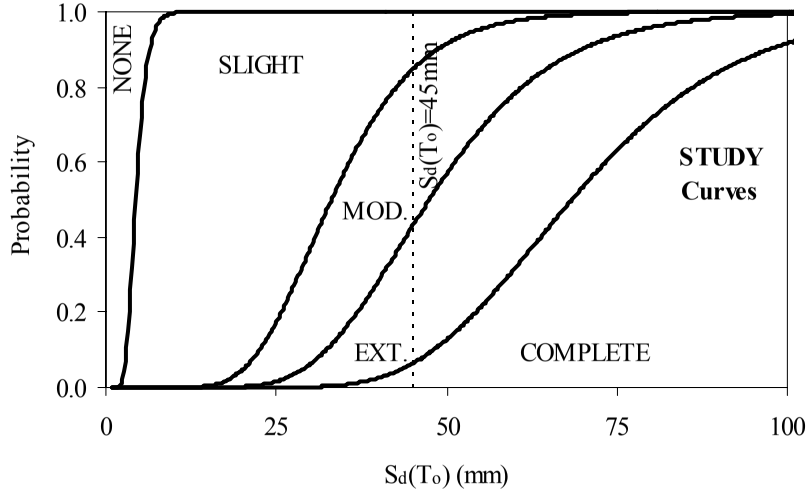

Figure 5.4.b Damage Distribution using Study Curves

interpretation of the spectral displacement as a seismic hazard parameter. They also encourage the use of the conversion procedure to obtain HAZUS-compatible fragility information as described in the following section.

Table 5.2 Comparison of Damage Distribution by Using HAZUS and Study Curves

	None	**Slight**	**Moderate**	**Extensive**	**Complete**
HAZUS Curves	-	3%	36%	40%	21%
Study Curves	-	14%	42%	36%	8%

Procedure to obtain HAZUS-compatible fragility curves:

The procedure enables the use of previously obtained seismic response from time-history analysis together with the data obtained from CSM. For each time-history simulation, the spectral displacement at the intersection of the related capacity spectrum and the demand spectrum of the related scaled ground motion is obtained. A similar procedure was used by Porter et al (2001) to develop HAZUS-compatible fragility curves for woodframe buildings with some differences. First, they associated their sample buildings with HAZUS building types. In other words, they used the pushover parameters available in HAZUS for woodframe buildings. On the contrary, the corresponding pushover curve for each structural simulation is constructed in this current procedure. Another point is that they did not employ the classical CSM to obtain the required spectral displacement values. Instead, they directly compared the HAZUS-based pushover curves with the response spectrum of the ground motions that they used in time-history analysis without considering the hysteretic damping and obtained the spectral displacement values without any iteration. However, the current procedure uses a Capacity Spectrum Procedure proposed by Freeman (1998), which is very similar to the ATC-40 (1996) Procedure. It takes hysteretic damping into account based on the principles given in ATC-40. The relationship between damped linear elastic response spectra and inelastic response spectra is considered such that the elastic damping ratios can be equated to ductility ratios for various characteristics of hysteretic behavior.

Details of each step of this procedure, for using time-history data with CSM to develop fragility curves, is presented below.

1) The pushover curves are constructed. To achieve this, the structural analysis software, ZEUS-NL, is utilized. The pushover curves are derived for each input data line shown in Table 3.7 to account for the material variability. Hence 30 different pushover curves are constructed. Then the curves are converted to the ADRS format by employing Equations 5.1-5.4. The resulting capacity spectra are shown in Figure 5.5.

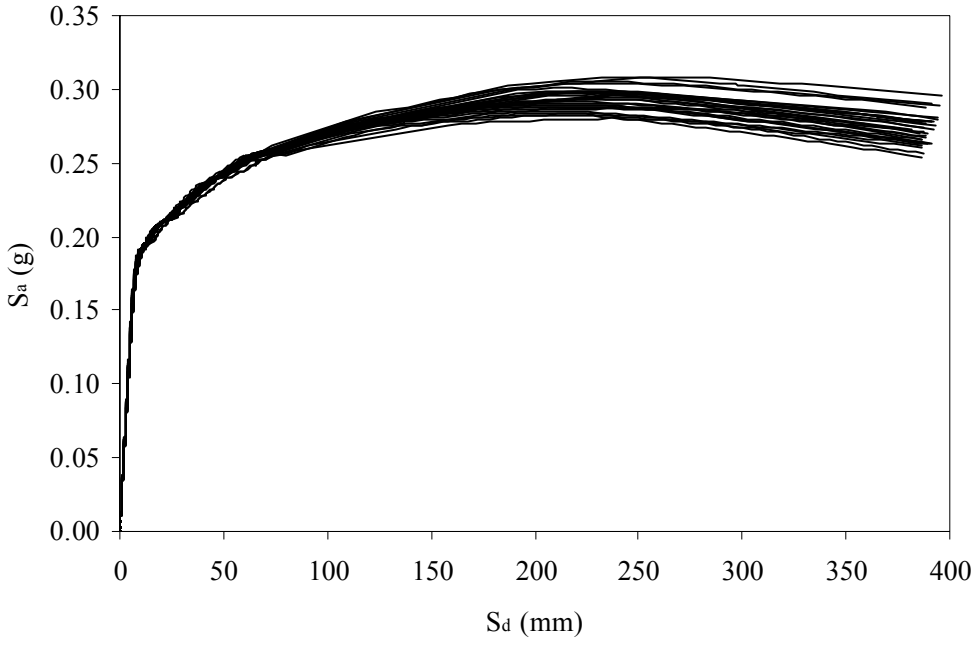

Figure 5.5 The Capacity Spectra for Each Set of Material Properties

For simplicity, a bilinear approximation is fitted to each curve. Equal energy principle is used in the approximation. In other words, the area under the bilinear curve is set approximately equal to the area under the capacity spectrum.

2) The response spectra of the ground motions used in the study are constructed for different values of damping. Obviously, 5% damped response spectrum represents the demand when the

structure is responding linearly elastic whereas higher damped response spectra are used to represent inelastic response spectra to account for hysteretic nonlinear response of the structure. A sample family of response spectra is illustrated in Figure 5.6 for GM7 (from 1994 Northridge Earthquake).

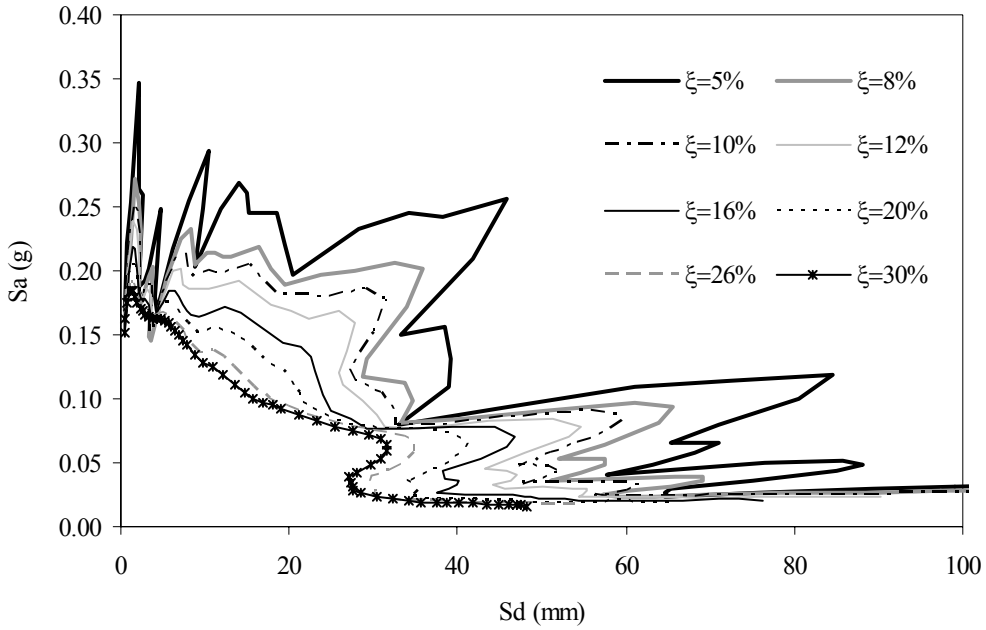

Figure 5.6 Family of Response Spectra in ADRS Format for GM7

3) After defining both the capacity and the response spectra with the same set of coordinates (S_a-S_d format), the CSM can be applied to match with each simulation that has been defined before in the development of fragility curves for flat-slab structures. However this indicates that CSM should be used for 3300 times to account for each simulation, corresponding to each time-history analyses. The number of CSM that should be applied to develop HAZUS-compatible fragility curves can be reduced by assuming mean structural properties. Figure 5.5 encourages the use of this assumption since the material variability does not have a significant effect on the capacity curves. Hence it is possible to match the results of simulations obtained by considering mean values with the CSM results for the same structural properties.

An important aspect of CSM is to define the relationship between the inelastic response spectra and the equivalent linear elastic response spectra, or in other words, relate effective damping to ductility. The method used in this study is based on ATC-40, which states that hysteretic damping is related to the area inside the loops that are formed when seismic force is plotted against structural displacement. Hence equivalent viscous damping, denoted as β_{eq}, can be written in the form

$$\beta_{eq} = \beta_o + 0.05 \qquad \textbf{(5.5)}$$

where β_o is hysteretic damping represented as equivalent viscous damping. In the formulation, a viscous damping value of 5% is assumed to be inherent in the structure. There are several ways to represent hysteretic damping in the form of equivalent viscous damping. The one used in ATC-40 is proposed by Chopra (1995)

$$\beta_o = \frac{1}{4\pi}\frac{E_D}{E_{So}} \qquad \textbf{(5.6)}$$

In this equation, E_D is the energy dissipated by damping and E_{So} is the maximum strain energy. Representing a typical hysteresis loop in the shape of a parallelogram (Figure 5.7) and referring to Equations 5.5 and 5.6, β_{eq} can be written as (in terms of percent critical damping)

$$\beta_{eq} = \frac{63.7\left(a_y d_{pi} - d_y a_{pi}\right)}{a_{pi} d_{pi}} + 5 \qquad \textbf{(5.7)}$$

where a_y, d_y, a_{pi} and d_{pi} are defined on the figure. It should be kept in mind that the derivations for equivalent damping are for a hysteresis loop with an idealized behavior (no stiffness or strength degradation, or pinching). However this is not the case for most of the building structures and using the results of idealized behavior can cause overestimations of equivalent viscous damping. In order to prevent this, a damping modification factor, κ, is introduced in ATC-40 to simulate the imperfect loops and the degraded structural behavior. By the addition of κ–factor, Equation 5.7 takes the form

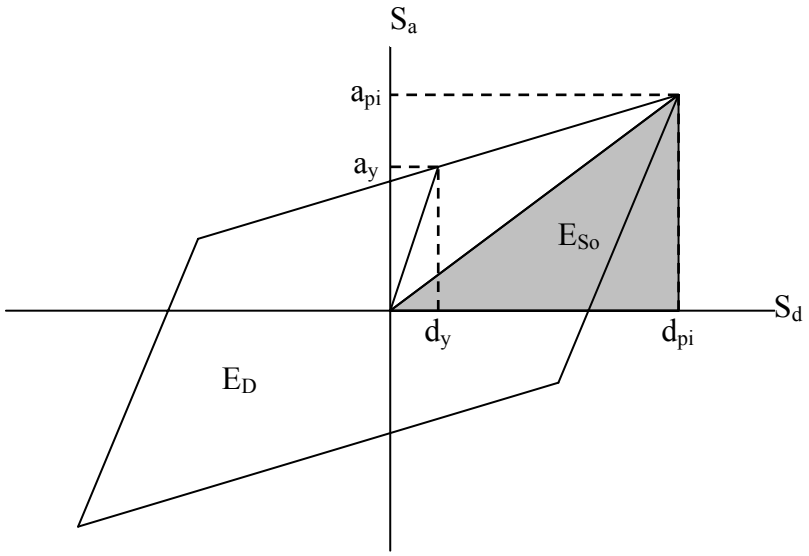

Figure 5.7 Bilinear Representation of Capacity Spectrum

$$\beta_{eq} = \frac{63.7\,\kappa\left(a_y d_{pi} - d_y a_{pi}\right)}{a_{pi} d_{pi}} + 5 \qquad \textbf{(5.8)}$$

ATC-40 simulates three categories of structural behavior. Structural behavior Type A represents stable, reasonably full hysteresis loops. Type B represents a moderate structural performance, therefore a moderate reduction of area is considered in the hysteresis loops. Type C represents poor hysteretic behavior (severe pinching) with a substantial reduction of loop area. The values assigned to κ for different structural behavior types are given in Table 5.3. In this study, the flat-slab building is assumed to be a Type B Structure, to account for the structural weaknesses and imperfections and κ-value is calculated accordingly.

Since d_{pi}/d_y is equal to ductility, β_{eq} values can be computed for different values of ductility by employing the properties of the bilinear approximation fitted to the capacity spectrum with the mean structural properties. Samples of calculated values are given in Table 5.4 along with κ-values.

Table 5.3 Values for Damping Modification Factor, κ (ATC-40)

Structural Behavior Type	β_o (percent)	κ
Type A	≤ 16.25	1.0
	> 16.25	$1.13 - \frac{0.51\left(a_y d_{pi} - d_y a_{pi}\right)}{a_{pi} d_{pi}}$
Type B	≤ 25	0.67
	> 25	$0.845 - \frac{0.446\left(a_y d_{pi} - d_y a_{pi}\right)}{a_{pi} d_{pi}}$
Type C	Any value	0.33

Table 5.4 Displacement Ductility (μ) vs. Equivalent Damping (β_{eq})

μ	1	1.5	2	2.5	3	4	5	6	7	8	9	10
κ	0.67	0.67	0.62	0.58	0.55	0.51	0.49	0.47	0.46	0.45	0.45	0.44
β_{eq}	5.00	19.23	24.81	27.07	28.26	29.39	29.88	30.13	30.26	30.35	30.40	30.43

CSM can now be applied to obtain the spectral displacement values at the intersection of the bilinear approximation of the mean capacity curve and the elastic response spectrum (with appropriate equivalent damping value) of the ground motions scaled to intensities defined during the development of the original fragility curves. For demonstration purposes, the procedure is explained by using a specific CSM example. The selected ground motion record is GM8, taken from a 14 Story Office Building during the 1994 Northridge Earthquake. The analysis is performed at the fifth intensity level (which corresponds to $S_d(T_o)$=30mm). As it has been discussed before, there are 11 intensity levels defined according to the spectral displacement values calculated at the fundamental period of the flat-slab building. The same intensity scale is used with CSM in order to match the results with the ones obtained from time-history analysis. The procedure is explained by the help of Figure 5.8. The points on the bilinear mean capacity spectrum symbolize specific ductility ratios and the corresponding values of β_{eq}. A capital letter from A to F is also assigned to each point. The ductility ratios and β_{eq} values for these data

points are listed in Table 5.5. Response spectra with five different values of effective damping are shown on the same figure. Each number in capital roman letters correspond to a response spectrum with an equivalent damping value, in increasing order. Response Spectrum Curve III (ξ=24%) intersects the capacity curve at a ductility ratio of approximately 2.5 (β_{eq} value of 27%) whereas Curve V (ξ=30%) cuts the capacity spectrum at a ductility ratio of nearly 2 (β_{eq} value of 24%). Hence the performance point, or the expected response, should be somewhere between these two curves. The next trial is Curve IV (ξ=26%), which intersects the capacity curve at a ductility ratio of 2.245 (β_{eq} value of 26.11%). The response spectrum seems to intersect the capacity spectrum with acceptable tolerance, hence point O is taken as the performance point and the spectral displacement at the intersection of demand and capacity curves is calculated as 59.8 mm for this specific example. In the same way, CSM is applied with each ground motion at each intensity to obtain the values of spectral displacement at the intersection point.

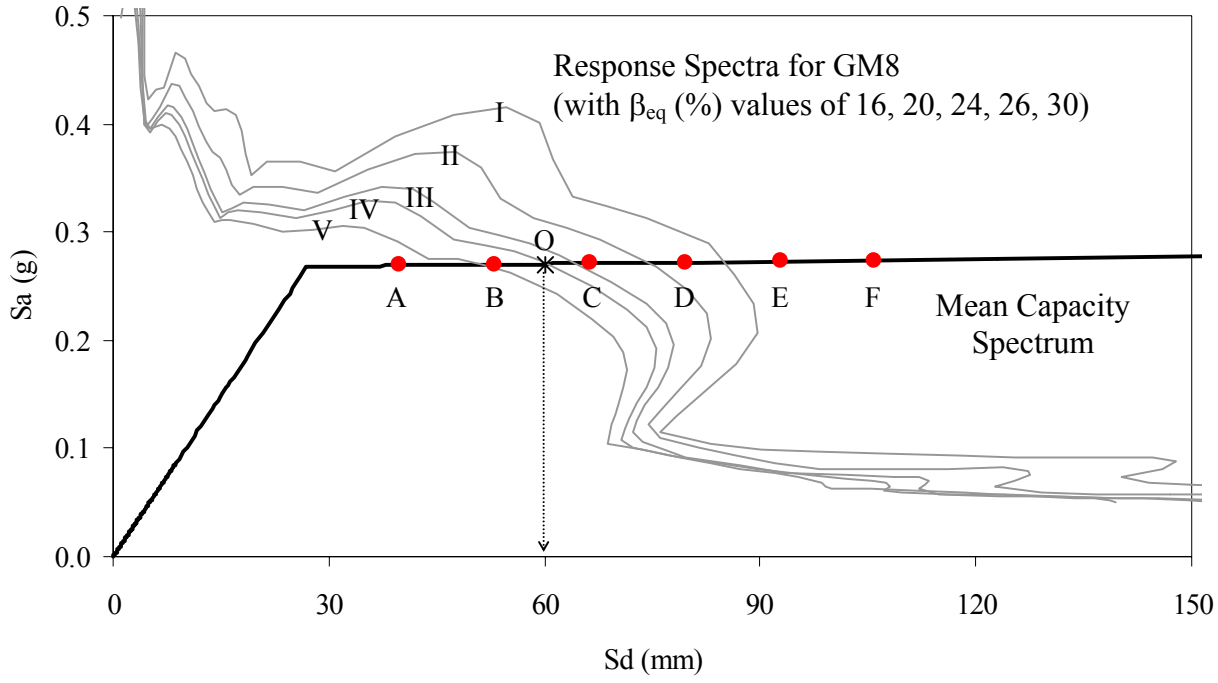

Figure 5.8 CSM with Mean Capacity Spectrum and Response Spectra for GM8

Table 5.5 Ductility (μ)–Equivalent Viscous Damping (β_{eq}) Values on Mean Capacity Spectrum

Points	**A**	**B**	**C**	**D**	**E**	**F**
μ	1.5	2.0	2.5	3.0	3.5	4.0
β_{eq} (%)	24.8	27.1	28.3	29	29.4	29.7

4) Time-history simulations with mean material properties have already been performed as a trial analysis before the start of the main time-history analysis which accounts for the material variability. Therefore, the response data of this set of analysis are available. The next step is to compile the set of pairs ($S_d(T_c)$, δ_{max}), where $S_d(T_c)$ is the spectral displacement at the intersection period and obtained by CSM and δ_{max} is the maximum story drift and obtained by the time-history analysis. Once these data pairs are obtained, the probability of exceedence of each damage state can be determined as done previously to develop the fragility curves of the flat-slab structure. The resulting HAZUS-compatible fragility curves are shown in Figure 5.9. Lognormal fragility parameters, the mean and the standard deviation values for each limit state (LS), are given as follows:

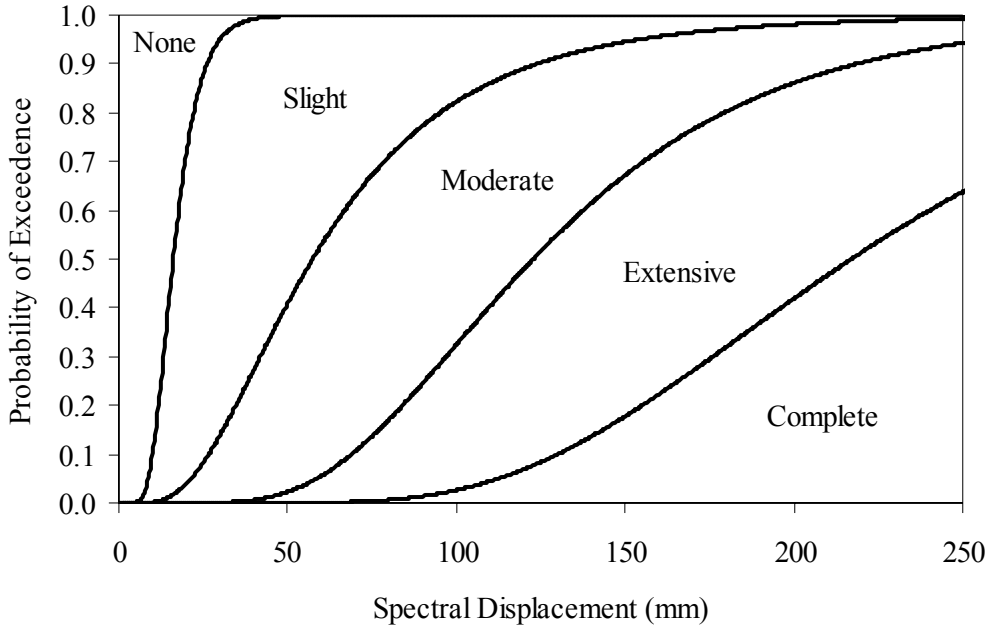

Figure 5.9 HAZUS Compatible Fragility Curves for Flat-slab Structures

LS1 (None to Slight Damage): $\mu = 17.29$, $\sigma = 6.72$

LS2 (Slight to Moderate Damage): $\mu = 68.72$, $\sigma = 45.24$

LS3 (Moderate to Extensive Damage): $\mu = 135.81$, $\sigma = 64.34$

LS4 (Extensive to Complete Damage): $\mu = 235.10$, $\sigma = 97.93$

5) Finally, the HAZUS-compatible curves are compared with some available HAZUS curves for verification purposes. For this comparison, two different building categories in HAZUS are selected as the most similar structural types to flat-slab structures: mid-rise concrete moment frame with moderate-code level of design and mid-rise concrete frame with unreinforced masonry (URM) infill walls with low-code level of design. In HAZUS, these building categories are abbreviated as C1MM and C3ML, respectively. The fragility curve parameters, i.e. the median and the log-normal standard deviation values for each damage state, of these building categories are available in the HAZUS Technical Manual (National Institute of Building Sciences, 1999b). Hence it is possible to make a direct comparison between any two sets of fragility curves. Figure 5.10 shows such a comparison between the HAZUS-compatible fragility curves for flat-slab structure (solid lines) and the original HAZUS curves for building types C1MM and C3ML (dashed lines). In the figures, the Roman numerals I, II, III and IV represent the limit states LS1 (None to Slight Damage), LS2 (Slight to Moderate Damage), LS3 (Moderate to Extensive Damage) and LS4 (Extensive to Complete Damage), respectively for each set of curves. It can be clearly observed that there is agreement between the HAZUS-compatible and the original HAZUS curves in both cases. Flat-slab structures seem to be more vulnerable to damage for low levels of seismic intensity when compared to other building types. For moderate intensity, the curves are close to each other. On the other hand, under high seismic intensity, flat-slab structures are significantly more vulnerable to damage, which is in agreement with the expected performance of these types of structures.

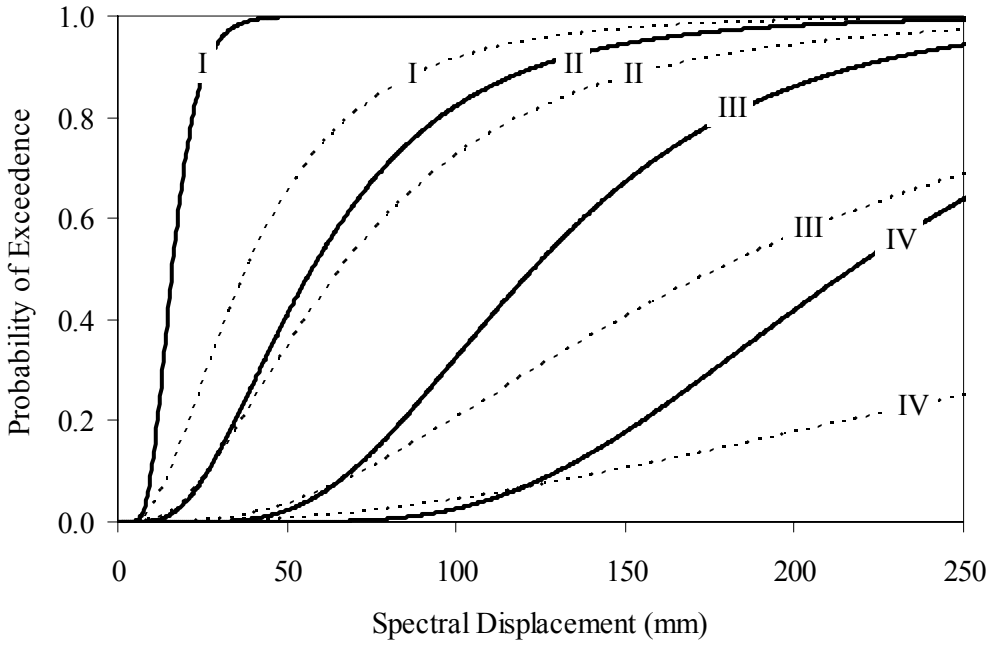

Figure 5.10.a Comparison of HAZUS-compatible Fragility Curves for Flat-slab Structures (Solid Lines) with HAZUS Curves for Concrete Moment Frame - C1MM (Dashed Lines)

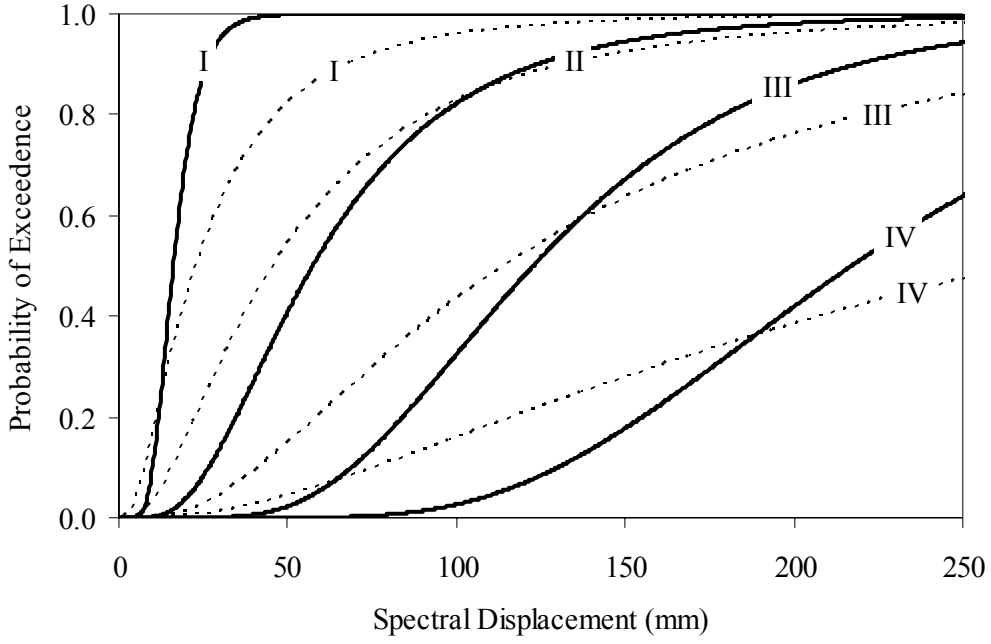

Figure 5.10.b Comparison of HAZUS-compatible Fragility Curves for Flat-slab Structures (Solid Lines) with HAZUS Curves for Concrete Frame with URM Walls– C3ML (Dashed Lines)

5.3 Employment of HAZUS AEBM in the Implementation Process

General information about HAZUS AEBM was provided in the previous chapter. The module is developed for experienced users to create building-specific damage and loss functions for an individual type of building or a group of similar buildings. As the main goal of this study is to implement the fragility curves for flat-slab structures into HAZUS and then to assess the vulnerability of flat-slab structures with respect to the default building types in HAZUS, it is more appropriate to use a 'Level 3 Type' AEBM analysis in which one can conduct building specific loss estimation analysis. The flow of AEBM analysis is not different from the default HAZUS analyses of 'Level 1' or 'Level 2' except 'Level 3' needs extra input data regarding the inventory and structural characteristics of buildings. Three buildings with different types are selected for comparison. Two of them are default HAZUS building types with built-in fragility information and the third one is the flat-slab building. Two different study regions are selected for the study: Urbana, IL and Shelby County, Memphis, TN. The selection of the study region and the scenario earthquakes, the preparation of input data for the selected buildings, running the AEBM analyses and obtaining the AEBM results for each study region are explained in detail in the following sections.

5.4 Study Region 1: Urbana, IL

The first step is to define a study region that includes the location (latitude and longitude) of all buildings to be evaluated. Urbana, IL is selected as the first study region for the AEBM analysis to provide a basis for comparing the individual building losses with those for the region. Ten census tracts are used in HAZUS to match the city boundary of Urbana. Figure 5.11 shows the census tracts in the Urbana region. The population of the region is more than 45,000 according to the US Bureau of Census. The default HAZUS inventory data indicate that there are 10,844 buildings in the selected region. Among these, 63% of the buildings are woodframe and 19% of the buildings are unreinforced masonry (Table 5.6). Considering the rest of the building stock, the number of reinforced concrete buildings is very small, even less than 1% of the total inventory.

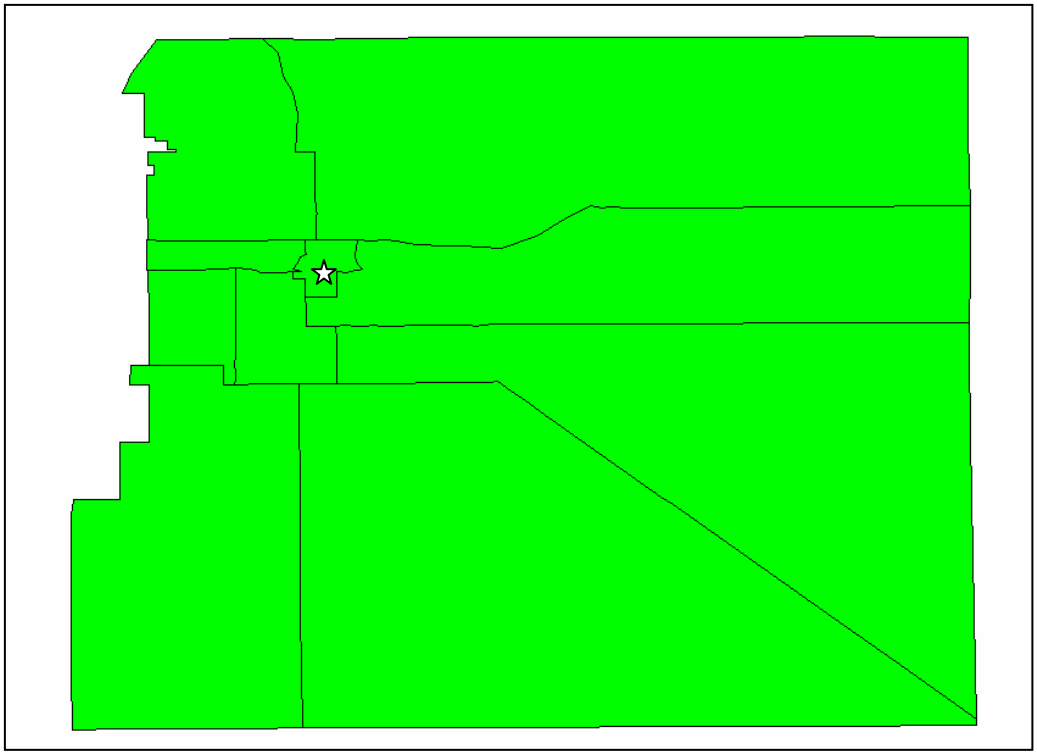

Figure 5.11 Census Tracts Selected in HAZUS to Match the City Boundary of Urbana

Table 5.6 Number of Buildings per General Building Type in Urbana Region

	Wood	Steel	RC	Precast	RM	URM	Mobile
C. Tract 1	19	10	2	2	1	14	0
C. Tract 2	172	4	3	1	2	54	0
C. Tract 3	585	21	16	10	2	186	202
C. Tract 4	919	17	16	5	3	278	1202
C. Tract 5	1270	11	20	4	2	374	247
C. Tract 6	1314	3	17	1	1	379	0
C. Tract 7	1504	15	22	3	3	443	0
C. Tract 8	764	4	11	1	2	225	0
C. Tract 9	168	8	33	41	6	101	0
C. Tract 10	75	0	1	1	1	23	0
Total	**6790**	**93**	**141**	**69**	**23**	**2077**	**1651**

5.4.1 Selection of Scenario Earthquakes

There are three types of scenarios that can be used. These include a deterministic event, a probabilistic analysis of seismic hazard or a user-supplied map of the ground motion. The deterministic event option will likely be the most useful and the most convenient method of defining AEBM ground shaking. A deterministic scenario in HAZUS requires magnitude, location, the focal depth of the event and the attenuation relationship for study regions selected from the Central or Eastern US. However, it is necessary to have general information about the seismicity of the Mid-America Region before being able to define scenario earthquakes with reasonable event parameters.

Seismicity of Mid-America Region

The Mid-America region is an area of low probability but high risk for earthquake damage. The New Madrid Seismic Zone (NMSZ) is active and regarded as potentially one of the most dangerous tectonic features in the United States. Arkansas, Illinois, Indiana, Kentucky, Mississippi, Missouri and Tennessee are all states located within the NMSZ region.

The Mid-America Region has had several devastating earthquakes in the years 900, 1450 and during the winter of 1811-1812. The 1811-1182 earthquake sequence, also known as the "New-Madrid Earthquakes", includes four consecutive earthquakes that had magnitudes >7.5. These are by far the largest earthquakes known in the history of the continental U.S. based on the large area of damage (600,000 square kilometers) and the widespread area of perceptibility (5,000,000 square kilometers). Figure 5.12 shows he isoseismal map of the 1811-1812 New Madrid Earthquakes. This map clearly shows that the earthquakes were felt in a very large area, extending to Boston, Massachusetts and Ottawa, Canada. The first and second earthquakes occurred in Arkansas on December 16, 1811 and had an estimated magnitude of 8.5 and 8.0, respectively (Stover and Coffman, 1993). Obviously, these magnitude values were approximated and depended on the estimates taken from the isoseismal maps. The third and the fourth earthquakes occurred in Missouri on January 23, 1812 and February 7, 1812 and had estimated magnitudes of 8.4 and 8.8, respectively. The maximum intensities at the epicenter of the first two earthquakes were estimated at the MMI Intensity X-XI Level. It is not easy to assign intensities

to the shocks that occurred after 1811 events since it is not clear if the information included the cumulative effects of all the earthquakes or just the individual events. However, it is accepted that the intensity of the third event is close to the others at similar locations. The fourth earthquake was also the largest of the 1811-1812 series. The shock that occurred on February 7 surpassed the magnitude of the previous events and as a result the town of New Madrid was destroyed*.

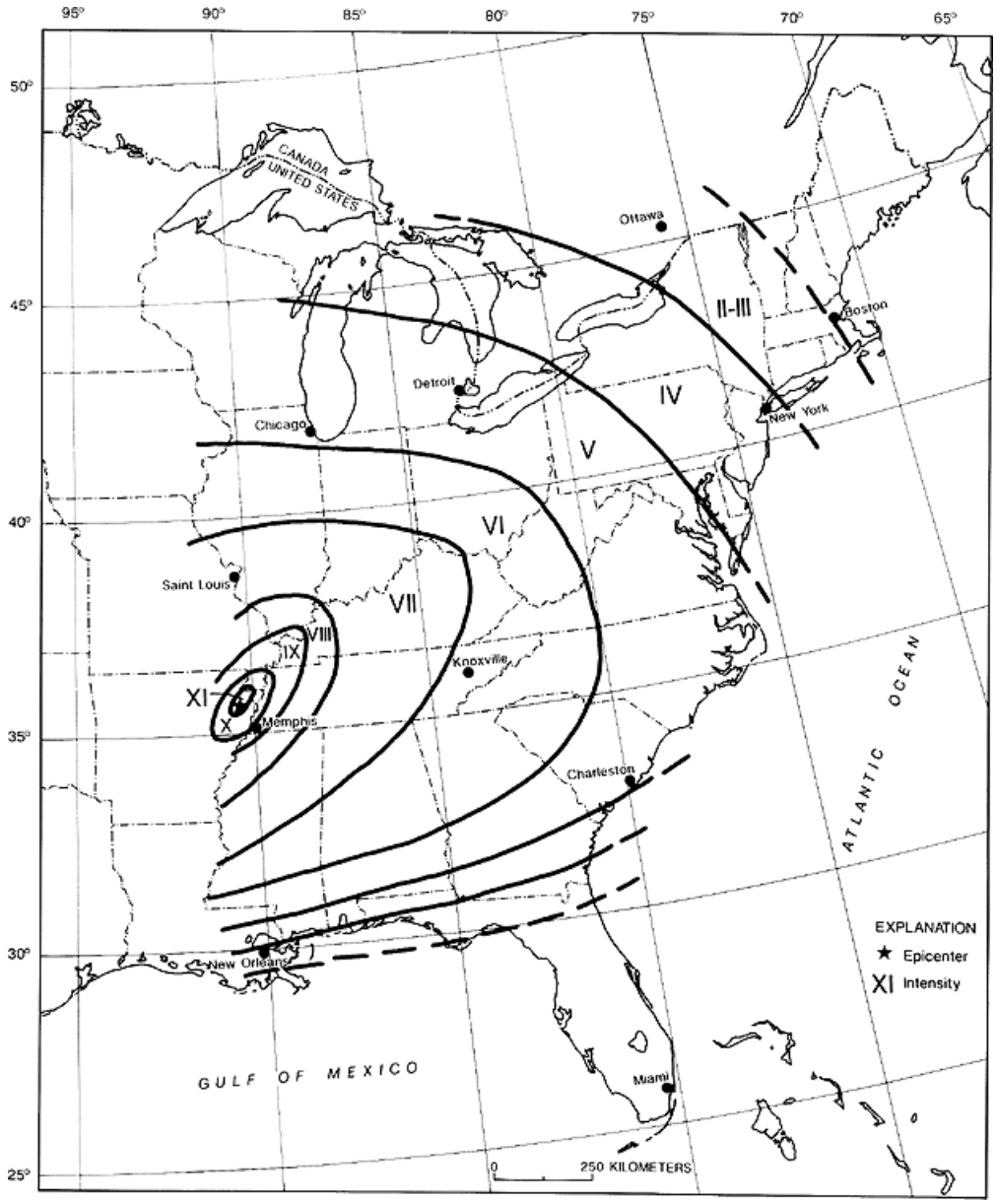

Figure 5.12 Isoseismal Map of 1811-1812 New Madrid Earthquakes (from USGS Web Site)

* The information about the 1811-12 New Madrid Earthquakes is taken from USGS Web Site (http://www.usgs.gov)

The next largest earthquake occurred near Charleston, Mississippi County, Missouri in 1895. The earthquake had an estimated magnitude of 6.7 and an Intensity of VIII. Structural damage and liquefaction phenomena were reported after the earthquake. The earthquake caused extensive damage to school buildings, churches, private houses, and to almost all the buildings in the commercial section of Charleston.

Until then many earthquakes occurred in the region without devastating consequences. Currently, it is not expected that an earthquake with a magnitude 8-9 earthquake will shake the region again. It is more probable that an earthquake with a moderate magnitude will occur. According to Johnston and Nava, 1985, the probability of an occurrence of a moderate earthquake with a magnitude of 6.3 or greater by the year 2035 is 86-97%.

An interesting observation about the earthquakes in the Central US is that they affect much larger areas than earthquakes of similar magnitude in the western United States. For instance, the area of strong shaking associated with the first two shocks of the New Madrid Earthquake Sequence is two to three times larger than that of the 1964 Alaska earthquake and 10 times larger than that of the 1906 San Francisco Earthquake. Another example is illustrated in Figure 5.13. This figure compares the areas of the U.S. affected by the 1895 Charleston, Missouri Earthquake (M=6.8) and the 1994 Northridge, California Earthquake (M=6.7), earthquakes of similar magnitudes. The differences in geology east and west of the Rocky Mountains cause this strong contrast.

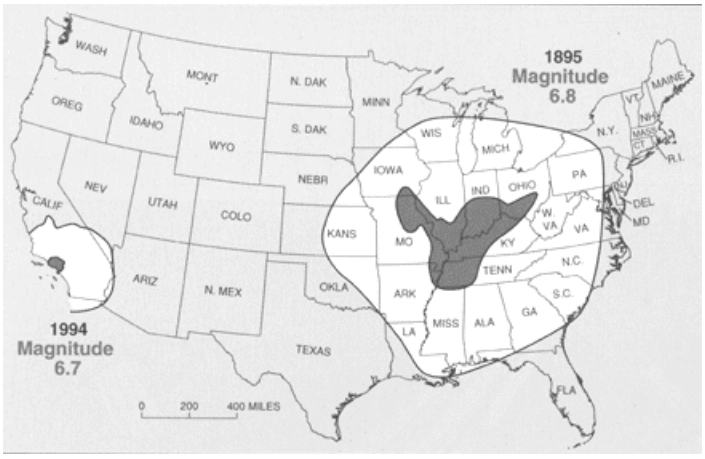

Figure 5.13 The Areas Affected by the 1895 Charleston and 1994 Northridge Earthquakes.

Seismicity of Urbana, Illinois

One of the largest earthquakes in Northern or Central Illinois occurred on May 26, 1909, a shock with a magnitude of 5.1 and an Intensity of VII. The effects of this earthquake were felt over 500,000 square miles and were also strongly felt in Iowa and Wisconsin. It also caused buildings to sway in Chicago.

Another earthquake with an Intensity VII occurred on November 9, 1968. This was the strongest earthquake felt in Southern Illinois since the 1895 Missouri Event. It had a magnitude of 5.5 and was felt over 580,000 square miles in 23 states. Damage consisted of bricks being knocked from chimneys, broken windows, toppled television antennae and cracked plaster. Other significant earthquakes occurred in the region from the 1800's to the present had magnitudes ranging between 4.0 and 5.0 with no significant damage reported.

Based on the 1996 USGS Seismic Hazard Map for the Central and Eastern US, Urbana has a 10% probability of experiencing ground shaking of 0.0368g or greater in 50 years.

Criteria for Scenario Earthquake

As stated above, a deterministic event is the most useful and the most convenient to use as an earthquake scenario event. Four parameters should be defined for the Eastern US in the HAZUS methodology. These are magnitude, location, the focal depth and the attenuation function. In addition, several assumptions are used to identify the seismic hazard. The first assumption is that earthquakes with $M<7$ are assumed to have a moderate intensity whereas earthquakes with $M>7$ are assumed to have a large intensity. The lower boundary of magnitude for a moderate earthquake is considered as 5.

Assumptions made by Olshansky et al. (2002) concerning the location of the earthquakes are used. According to these assumptions, large earthquakes are likely to occur anywhere along the New Madrid seismic fault and moderate earthquakes are equally likely to occur anywhere in the "reference zone" of a community under study. The "reference zone" is defined as the area of a community that contains all the earthquakes. Considering the relatively low attenuation in Mid-America, Olshansky et al. assumed such a distance to be 500 km which is also in accordance

with the recent studies of Frankel et al (1996) and Wu (2000). Based on this information, the reference zone for Urbana is determined to be a circle with a 500 km radius.

The focal depth, the third assumption is determined by using Wheeler and Johnston (1992) focal depth distribution model which uses previous earthquake data from the Central and Eastern US. The median depth of the selected earthquakes was calculated as 10 km. They also concluded that Large earthquakes (M>7) have a hypocentral depth of 12 km whereas moderate earthquakes have a hypocentral depth of 15 km.

In HAZUS, there are three different attenuation functions to be used in Mid-America Region. These attenuation relationships belong to Frankel et al. (1996), Toro et al (1997) and Savy (1998). In addition, the methodology provides a default combination of the first two attenuation functions given above based on the theory developed by USGS for "Project 97". This weighted attenuation relationship is also recommended by HAZUS. Hence attenuation "Project 97" is selected for the earthquake scenario design.

Table 5.7 Scenario Earthquakes Selected for the Urbana Study Region

Scenario	Magnitude	Location (Degree)	Distance (km)	Depth (km)
SE-1	5.0	(-88.21, 40.11)	0	15
SE-2	5.5	(-88.21, 40.11)	0	15
SE-3	6.0	(-88.21, 40.11)	0	15
SE-4	7.0	(-89.10, 37.24)	368	12
SE-5	8.0	(-89.10, 37.24)	368	12

Based on the above considerations and assumptions, 5 different scenario earthquakes are selected for Urbana (Table 5.7). The scenario earthquakes are abbreviated as SE-1, SE-2, SE-3, SE-4 and SE-5, respectively. The first three scenarios are moderate earthquakes with on-site hits. The location of these events in Figure 5.11 is represented by the star shape. They are assumed to occur at a depth of 15 km. The other two earthquakes are assumed to be large earthquakes and

occur on the New Madrid Seismic fault (368 km from downtown Urbana). Focal depth estimations made for the 1811-1812 earthquake sequence by USGS indicate that their focal depths were probably between 5 and 20 kilometers. A similar range for the focal depth was suggested by Youssef Hashash, a professor at the University of Illinois.* Therefore the focal depth of 12 km will be used for the last two scenario earthquakes. These five scenario earthquakes are in accordance with the worst scenario earthquakes defined by Olshansky et al. (2002) to evaluate the seismic risk in Mid-American Communities.

5.4.2 Defining AEBM Input Data

Before running the AEBM Analysis, the individual buildings to be analyzed are selected and the corresponding AEBM Inventories and Profiles are defined. Three buildings with different structural types are selected for this study. The first two buildings that are selected are a mid-rise reinforced concrete moment frame and a mid-rise reinforced concrete frame with URM walls. The data for these building types are already contained in the HAZUS Methodology. The third building is selected as a mid-rise flat-slab structure in accordance with the structural model investigated in this study. The fragility information for the first two buildings is already built-in and the HAZUS-compatible fragility parameters of the flat-slab structure were developed previously in this chapter. The comparison of fragility curves derived for flat-slab structures with the other two building types is shown in Figure 5.10.

The AEBM Inventory contains 22 data fields to be filled by the user. These parameters are listed in Table 5.8. Since there are three buildings in the case study, there should also be three different inventory records. The buildings are abbreviated as MRF (moment frame), MRW (frame with URM) and FSS (flat-slab). Since the goal is to assess the performances of the building types with different fragility characteristics, all the parameters, except the fragility information, are assumed to be the same in the case study buildings. All the buildings are assumed to be at the same location (same latitude and longitude). The values of the other AEBM parameters, the number . of occupants and other economical parameters, are estimated .

* Personal communication by e-mail.

Table 5.8 AEBM Inventory Data for the Case Study Buildings

Parameter Field Name	**Moment Frame**	**Frame with URM**	**Flat-slab with URM**
ID No	MRF	MRW	FSS
Name	R/C MRF in Urbana	R/C MRW in Urbana	R/C FSS in Urbana
Profile Name	*Moment Frame*	*Frame with URM*	*Flat-Slab*
Address	Downtown Urbana	Downtown Urbana	Downtown Urbana
City	Urbana	Urbana	Urbana
State	IL	IL	IL
Zip Code	61801	61801	61801
Latitude	40.11	40.11	40.11
Longitude	-88.2	-88.2	-88.2
Daytime Occupants	250	250	250
Nighttime Occupants	20	20	20
Building Area (sq.ft)	18,000	18,000	18,000
Building Value ($)	3,500,000	3,500,000	3,500,000
Contents Value ($)	700,000	700,000	700,000
Business Inventory ($)	_	_	_
Business Income ($/day)	20,000	20,000	20,000
Wages Paid ($/day)	7,500	7,500	7,500
Relocation Disruption Costs ($)	12,500	12,500	12,500
Rental Costs ($/day)	1,000	1,000	1,000
Ratio of Building Owner Occupied	70	70	70
County FIBS	17019	17019	17019

The HAZUS software uses a profile name to link the buildings listed in the AEBM Inventory to the corresponding AEBM Profile data set. All three buildings should have different profiles since they have different fragility information. The AEBM profile data is composed of eight sets of databases:

1- Building Characteristics,

2- Structural Fragility Curves,

3- Nonstructural Drift Fragility Curves,

4- Nonstructural Acceleration Fragility Curves,

5- Casualty Ratios (per occupant),

6- Building Related Repair Cost Ratios,

7- Contents & Building Inventory Replacement Cost Ratios,

8- Loss of Function Parameters (no. of days).

Table 5.9 Selection of Building Characteristics for the Case Study Buildings

Profile Characteristics	Moment Frame	Frame with URM	Flat-slab with URM
Occupancy Class	COM4	COM4	COM4
Building Type	C1M	C3M	C3M
Seismic Design Level	Moderate	Moderate	Moderate
Building Quality	Code	Code	Code

The "Building Characteristics" data set includes information about the occupancy class, the building type, the design level and the quality of construction. These four parameters should be selected for each example building before defining any other profile data set, because the data fields in the other seven data sets are populated with default values according to this selection. The selections made for the case study buildings are listed in Table 5.9. The buildings are assumed to be for commercial use and include offices for professional or technical services, which fall in HAZUS occupancy class of COM4. The first two buildings are built-in types in HAZUS so the default building types are C1M and C3M. For the flat-slab building, all the damage and loss data other than structural fragility information are assumed to be similar to the reinforced concrete frame with URM walls. Seismic design level of the buildings are selected as "Moderate" and the building quality is selected as "Code", indicating that the buildings are designed and constructed according to regular code provisions.

The data set modified for the flat-slab structure is the second one, which is related to the structural fragility curves. Hence the default median and beta values for Slight, Moderate,

HAZUS AEBM- Individual Building Report (FSS-SE3)

Building Information

Id Number : FSS
Building Name : FLAT SLAB WITH URM WALLS
Address : DOWNTOWN URBANA
Latitude / Longitude : 40.11 / -88.20
Building Profile : FSS

Ground Motion

SA @ 0.3 seconds (g) : 0.27
SA @ 1.0 seconds (g) : 0.13
PGA (g) : 1.13
Soil Type : Very thick soft / medium stiff clays

Building Intersection Points

Displacement (in) : 4.34
Acceleration (g) : 0.57

Building Damage

Damage State	Damage State Probabilities (%)		
	Structural	Non-Structural Drift	Non-Structural Acc.
None	1	55	25
Slight	71	26	40
Moderate	28	16	28
Extensive	1	2	7
Complete	0	1	1

Casualties

Casualty Level	Estimated Number of Occupants and Casualties		
	Description	Day-time Scenario	Night Time Scenario
Occupants	No. of people in the building	250	20
Level 1	Req. medical attention	0	0
Level 2	Req. hospitalization	0	0
Level 3	Life-threatening injury	0	0
Level 4	Death	0	0
Total		0	0

Economic Loss

Loss Category	Building Exposure $ Economic Loss		
	Exposure ($)	Loss ($)	% of Total Loss
Building Structural	3,500,000	30,085	11.03
Building Nonstructural		172,712	63.34
Contents	700,000	26,992	9.9
Business Interruption	-	42,903	15.73
Total	4,200,000	272,692	

Study Region : Urbana
Scenario : ES3

Figure 5.14 Example Summary Report – Flat-slab Structure subjected to SE-3

Extensive and Complete damage are replaced by the calculated values for the flat-slab model investigated in the study. No further modifications are made in any of the other data sets.

5.4.3 Assessment of AEBM Results

The results of the AEBM analysis are provided in a table format. The "Results Table" includes damage state probabilities, casualty and direct economic losses for each individual building and for each scenario earthquake. There are 5 scenario earthquakes and 3 different building types, so at the end of the AEBM analysis there are 15 individual building summary reports. An example of the summary report is presented in Figure 5.14. The other summary reports, the damage and loss data, are presented in graphical form (Figures 5.15-5.19) for direct comparison.

An important observation about the AEBM results is that the scenario earthquakes that are assumed to occur on the New Madrid seismic fault do not cause any damage at all. This is because of the epicenter of these earthquakes are too far away from the investigated site (368 km) although they are events with large magnitudes. On the other hand the moderate on-site earthquakes with smaller magnitudes cause damage and loss in the study region. Similarly, in a recent study (Olshansky et al. 2002), it was observed that two scenario earthquakes with magnitudes of 7 and 8 on the New Madrid seismic fault would not affect any of the buildings located in Urbana region.

Figure 5.15 presents the building damage in terms of damage state probabilities for the first three scenario earthquakes. The abbreviations used for moment frame, frame with URM walls and the flat-slab structure are MRF, MRW and FSS, respectively. The damage distribution shifts from No Damage to Moderate Damage as the magnitude of the scenario earthquake increases. In the first scenario earthquake (M=5), there is a very low probability of damage. In the second scenario earthquake (M=5.5), the probability that MRF and MRW will suffer moderate damage is higher than the probability that FSS will suffer the same level of damage. On the other hand, it

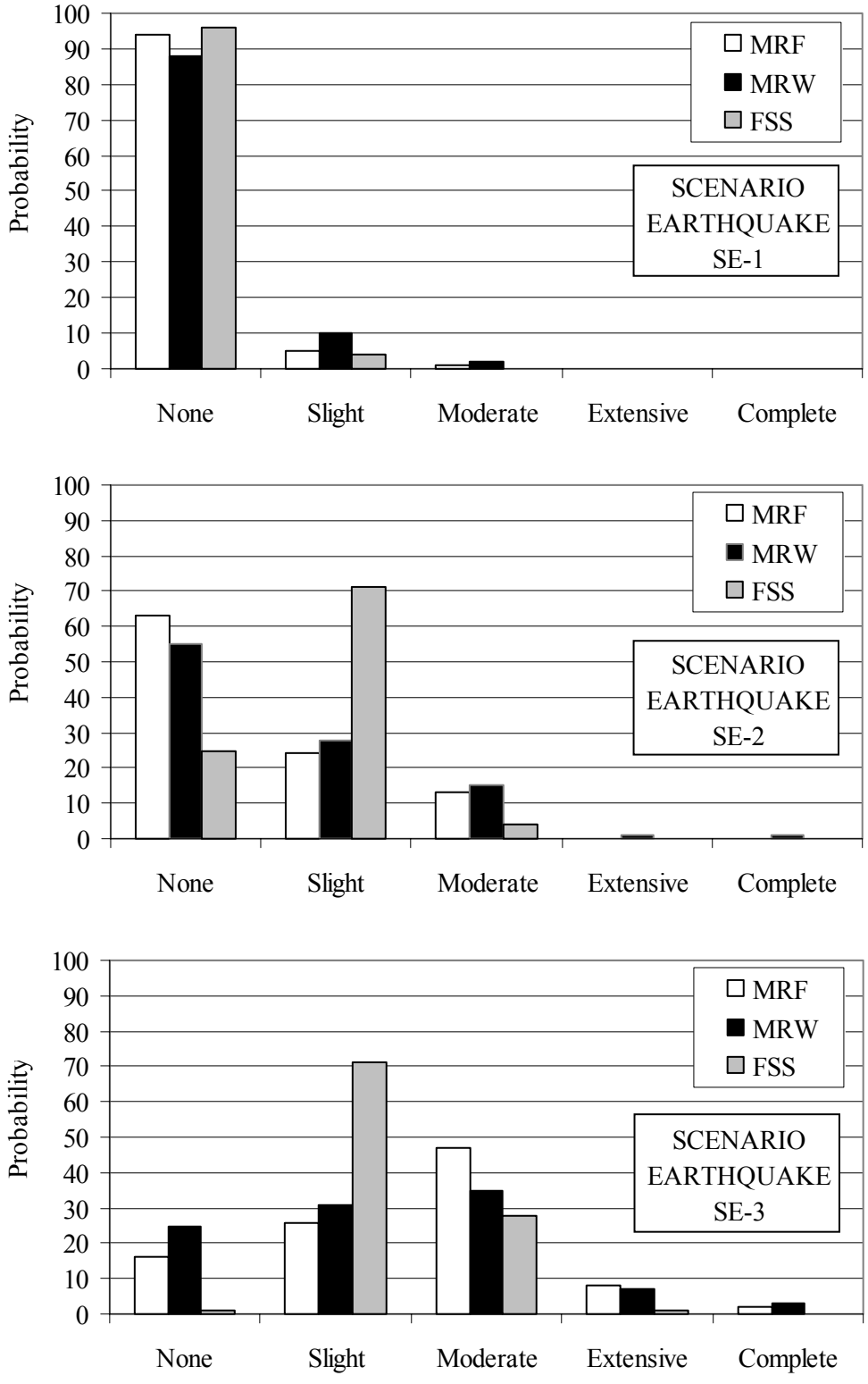

Figure 5.15 Building Damage in terms of Damage State Probabilities for Urbana Region

is a low probability that the FSS will suffer no damage when compared with the probabilities of the other two example buildings. The same trend is also observed when the magnitude of the earthquake is increased by using the third scenario earthquake with M=6.0 although the damage distribution is shifted to higher levels. The nature of such a damage distribution is better understood by investigating the fragility curves in Figure 5.10. The Slight Limit State fragility curve of the flat-slab structure is much steeper than the corresponding fragility curves of other building types. In other words, the flat-slab structure is much more vulnerable to a slight damage state due to its low lateral stiffness. For moderate levels of seismic intensity, MRF or MRW can sustain more damage than FSS due to the fact that they are stiffer than FSS, so they are subjected to higher lateral loads. When the seismic intensity is high, FSS is more vulnerable than the other two types since the structural system cannot withstand the excessive lateral displacement due to insufficient lateral resistance. The scenario earthquakes were moderate events, so the damage levels of the building systems in the case study were similar. However in the case of a devastating event, the FSS will be far more damaged than the other two building types.

Figures 5.16-5.18 present the percentages of the four loss categories; building structural, building non-structural, contents and business interruption with respect to the total economic loss for each scenario earthquake. Economic loss due to the damage to non-structural components is significantly much more in all of the cases followed by the contents damage in the first Scenario Earthquake. However the share of losses due to structural damage and business interruption gets larger with increasing ground motion intensity. Moreover, the percentage of losses due to non-structural damage is the highest for FSS. This is in accordance with the fact that the flat-slab system sustains significant non-structural damage even under moderate shaking intensities. However losses are also dependent on non-structural fragility curves for which the default values given in HAZUS were assumed.

Figure 5.19 illustrates the total losses in dollars for the example buildings when they are subjected to scenario earthquakes with different magnitudes. The losses increase with the severity of the ground motion. The losses estimated for FSS is less than MRF and MRW since the probability of exceeding moderate damage is less than the others for the third scenario earthquake.

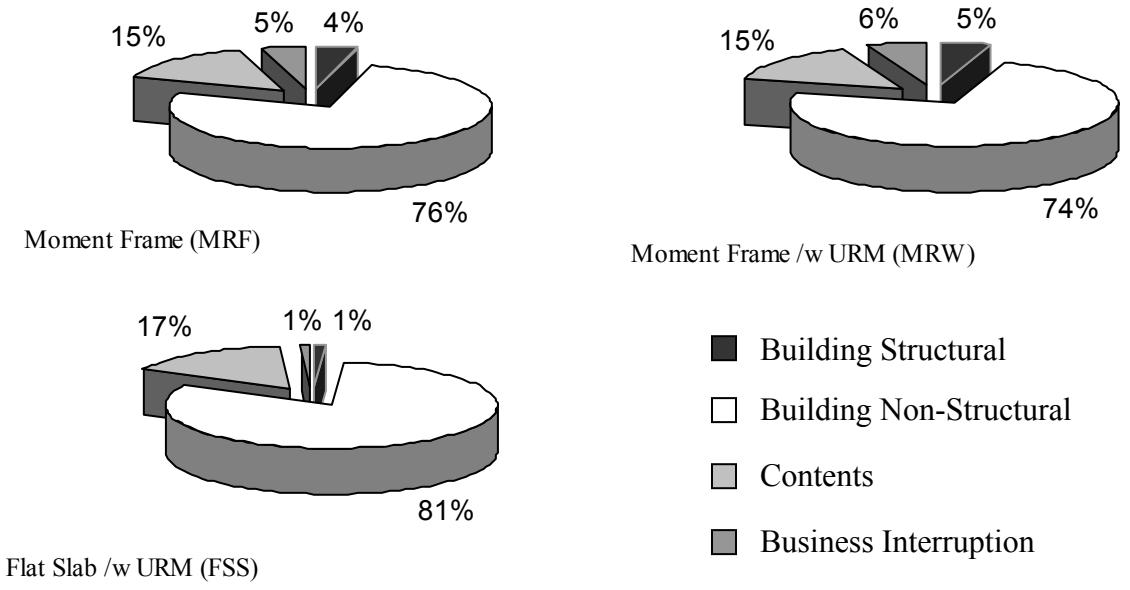

Figure 5.16 Distribution of Losses w.r.t. Total Economic Loss in SE-1 (M=5)

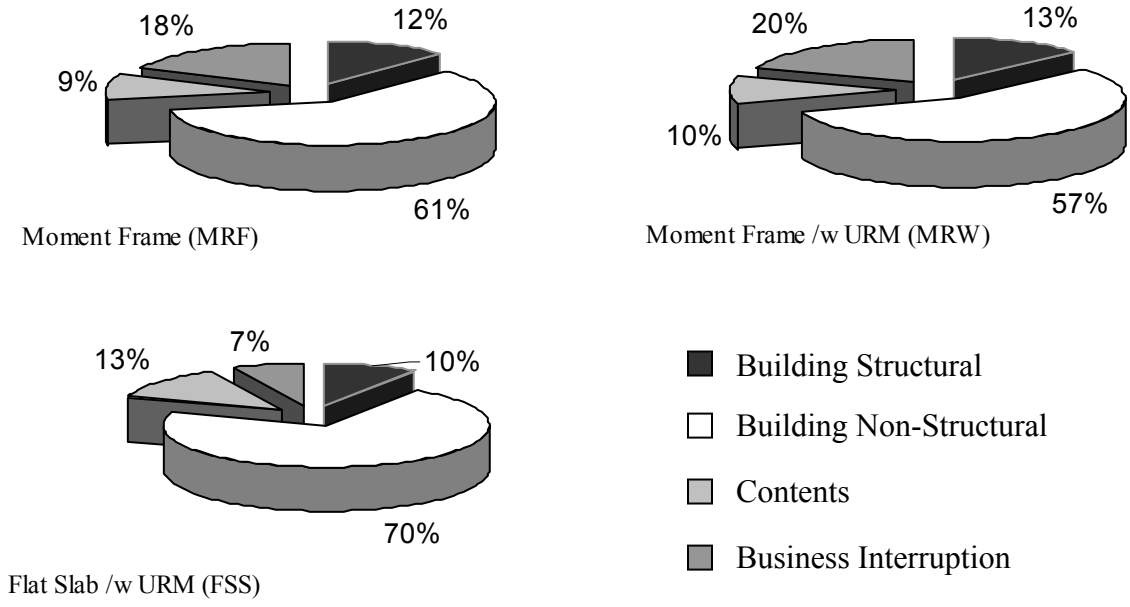

Figure 5.17 Distribution of Losses w.r.t. Total Economic Loss in SE-2 (M=5.5)

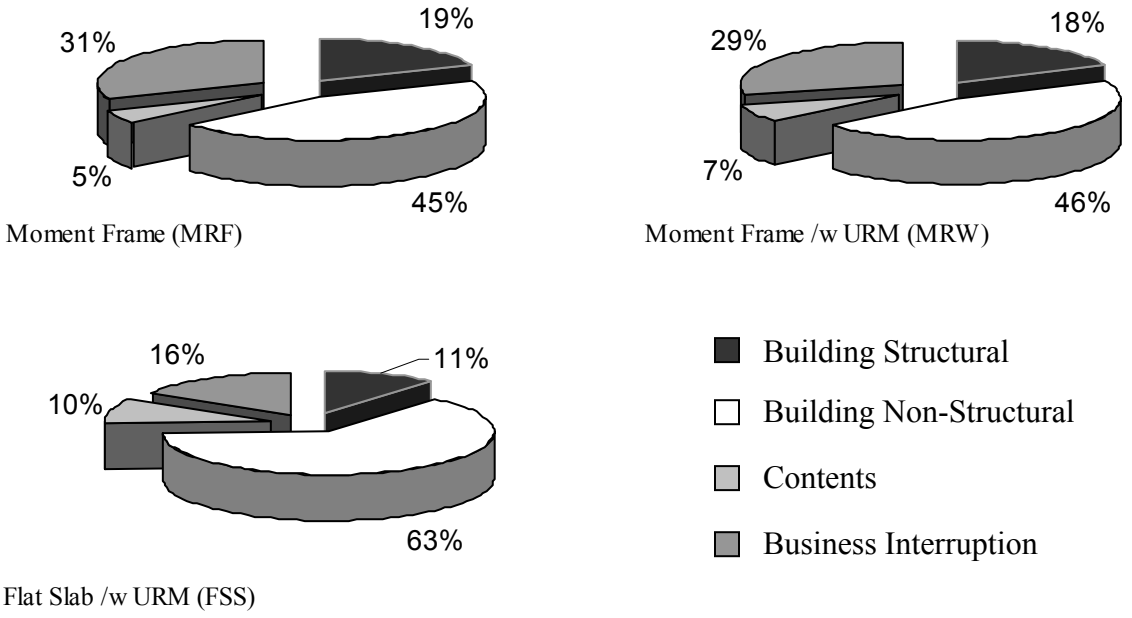

Figure 5.18 Distribution of Losses w.r.t. Total Economic Loss in SE-3 (M=6)

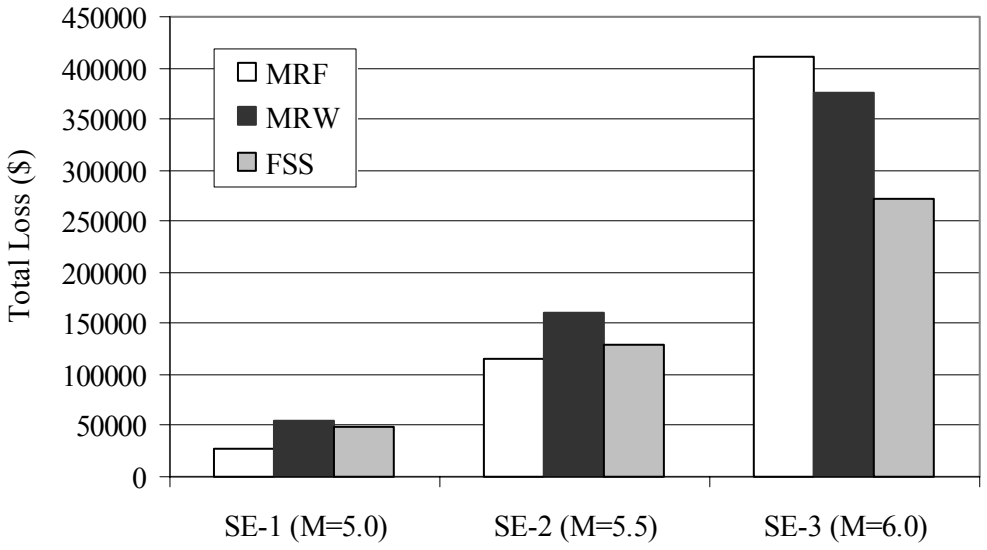

Figure 5.19 Total Economic Losses in the Example Buildings When Subjected to SE-1, SE-2 and SE-3.

Checking the AEBM building summary reports, it is observed that the estimated number of day-time casualties in the buildings is nearly zero. There is only one occupant which requires medical attention (Severity Level 1) in each of the buildings under the third scenario earthquake (M=6).

The AEBM results from individual buildings can be better evaluated by comparing the results of the regional loss estimation studies for the same region using the same scenario earthquakes. For this purpose, the third scenario earthquake (M=6) is employed for the regional loss estimation analysis of the Urbana region. There are 10,844 buildings with an exposure of $2.5 billion. After the analysis, the share of structural damage, non structural damage and contents damage with respect to the total economic loss for the building stock is investigated. The economic losses due to structural damage, non-structural damage and contents damage are estimated to be $81 million, $296 million and $115 million, respectively, or in terms of a percent ratio of the total loss; 3.3%, 12.1% and 4.7%, respectively. Although it may be misleading to make a one-to-one comparison between loss values obtained from individual buildings and the average losses for the study region, the values indicate that losses due to non-structural damage is much more pronounced in the case of individual buildings than the corresponding average losses obtained for the general building stock.

One last comment is devoted to the comparison of the number of occupants and the estimated casualties in AEBM versus regional analysis. For the individual buildings, the number of occupants for a day-time and a night-time scenario are assumed to be 250 and 20, respectively. As mentioned above there was only one minor injury when SE-3 was used for the analysis. Considering the regional loss estimation analysis, for a population of 45,063 in the Urbana study region, the number of day-time casualties is 707, where the number of deaths (Severity Level 4) are 39. The average casualty/occupant ratio including all severity levels is 1.6 % for regional analysis whereas this ratio is 0.5 % for the individual buildings. This indicates that the estimated casualties are below the average values for the example buildings.

5.5 Study Region 2: Shelby County, Memphis, TN

The city of Memphis is a fast-developing region in the Central US. Memphis' metropolitan area includes Fayette, Shelby and Tipton Counties in Tennessee and De Soto County in Mississippi. However Memphis, with a population of approximately 1,000,000 persons, is under high seismic risk since it is geographically very close to the southwestern segment of the NMSZ. Hence Shelby County was selected as the second study region to be used in loss estimation studies.

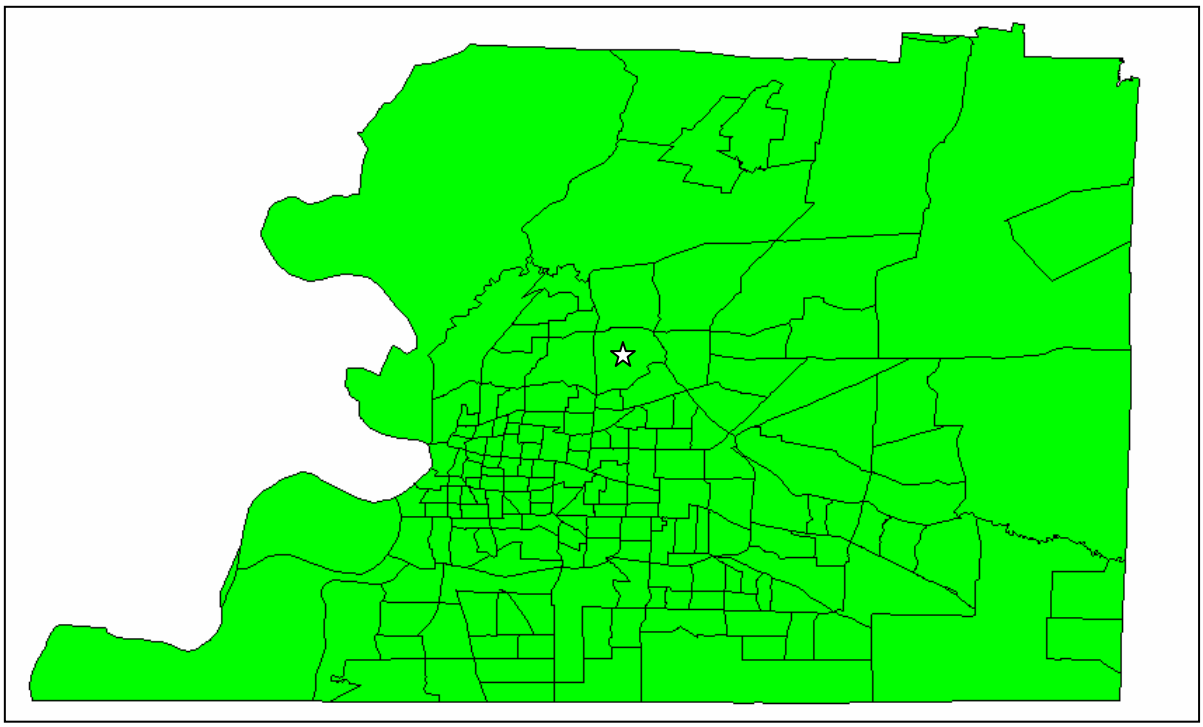

Figure 5.20 Study Region 2: Shelby County, Memphis, TN

Shelby County is composed of 185 census tracts (Figure 5.20). The population of the county is 826,330 persons according to the US Bureau of Census. The default HAZUS inventory data indicate that there are 238,064 buildings in the selected region. Among these, 80% of the buildings are woodframe and 11% of the buildings are unreinforced masonry. Just like the previous study region, the percentage of reinforced concrete buildings is very small (1 %). This verifies that reinforced concrete construction is not typical in Mid-America communities.

5.5.1 Selection of Scenario Earthquakes

The scenario earthquakes are selected based on the same principles as in the first study region. Before discussing the scenario earthquakes in more detail, additional information about the seismicity of the Memphis Region is provided.

Seismicity of Memphis Region

Memphis City is close to the NMSZ, known as the most seismically active region in North America, east of the Rockies. The southwestern segment of the NMSZ ends near Marked Tree, Arkansas. A strongly damaging earthquake struck Marked Tree, Arkansas in 1843 (M=6.3) with an estimated Intensity of VIII. Memphis experienced additional damage from an earthquake on July 19, 1895, with an Intensity of VI. Since then, about twice a decade, smaller damaging earthquakes have struck the seismic zone and about two or three times a year, smaller earthquakes that do not cause damage can be felt.

Table 5.10 Scenario Earthquakes Selected for the Shelby County Study Region

Scenario	Magnitude	Location (Degree)	Distance (km)	Depth (km)
SE-6	5.0	(-89.95, 35.21)	0	15
SE-7	5.5	(-89.95, 35.21)	0	15
SE-8	6.0	(-89.95, 35.21)	0	15
SE-9	7.0	(-90.5, 35.5)	60	12
SE-10	8.0	(-90.5, 35.5)	60	12

Criteria for Scenario Earthquake

Similar to the first case study, five different earthquake scenarios are selected (Table 5.10). The scenario earthquakes are abbreviated as SE-6, SE-7, SE-8, SE-9 and SE-10, respectively. The first three of them are moderate earthquakes and the last two are large earthquakes on the New Madrid Seismic Fault. The selected on-site location for SE-6, SE-7 and SE-8 is represented by the star shape in Figure 5.20. The site location with the coordinates (-89.95, 35.21) was

arbitrarily selected. For SE-9 and SE-10, it is assumed that the shaking occurs very close to Marked Tree, Arkansas, the closest segment of NMSZ to Memphis. Hence the epicenter of the last two scenario earthquakes are located at (-90.5, 35.5), approximately 60 kilometers to the site. The assumptions used to define the focal depths in the first case study are also valid for this case. In addition, the same attenuation relationship is employed.

5.5.2 Defining AEBM Input Data

The selected individual buildings are exactly the same ones used in the first case study. Hence the same AEBM Inventory and Profile data are employed. The example buildings will again be abbreviated as MRF, MRW and FSS. They are all located at the site with the coordinates (-89.95, 35.21).

5.5.3 Assessment of AEBM Results

The damage state probabilities of the example buildings subjected to the scenario earthquakes SE-8 to SE-10 are shown in Figure 5.21. The damage state probabilities obtained for SE-6 and SE-7 are not included in the figure since the damage state probabilities belonging to on-site earthquakes are very similar to the ones obtained in the Urbana Study Region, This is obvious because the properties of the general building stock of these two Mid-American Communities are very similar to each other. Another observation is that the large earthquakes on the New Madrid Seismic Fault, which did not treat the Urbana Study Region and have a significant damage potential for the Shelby County Region. It is probable that these large earthquakes will cause equal or more damage than the on-site moderate earthquakes.

The distribution of losses (building structural, building non-structural, contents, and business interruption) with respect to total economic loss in scenario earthquakes SE-8, SE-9 and SE-10 are presented in Figures 5.22-5.24. The economical loss due to non-structural damage in FSS is about 50%-60% of the total loss whereas the same ratio is reduced to 40%-45% in the

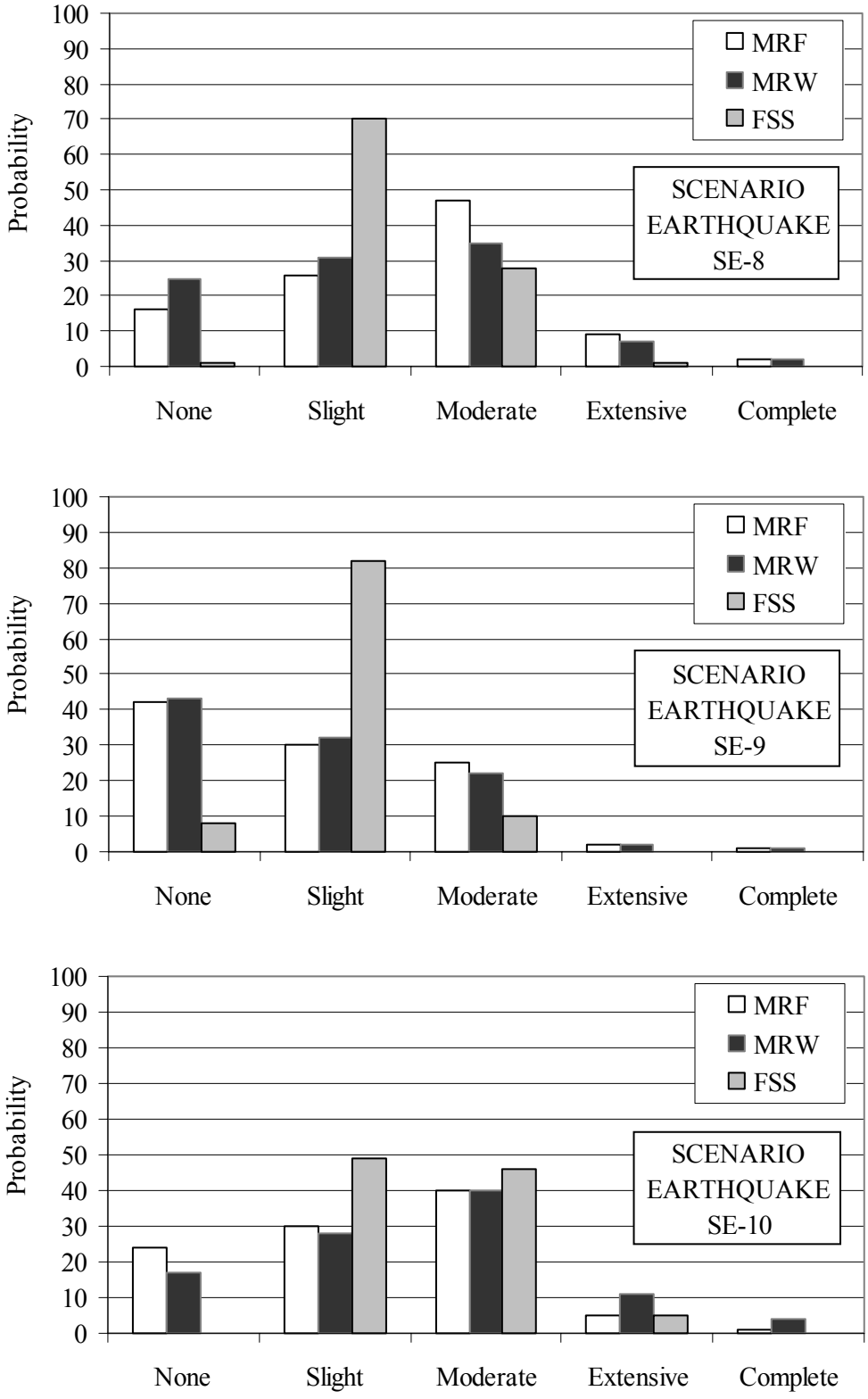

Figure 5.21 Building Damage in terms of Damage State Probabilities for Shelby County Region

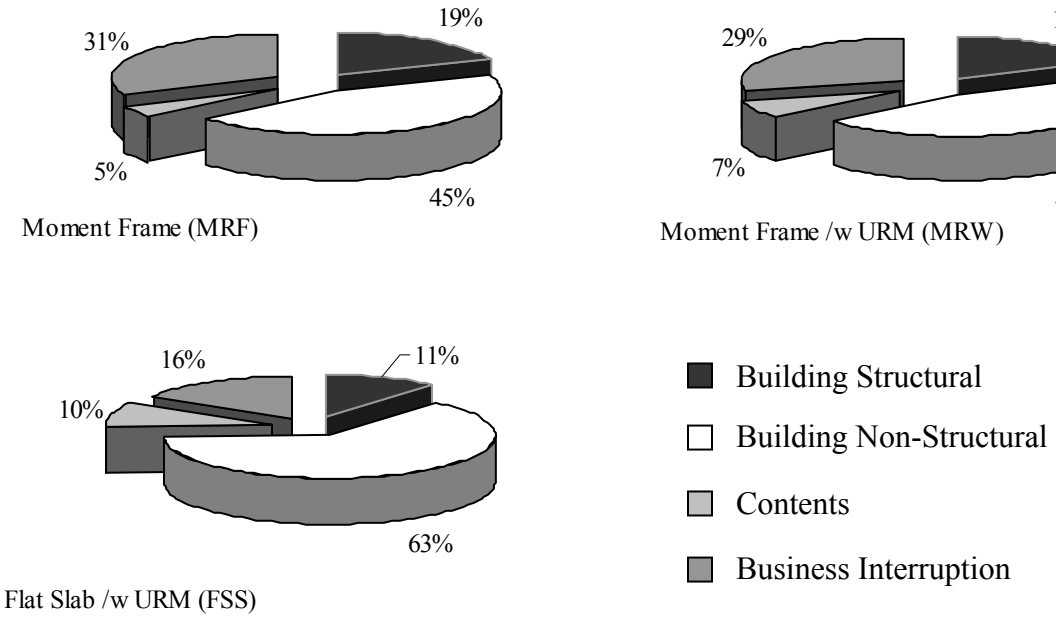

Figure 5.22 Distribution of Losses w.r.t. Total Economic Loss in SE-8 (M=6)

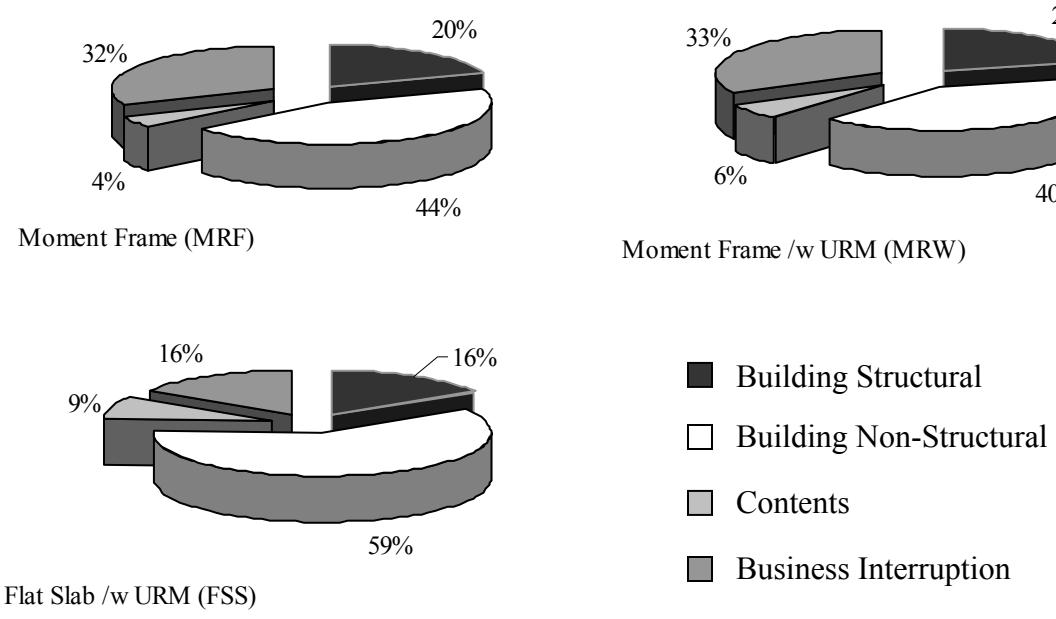

Figure 5.23 Distribution of Losses w.r.t. Total Economic Loss in SE-9 (M=7)

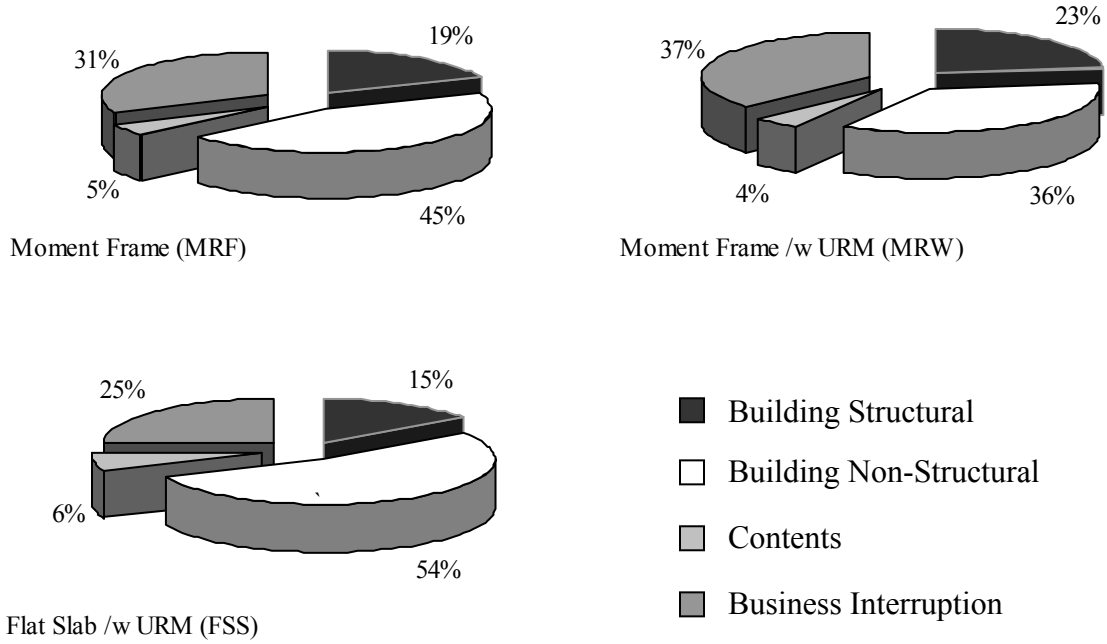

Figure 5.24 Distribution of Losses w.r.t. Total Economic Loss in SE-10 (M=8)

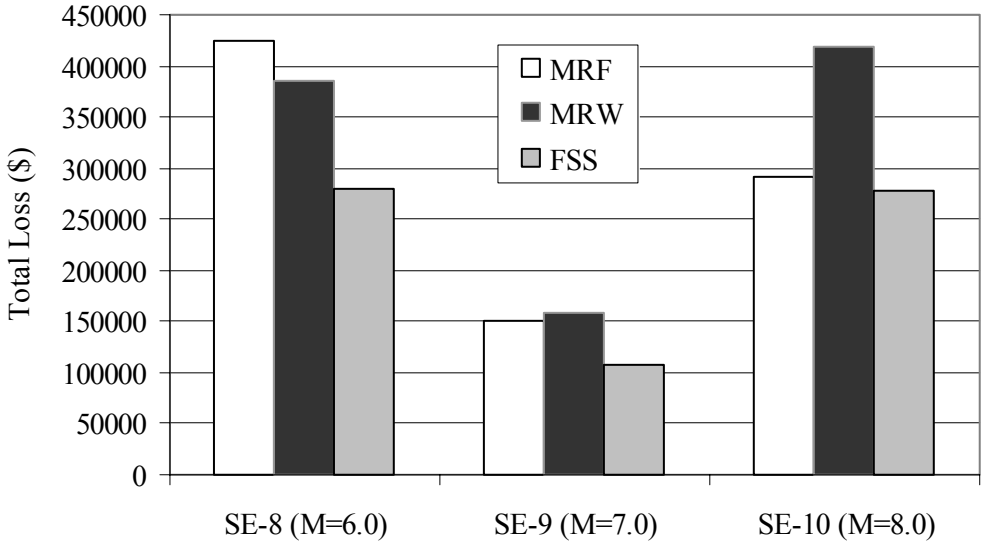

Figure 5.25 Total Economic Losses in the Example Buildings When Subjected to SE-8, 9 and 10

case of MRF and MRW. Furthermore, approximately 15% of the losses are due to structural damage considering all the buildings types in general. Losses due to contents damage constitute the smallest portion in the pie-charts.

Figure 5.25 shows the estimated economic losses that the example buildings will suffer when they are exposed to the scenario earthquakes SE-8, SE-9 and SE-10. Total loss estimates in SE-8 and SE-10 are close to each other, which means that a M6 on-site earthquake and a M8 large earthquake in the southwestern segment of the New Madrid seismic fault will affect the concrete structures in a similar way. On the other hand, the estimates obtained for SE-9 indicate that this event does not cause as much damage as the SE-8 and the SE-10, when considering the individual buildings in the loss estimation study. Total losses in FSS are not as high as the losses in MRF or MRW since inertia forces acting on this structural type are less than the other two types due to its inherent flexibility. Moreover, the scenario earthquakes are not able to cause very severe damage in any of the buildings, which would be a good basis for comparing the ultimate performances of the three structural types.

Finally, the AEBM results are compared with the results of the regional loss estimation analysis for Shelby County, TN. The scenario earthquake SE-10 (M=8) is employed for this comparison. There are 238,064 buildings in the study region with a total exposure of $38 billion. The total economic loss of the scenario is estimated as $8.76 billion. The share of losses due to structural damage, non-structural damage and contents damage are approximately 14%, 40% and 13%, respectively. These average values are very close to the estimates obtained for MRF and MRW. The percentage of losses due to non-structural damage for FSS is above the average (Figure 5.24).

The day-time casualty estimates are 23,509 persons in the earthquake scenario of which 1420 of them or 6% are fatalities. The average casualty per occupant ratio is equal to 2.8%. This is a high value when compared to the 1.2% obtained for the individual buildings using the same scenario earthquake in the AEBM analysis.

6. SUMMARY AND CONCLUSIONS

The studies performed to achieve the main objectives of the study and the results obtained are summarized in this chapter. It also includes the conclusions drawn in relation with the obtained results.

The first goal was to develop fragility information of the flat-slab system. For this purpose, a mid-rise building was designed and modeled, considering the structural characteristics of the flat-slab system. The preliminary evaluation of the seismic response indicated that the model structure is very flexible due to the absence of deep beams and shear walls. The performance of the structures was investigated through push-over analysis and the limit states of the structure were attained accordingly. For the time history simulations, ten spectrum-compatible ground motions were selected. Compressive strength of concrete and yield strength of steel were employed as random variables to define the material variability. Dynamic time-history analyses were conducted at different levels of seismic intensity and the probability of exceeding each damage state was calculated using the response statistics. The fragility curves for the flat-slab structure were obtained and then compared with the similar curves in the literature. It was observed that differences exist, but the developed curves were in the same range with the ones in the literature, and the differences were justifiable on grounds structural response characteristics.

The second objective was to assess the HAZUS Earthquake Loss Estimation Methodology as an open-source, nationally-applicable software. The advantages and the limitations of the study were discussed from the user's point of view. The sources of uncertainty in the HAZUS methodology were also considered. It was stated that there are ways to treat the uncertainty in HAZUS although it is not explicitly accounted for. Then the building-related modules in HAZUS and their interactions with each other were investigated in detail to get a better understanding of the flow of the methodology.

The last objective was to implement the developed fragility curves for flat-slab structures into HAZUS. First the differences between the methodology used in this study and in HAZUS were stated. Then the procedure to develop HAZUS-compatible fragility curves was discussed. The

implementation of the compatible curves into HAZUS modules were explained in detail. The new fragility curves were compared with the built-in fragility information through two different case studies. The study regions, Urbana, IL and Shelby County, Memphis, TN. were selected from two different Mid-American communities. Finally, the results of the loss estimation analyses in relation to different types of building structures and different scenario earthquakes were discussed.

Based on the observations and the results obtained during the course of this study, the following conclusions can be stated:

Related with the development of the fragility curves for the flat-slab structure:

- There are different methodologies to develop fragility curves. The resulting curves are strongly dependent on the choices made for the analysis method, structural idealization, seismic hazard identification and the damage models used. These choices can cause significant discrepancies in the vulnerability predictions by different researchers, even in the cases where similar structural types and the same seismicity information are employed.

- Fragility curves derived for the flat-slab structure reflect the inherent characteristics of this structural form. When compared with the curves of regular moment frames of similar structural class, it is observed that the fragility curves are more vulnerable to seismic hazard because of their insufficient lateral resistance and undesired performance at high levels of seismic demand.

- The fragility curves developed for flat-slab system gets flatter as the limit state shifts from slight to complete. This is due to the nature of the statistical distribution of the response data. The variability of the interstory drift at high seismic intensity levels is much more pronounced relative to the variability at low intensity levels. Hence small variations in low intensity cause significant differences in the limit state exceedence probabilities.

- The steep shape of the Slight limit state curve is because of the flexibility of the flat-slab structures and the infill panel stiffness and strength.

Related with HAZUS Loss Estimation Methodology:

- HAZUS is a pioneer in Standardization of Loss Estimation and is the first program that has been widely used as a seismic hazard reduction tool. Obviously, its current version is far from being perfect and has many pitfalls and limitations. It is just a tool to help the users do a better job in estimating the earthquake losses. The default HAZUS data needs updating and should only be used as a starting point. Moreover, the calculated estimates should only be used as an indicator, not as the exact results that all decisions are based on. The users should be aware of the limitations and uncertainties involved in the methodology. The results should only be used as a guide when making final decisions.

- Uncertainty in HAZUS is not considered explicitly and seems to be the major drawback of the methodology. However it is possible to examine the variability of the model by performing a sensitivity analysis.

Related with the implementation of the fragility curves for flat-slab structure into HAZUS:

- Fragility curves in HAZUS are created using a combination of engineering analysis, laboratory and other empirical component data, as well as the expert opinion of several structural engineers. The structural analysis method used in HAZUS is the Capacity Spectrum Method (CSM). On the other hand, the methodology used in this study utilizes nonlinear time-history analysis as the computation method, which is the most elaborate and accurate way of calculating the seismic response.

- A very significant distinction between the methodology used in this study and the HAZUS methodology is that the HAZUS fragility curves are derived based on the damped elastic spectral displacement at the intersection of a pushover curve and the earthquake response spectrum. However the fragility curves derived in this study are functions of spectral displacement at fundamental period of the building. Because of this period discrepancy, there is not a one-to-one correspondence between the two sets of

curves. Additional effort is required to transform the derived fragility curves into the HAZUS format.

- HAZUS-compatible curves are in agreement with the HAZUS built-in curves for reinforced concrete frames. The specific characteristics of these structural forms are very well reflected in the fragility curves. For low levels of seismic intensity, the probability of sustaining damage for flat-slab structure is higher than the corresponding probability for moment frame due to the inherent flexibility of this type of construction. For moderate levels of seismic intensity, it is probable that reinforced concrete frames can experience more damage since they are more rigid and attract higher seismic loads. For high levels of seismic intensity, the insufficient lateral resistance of the flat-slab system causes extensive damage, which is far more than the damage observed in regular concrete frame system.

Related with the earthquake loss estimation analysis conducted for Mid-American communities:

- The scenario earthquakes for Mid-American communities are generally events with moderate magnitude. When exposed to such earthquakes, flat-slab structures exhibit a similar behavior when compared with other reinforced concrete frame type structures. The loss estimation results indicate that a greater portion of the total economic losses are due to non-structural damage in flat-slab structures. However these results may be misleading since no study is conducted on the development of non-structural fragility curves for the flat-slab structure and the default values are used.

- The results of the HAZUS loss estimation analyses show that the New Madrid Seismic Zone is not a threat for the Urbana Study Region. An on-site moderate earthquake will be more devastating for Urbana. However, this is not the case for the second study region, Shelby County, TN. A large earthquake originated by the New Madrid seismic fault can cause as much damage as a moderate on-site earthquake for this study region.

REFERENCES

ACI-ASCE Committee 352, 1988. "Recommendations for Design of Slab-column Connections in Monolithic Reinforced Concrete Structures", ACI Structural Journal, Vol.85, No.6, pp. 675-696.

ACI Committee-318, 1999. "ACI 318-99, Building Code Requirements for Structural Concrete", American Concrete Institute, Detroit, Michigan.

Allen, D.E., 1972. "Statistical Study of the Mechanical Properties of Reinforcing Bars", Building Research Note No.85, Division of Building Research, National Research Council, Ottawa, Canada.

Alpsten, G.A. "Variations in Mechanical and Cross-Sectional Properties of Steel", Proceedings, International Conference on Planning and Design of Tall Buildings, Vol. 1b, Tall Building Criteria and Loading, Lehigh University, Bethlehem, pp. 775-805.

Ang, A. H.-S. and Cornell, C.A., 1974. "Reliability Bases of Structure Safety and Design", Journal of Structural Engineering, ASCE, Vol.100, No.9, pp.1755-1769.

Applied Technology Council (ATC), 1996. "Seismic Evaluation and Retrofit of Concrete Buildings", Report No. SSC 96-01: ATC-40, Vol.1, Redwood City, CA.

ASTM Task Group 70-3, 1972. "Reinforcing Bar Testing Program", ASTM A.01.05, American Society for Testing and Materials, Philadelphia, PA.

Ayyub, B.M. and Lai, K.-L., 1989. "Structural Reliability Assessment using Latin Hypercube Sampling", Proceedings, 5th International Conference on Structural Safety and Reliability, ICOSSAR'89, Vol.2, ASCE, New York, pp. 1177-1184.

Bannister, J.L., 1968. “Steel Reinforcement and Tendons for Structural Concrete, Part I: Steel for Reinforced Concrete”, Concrete, Vol.2, No.7, pp.295-306.

Barron-Corvera, R., 2000. “Spectral Evaluation of Seismic Fragility of Structures”, Ph.D. Dissertation, Development of Civil, Structural and Environmental Engineering, State University of New York at Buffalo, N.Y.

Bazzuro, P. and Cornell, C. A., 1994. “Seismic Hazard Analysis of Nonlinear Structures I: Methodology”, Journal of Structural Engineering, ASCE, Vol.120, No.11, pp. 3320-3344.

Bertero V. V. and Brokken, S. T., 1983. “Infills in Seismic Resistant Building”, Journal of Structural Engineering, ASCE, Vol.109, No.6.

Building Seismic Safety Council, 2001. NEHRP Recommended Provisions for Seismic Regulations for New Buildings and Other Structures, Part.1 Provisions (FEMA 368), Washington D.C.

Chopra, A.K., 1995. Dynamics of Structures, Theory and Applications to Earthquake Engineering, Prentice Hall International, Englewood Cliffs, New Jersey.

Chow, H. L. and Selna, L. G., 1995. “Seismic Response of Nonductile Flat Plate Buildings”, Journal of Structural Engineering, ASCE, Vol.121, No.1, pp. 115-123.

Dymiotis, C., Kappos, A. J., Chryssanthopoulos, M. K., 1999. “Seismic Reliability of RC Frames with Uncertain Drift and Member Capacity”, Journal of Structural Engineering, ASCE, Vol.125, No.9, pp. 1038-1047.

Ellingwood, B., 1977. “Statistical Analysis of RC Beam Column Interaction”, Journal of Structural Engineering ASCE, Vol.103, pp.1377-1388.

Elnashai, A. S. and Borzi, B., 2000. "Deformation-based Analytical Vulnerability Functions for RC Bridges", Engineering Seismology and Earthquake Engineering Report No. ESEE 00-6, Imperial College, London,UK.

Elnashai, A.S., Papanikolaou, V. and Lee, D.H., 2002. ZeusNL User Manual, Civil and Environmental Engineering Department, University of Illinois at Urbana-Champaign.

Ersoy, U., 1994. Reinforced Concrete. Middle East Technical University, Ankara, Turkey, 436 pages.

Federal Emergency Management Agency, 1997. NEHRP Guidelines for the Seismic Rehabilitation of Buildings, FEMA Publication 273, Washington D.C.

Federal Emergency Management Agency, 1999. Evaluation of Earthquake Damaged Concrete and Masonry Wall Buildings, FEMA Publication 307, Washington D.C.

Frankel A.D., Mueller, C., Barnhard, T., Perkins, D., Leyendecker E. V., Dickman, N., Hanson, S. and Hopper, M., 1996. "Natural Seismic Hazard Maps: Documentation.", US Geological Survey Open-File Report 96-532, United States Government Printing Office, Washington, D.C.

Freeman, S.A., 1998. "Development and Use of Capacity Spectrum Method", Proceedings, 6th US National Conference on Earthquake Engineering, Seattle (in CDROM)

Ghobarah, A., Aly, N. M. and El-Attar, M., 1998. "Seismic Reliability Assessment of Existing Reinforced Concrete Buildings", Journal of Earthquake Engineering, Vol.2, No.4, pp.569-592.

Greek Code for Earthquake Resistant Structures, 99-10 edition. Ministry of the Environment and Public Works, Greece.

Grossi, P., 2000. Quantifying the Uncertainty in Seismic Risk and Loss Estimation", Ph.D. Dissertation, University of Pennsylvania.

Holmes, M., 1961. “Steel Frames with Brickwork and Concrete Infilling”, Proceedings, Institute of Civil Engineers, London, England, Part 2, Vol.19, pp. 473-478.

Hueste, M.B.D. and Wight, J.K., "Evaluation of a Four-Story Reinforced Concrete Building Damaged During the Northridge Earthquake", Earthquake Spectra, Vol. 13, No. 3, pp. 387-414.

Hwang, H. and Huo, J-R., 1997. “Chapter 7.b: Development of Fragility Curves for Concrete Frame and Shear Wall Buildings”, Loss Assessment of Memphis Buildings, Technical Report NCEER 97-0018, pp 113-137.

Iman, R.L. and Conover, W.J., 1982. “Sensitivity Analysis Techniques: Self-teaching Curriculum”, Nuclear Regulatory Commission Report, NUREG/CR-2350, Technical Report SAND81-1978, Sandia National Laboratories, Albuquerque, NM.

Iman, R.L., Helton, J.C. and Campbell, J.E., 1981a. “An Approach to Sensitivity Analysis of Computer Models, Part 1”, Journal of Quality Technology, Vol.13, No.3, pp. 174-183.

Iman, R.L., Helton, J.C. and Campbell, J.E., 1981b. “An Approach to Sensitivity Analysis of Computer Models, Part 2”, Journal of Quality Technology, Vol.13, No.4, pp. 232-240.

Johnston, A.C. and Nava, S.J., 1985. “Recurrence Rates and Probability Estimates for the New Madrid Seismic Zone”, Journal of Geophysical Research, Vol.90 (B8), pp. 6737-6753.

Julian, E.G., 1955. “Discussion of Strength Variations in Ready-mixed Concrete” by A.E. Cummings, ACI Structural Journal, Vol.51, No.12, pp.772-778.

Kappos, A. J., 1991. “Analytical Prediction of the Collapse Earthquake for R/C Buildings: Case Studies”, Earthquake Engineering and Structural Dynamics, Vol.20, pp. 177-190.

Kennedy, R. P., Cornell, C. A., Campbell, R. L., Kaplan, S. and Perla, H. F., 1980. Probabilistic Seismic Safety of an Existing Nuclear Power Plant, Nuclear Engineering and Design Vol.59, No.2, pp. 315-338.

Klingner, R. E. and Bertero, V. V., 1978. "Earthquake Resistance of Infilled Frames", Journal of Structural Division, ASCE, Vol.104, No.ST6, pp. 973-989.

Krawinkler, H., 1996. "Pushover Analysis: Why, How, When and When Not to Use It", Proceedings, 65th Annual SEAOC Convention, Maui, Hawaii.

Limniatis, A., 2001. "Seismic Behavior of Flat-Slab RC Structures", MSc. Dissertation, Civil Engineering Department, Imperial College of Science, Technology and Medicine.

Luo, Y. H., Durrani, A., 1995a. "Equivalent Beam Model for Flat-Slab Buildings: Interior Connections", ACI Structural Journal, Vol.92, No.1, pp. 115-124.

Luo, Y. H., Durrani, A., 1995b. "Equivalent Beam Model for Flat-Slab Buildings: Exterior Connections", ACI Structural Journal, Vol.92, No.2, pp. 250-257.

Luo, Y. H., Durrani, A., Conte, J., 1995. "Seismic Reliability Assessment of Existing R/C Flat-slab Buildings", Journal of Structural Engineering, ASCE, Vol.121, No.10, pp. 1522-1530.

MacGregor, J.G., 1997. Reinforced Concrete: Mechanics and Design. Prentice Hall, Upper Saddle River, N.J., 939 pages.

Madan, A., Reinhorn, A. M., Mander, J. B. and Valles, R. E., 1997. "Modeling of Masonry Infill Panels for Structural Analysis", ASCE, Vol.123, pp. 1295-1302.

Mainstone, R. J., 1971. "On the Stiffness and Strength of Infilled Frames",Proceedings, Supplement(IV), Paper 7360S, Institution of Civil Engineers, London England.

Mander J. B., Priestley, M.J. N. and Park, R., 1988. "Theoretical Stress-Strain Model for Confined Concrete", Journal of Structural Engineering, ASCE, Vol.114, No.8, pp. 1804-1826.

Martinez-Rueda, J. E. and Elnashai, A. S., 1997. "Confined concrete model under cyclic load", Materials and Structures, Vol.30, No.197, pp. 139-147.

McKay, M.D., Conover, W.J. and Beckman, R.J., 1979. "A Comparison of Three Methods for Selecting Values of Input Variables in the Analysis of Output from a Computer Code", Technometrics, Vol.221, pp. 239-245.

Megally, S. and Ghali, A., 1994. "Design Considerations for Slab-column Connections in Seismic Zones", ACI Structural Journal, Vol.91, No.3, pp. 303-314.

Megally, S. and Ghali, A., 2000. "Seismic Behavior of Slab-column Connections", Canadian Journal of Civil Engineering, Vol.27, No.1, pp. 84-100.

Mexico Building Code, 1987. Reglamento da Construcciones para el Distrito Federal, Diario Oficial, Mexico.

Mirza, S.A. Hatzinikolas, M. and MacGregor, J.G., 1979. "Statistical Descriptions of Strength of Concrete", Journal of Structural Engineering, ASCE, Vol.105, No.ST6, pp.1021-1036.

Mirza, S.A. and MacGregor, J.G., 1979. "Variability of Mechanical Properties of Reinforcing Bars", Journal of Structural Engineering ASCE, Vol.105, No.ST5, pp.921-937.

Moehle, J. P., 1986. "Seismic Response of Slab-column Frames", Proceedings of the Third U.S. National Conference on Earthquake Engineering, Charleston, SC, Vol.2., pp. 1505-1516.

Mosalam, K., Ayala, G. and White, R., 1997. "Chapter 7.c: Development of Fragility Curves for Masonry Infill - Concrete Frame Buildings", Loss Assessment of Memphis Buildings, Technical Report NCEER 97-0018, pp 139-158.

National Institute of Building Sciences (NIBS), 1999a. HAZUS User's Manual, prepared for Federal Emergency Management Agency, Washington D.C.

National Institute of Building Sciences (NIBS), 1999b. HAZUS Technical Manual (3 volumes), prepared for Federal Emergency Management Agency, Washington D.C.

National Institute of Building Sciences (NIBS), 1999c. HAZUS Advanced Engineering Building Module (AEBM) Technical and User's Manual, prepared for Federal Emergency Management Agency, Washington D.C.

Olshansky, R., Wu, Y. and French, S., 2002. "Evaluating Earthquake Risk in Mid-American Communities", Final Report, Project SE-5, Mid America Earthquake Center, Civil and Environmental Engineering Department, University if Illinois at Urbana-Champaign.

Pan, A. and Moehle, J. P., 1989. "Lateral Displacement Ductility of R/C Flat Plates", ACI Structural Journal, Vol.86, No.3, pp. 250-258.

Park, R., Priestley, M. J. N. and Gill, W. D., 1982. "Ductility of Square Confined Concrete Columns", Journal of Structural Division, ASCE, Vol.ST4, pp. 929-950.

Paulay, T. and Priestley, M.J.N., 1992. Seismic Design of Reinforced Concrete and Masonry Buildings, John Wiley, New York.

Penelis, G.G. and Kappos, A.J., 1997. Earthquake Resistant Concrete Structures. E & FN Spon, London.

Porter, K.A., 2000. "Assembly-based Vulnerability of Buildings and Its Uses in Seismic Performance Evaluation and Risk Assessment Decision-Making", Doctoral Dissertation, Stanford University, Stanford, CA.

Porter, K. A., Beck, J. L., Seligson, H. A., Scawthorn, C. R., Tobin, L. T., Young, R. and Boyd, T., 2001. "Improving Loss Estimation for Wood-frame Buildings", Final Report of the CUREE-Caltech Wood-frame Project, published by the Consortium of Universities for Research in Earthquake Engineering, Richmond, CA.

Priestley, M.J.N., 1998. "Displacement Based Approaches to Rational Limit States Design of New Structures", Proceedings of the 11th European Conference on Earthquake Engineering, A.A. Balkema, Rotterdam (in CD-ROM)

Saneinejad, A. and Hobbs, B., 1995. "Inelastic Design of Infilled Frames", Journal of Structural Engineering, ASCE, Vol.121, pp. 634-650.

Savy, J., 1998. "Ground Motion Attenuation in the Eastern North America", Lawrence Livermore National Laboratory, Livermore, CA.

SEAOC, 1995. "Performance Based Seismic Engineering of Buildings", Vision 2000 Committee, Structural Engineers Association of California, Sacramento, California.

Singhal, A. and Kiremidjian, A.S., 1997. "A Method for Earthquake Motion-Damage Relationships with Application to Reinforced Concrete Frames", Technical Report NCEER 97-0008, National Center for Earthquake Engineering Research, Buffalo, NY.

Sozen, M. A., 1981. "Review of Earthquake Response of RC Buildings with a View to Drift Control", State-of-the-Art in Earthquake Engineering, Kelaynak Press, Ankara, Turkey.

Stafford Smith, B., 1966. "Behavior of Square Infilled Frames", Journal of Structural Engineering, ASCE, Vol.92, pp. 381-403.

Stafford Smith, B. and Carter, C., 1969. "A method of Analysis for Infilled Frames", Proceedings, Institute of Civil Engineers, London, England, Part 2, Vol.44, pp. 31-48.

Stafford Smith, B. and Riddington, J. R., 1978. “The Design of Masonry Infilled Steel Frames for Bracing Structures”, Journal of Structural Engineers, Vol.56B, pp. 1-7.

Stover, C.W. and Coffman, J. L., 1993. “Seismicity of the United States 1568-1989”, US Geological Survey Professional Paper No.1527, United States Government Printing Office, Washington.

Tantala, M.W. and Deodatis, G., 2002. “Development of Seismic Fragility Curves for Tall Buildings”, 15th ASCE Engineering Mechanics Conference, Columbia University, New York.

Toro, G. R., Abrahamson, N. A. and Schneider, J. F., 1997. “Engineering Model of Strong Ground Motions from Earthquakes in the Central and Eastern United States”, Seismological Research Letters, January/February.

Tsuobi, Y. and Kawaguchi, M., 1960. “On Earthquake Resistant Design of Flat-Slabs and Concrete Shell Structures“, Proceedings, 2nd World Conference on Earthquake Engineering, Tokyo, Vol.3, pp. 1693-1708.

Uniform Building Code (UBC), 1997. Structural Engineering Design Provisions, Vol.2, International Conference of Building Officials, Whittier, Calif.

Wen, Y.K., Ellingwood, G. T. and Bracci, J., 2003. “Vulnerability Function Framework for Consequence-based Engineering”, Draft Report, Project Title: DS-4, Vulnerability Functions, Mid-America Earthquake Center, University of Illinois at Urbana Champaign.

Wheeler, R.L. and Johnston, A.C., 1992. ”Geological Implications of Earthquake Source Parameters in Central and Eastern North America”, Seismological Research Letters, Vol.70, No.1, pp. 491-514.

Whitman, R. V., Anagnos, T., Kircher, C. A., Lagorio, H. J., Lawson, R. S., Schneider, P., 1997. "Development of a National Earthquake Loss Estimation Methodology", Earthquake Spectra, Vol.13, No.4, pp.643-661.

Wiss, Janney, Elstner (WJE) and Associates, Inc., 1970. "Final Report on Bar Tests", Committee of Concrete Reinforcing Bar Producers and American Iron and Steel Institute, Northbrook, IL.

Wu, C.L., 2000. "Earthquake Motion Simulation and Reliability Implications", Dissertation, University of Illinois at Urbana-Champaign.

Wyss, G.D. and Jorgensen, K.H., 1998. "A User's Guide to LHS: Sandia's Latin Hypercube Sampling Software", Technical Report SAND98-0210, Risk Assessment and Systems Modeling Department, Sandia National Laboratories, Albuquerque, NM.

Zarnic, R., 1990. "Masonry Infilled RC Frames as Subassemblies of Earthquake Resisting Buildings", Earthquake Damage Evaluation and Vulnerability Analysis of Building Structures, A. Koridze, ed., OMEGA Scientific, Wallingford, Oxon, UK, pp. 79-100.